UNIVERSIDADE FEDERAL DO PARANÁ

MIDORI GRAÇA FATORI DEGUCHI RAMOS PINTO

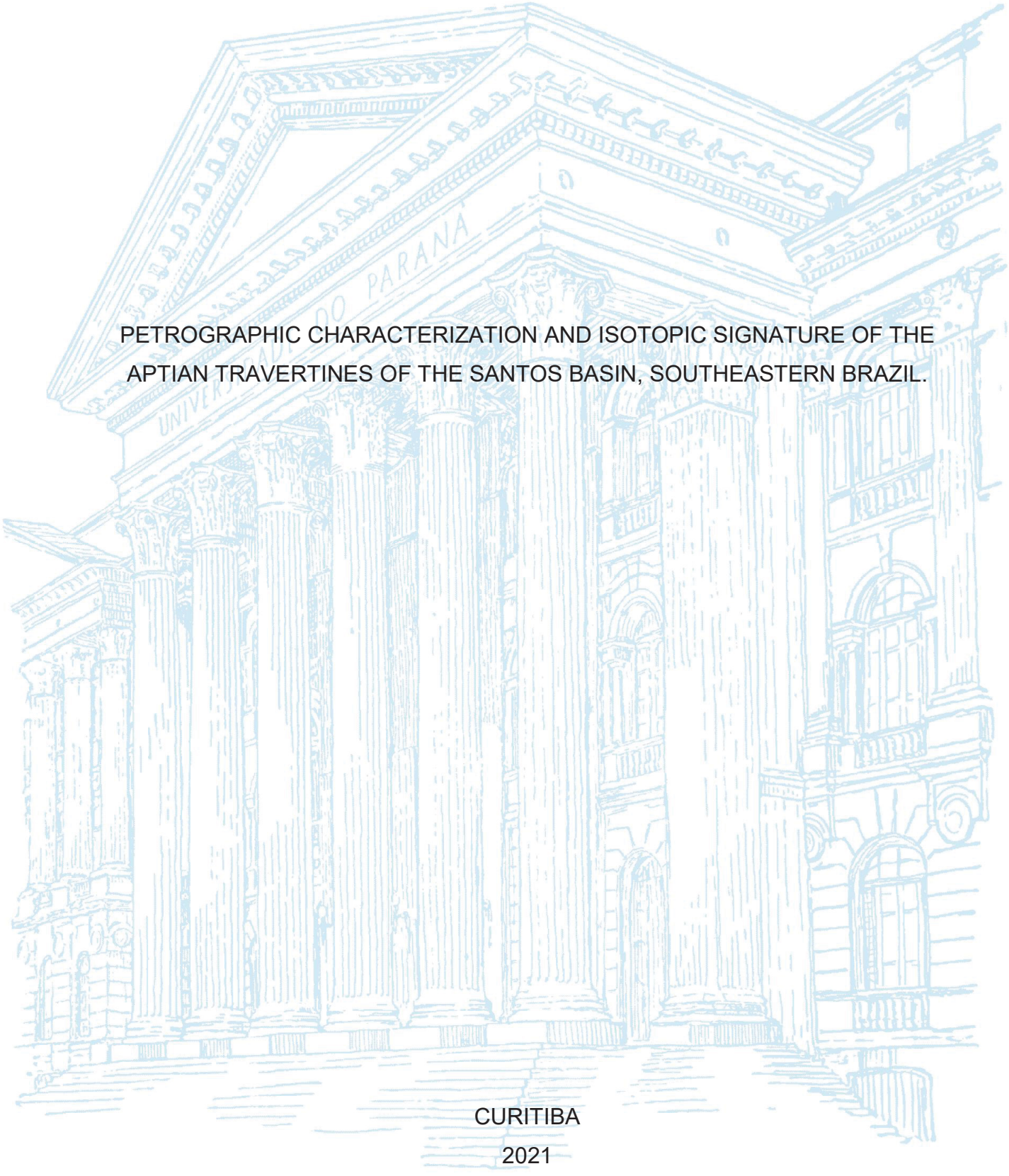

PETROGRAPHIC CHARACTERIZATION AND ISOTOPIC SIGNATURE OF THE APTIAN TRAVERTINES OF THE SANTOS BASIN, SOUTHEASTERN BRAZIL.

CURITIBA

2021

MIDORI GRAÇA FATORI DEGUCHI RAMOS PINTO

PETROGRAPHIC CHARACTERIZATION AND ISOTOPIC SIGNATURE OF THE APTIAN TRAVERTINES OF THE SANTOS BASIN, SOUTHEASTERN BRAZIL.

Dissertação apresentada ao curso de Pós-Graduação em Geologia, Setor de Ciências Exatas da Terra, Universidade Federal do Paraná, como requisito parcial à obtenção do título de Mestre em Geologia Exploratória.

Orientador: Prof. Dr. Almério Barros França

Coorientadora: Profa. Dra. Anelize Bahniuk Rumbelsperger

CURITIBA

2021

CATALOGAÇÃO NA FONTE – SIBI/UFPR

P659p Pinto, Midori Graça Fatori Deguchi Ramos

Petrographic characterization and isotopic signature of the aptian travertines of the santos basin, southeastern Brazil [recurso eletrônico]/ Midori Graça Fatori Deguchi Ramos Pinto – Curitiba, 2021.

Dissertação (Mestrado) – Curso de Pós-Graduação em Geologia, Setor de Ciências Exatas da Terra, Universidade Federal do Paraná, como requisito parcial à obtenção do título de Mestre em Geologia Exploratória.
Orientador: Prof. Dr. Almério Barros França
Coorientadora: Profa. Dra. Anelize Bahniuk Rumbelsperger

1. Petróleo. 2. Bacia - Santos. 3. Geoquímica. I. França, Almério Barros. II. Rumbelsperger, Anelize Bahniuk . III. Título. IV. Universidade Federal do Paraná.

CDD 338.981

Bibliotecária: Vilma Machado CRB9/1563

MINISTÉRIO DA EDUCAÇÃO
SETOR DE CIENCIAS DA TERRA
UNIVERSIDADE FEDERAL DO PARANÁ
PRÓ-REITORIA DE PESQUISA E PÓS-GRADUAÇÃO
PROGRAMA DE PÓS-GRADUAÇÃO GEOLOGIA - 40001016028P5

TERMO DE APROVAÇÃO

Os membros da Banca Examinadora designada pelo Colegiado do Programa de Pós-Graduação GEOLOGIA da Universidade Federal do Paraná foram convocados para realizar a arguição da dissertação de Mestrado de **MIDORI GRACA FATORI DEGUCHI RAMOS PINTO** intitulada: **PETROGRAPHIC CHARACTERIZATION AND ISOTOPIC SIGNATURE OF THE APTIAN TRAVERTINES OF THE SANTOS BASIN, SOUTHEASTERN BRAZIL**, sob orientação do Prof. Dr. ALMÉRIO BARROS FRANÇA, que após terem inquirido a aluna e realizada a avaliação do trabalho, são de parecer pela sua APROVAÇÃO no rito de defesa.
A outorga do título de mestra está sujeita à homologação pelo colegiado, ao atendimento de todas as indicações e correções solicitadas pela banca e ao pleno atendimento das demandas regimentais do Programa de Pós-Graduação.

CURITIBA, 15 de Dezembro de 2021.

Assinatura Eletrônica
24/12/2021 09:17:46.0
ALMÉRIO BARROS FRANÇA
Presidente da Banca Examinadora

Assinatura Eletrônica
16/12/2021 11:58:12.0
RICARDO JORGE JAHNERT
Avaliador Interno (UNIVERSIDADE FEDERAL DO PARANÁ)

Assinatura Eletrônica
17/12/2021 08:43:43.0
BRUNO EUSTAQUIO MOREIRA LIMA
Avaliador Externo (PETRÓLEO S.A.)

I dedicate this work to my boys: Antônio Pedro and Francisco Hiroshi. May it serve as an inspiration for you to never stop studying and being amazed by the world!

ACKNOWLEDGEMENTS

Firstly, I would like to express my gratitude to Almério Barros França and Anelize Bahniuk Rumbelsperger, who has supervised this work and contributed with invaluable advice and support. You are an inspiration to me, not only for academic research but in life.

I thank LAMIR/UFPR (Laboratory of Minerals and Rocks Analysis of the Federal University of Paraná) and its technical staff for their unrestricted support during the work.

I would like to thank Petrobras for all funding and support during my MSc study at UFPR, especially to the Research and Development Centre of Petrobras (CENPES). I also need to thank Roberta Alves Mendes, my manager at the time, who not only supported my decision but genuinely believed and fought to make this wish come true and, all Petrobras geoscientists and engineers who spent their time, whether 10 minutes or several hours, helping me with technical support or, more important than that, encouraging and rooting for me.

I cannot express my gratitude to my dear husband, Luiz Fernando Ramos Pinto Filho, for his enormous patience. Without his unconditional support, this study would not have been successful. Thank you for taking care of our home and our children Tunico e Chico during these years of work and research and for continuing to love me (especially during the pandemic).

I am indebted to all my friends and family, especially my siblings Thieme and Nani, who were always so helpful in numerous ways.

Finally, I would like to express my gratitude to my parents Lina Maria and Bernardo, for their tremendous support and encouragement throughout my life. Thank you for showing me which way to go and always supporting my choices (even when they did not agree with some of them). Thank you for teaching me by example what hard work, honesty, and integrity are all about!

’’Happiness is only real when shared.’’

Christopher McCandless (1968-1992)

RESUMO

O estudo de carbonatos travertínicos ganhou nova importância geológica e econômica quando gigantescas reservas de hidrocarbonetos foram descobertas na seção Aptiana da Bacia de Santos, na costa sudeste do Brasil. Estes reservatórios carbonáticos não convencionais da Formação Barra Velha foram batizados de Seção Pré-Sal e são atualmente responsáveis por metade da produção brasileira de petróleo. Desde os primeiros poços perfurados e descritos, muitos modelos geológicos e classificações de fácies foram propostos. Em comum, quase todas enfatizam o caráter peculiar dessas rochas precipitadas em um ambiente lacustre alcalino, semelhantes aos encontrados no Rift do Leste Africano. Este estudo concentrou-se em um poço perfurado no Alto Externo da Bacia de Santos, do qual amostras de rocha foram coletadas, analisadas e forneceram, num primeiro momento, indicativos de tratar-se de um depósito travertínico. Dados de petrografia, microscopia eletrônica de varredura e análises de isótopos estáveis foram integrados para desvendar a origem e o ambiente de deposição dessas rochas. Descrições macroscópicas e petrografia revelaram características tipicamente encontradas em travertinos, como carbonatos fortemente bandados com ângulos de inclinação elevados, crostas de calcita, *rafts,* e feições de micro-carste. Ao mesmo tempo, valores muito negativos de $\delta^{13}C$ e a presença de fases minerais comumente precipitadas em sistemas hidrotermais carbonáticos como pirita, barita, fluorita, anidrita, Sr-barita e betume sólido apontam uma história diagenética complexa e heterogênea, associada a fluidos hidrotermais transportados pelos sistemas de falhas e fraturas que atuaram na Bacia de Santos durante a abertura do Oceano Atlântico, mas em tempos geológicos distintos. O conjunto de dados analisados fornece evidências claras da presença de travertinos no Pré-Sal e também sobre as alterações hidrotermais pós-deposicionais. Estas últimas, provavelmente associadas à atividade magmática do Cretáceo Superior ou Paleógeno que influenciou a criação, dissolução e obliteração da porosidade nos reservatórios do Pré-Sal.

Palavras-chave: Pré-Sal. Carbonatos lacustres. Bacia de Santos. Travertinos. Geoquímica de carbonatos.

ABSTRACT

The study of travertine carbonates gained both geological and economic significance when gigantic hydrocarbon reserves were discovered in the Aptian section of the Santos Basin. Known as the Pre-Salt, located in the southeastern Brazilian coast, the unconventional carbonate reservoirs of the Barra Velha Formation are currently responsible for half of the Brazilian oil production. Since the first drilled and described wells, many geological models and facies classifications have been proposed. In common, almost all emphasize the unusual character of these rocks precipitated in an alkaline lacustrine environment, similar to those found in the East African Rift. This study highlights one specific well drilled in Santos Basin Outer High, in which rock samples were collected, analyzed, and suggested the occurrence of travertine facies. Thin section petrography, scanning electron microscopy, and stable isotopes analyses were integrated to unravel these peculiar rocks' origin and depositional environment. Macroscopic descriptions and detailed petrography revealed features typically found in travertine systems, such as strongly banded carbonates with high inclinations angles, calcite crusts, rafts, and micro-karst features. At the same time, $\delta^{13}C$ negative values and some mineral phases commonly precipitated by hydrothermal systems in carbonate deposits such as pyrite, anhydrite, fluorite, barite, Sr-barite, and bitumen point out to a complex and heterogeneous diagenetic history of these rocks, associated with hydrothermal fluids carried through the fault and fracture systems that act in the Santos during the opening of the Atlantic Ocean but in different geological times. The combined data set provides clear evidence of travertines' presence in Pre-Salt and also about post-depositional hydrothermal alterations. The latter one, likely associated with Late Cretaceous or Paleogene magmatic activity that controlled creation, dissolution, and obliteration of the porosity in Pre-Salt reservoirs.

Keywords: Pre-Salt. Lacustrine carbonates. Santos Basin. Travertines. Carbonate geochemistry.

LISTA DE FIGURAS

LISTA DE TABELAS

SUMMARY

1 INTRODUCTION

The study of travertine carbonates gained new geologic and economic significance when, in 2006, gigantic hydrocarbon reserves were discovered in southeastern Brazil. Since the first wells were drilled and described in the Aptian section of the Santos Basin (known as the Pre-Salt section), many geological models and facies classification have been proposed, usually based on petrographic, textural, and mineralogical observations. In common, almost all emphasize the unusual character of these rocks (Farias et al., 2019; Gomes et al., 2020; Lima et al., 2019; Sartorato, 2018; Terra et al., 2009).

The macroscopic similarity observed between the porous types described in outcrops of travertine systems in different regions of the world and those observed in the sampled rocks in Santos Basin Pre-Salt is striking and motivated the search for analogs that could help in understanding the genesis and the paleoenvironmental context in which these reservoir rocks were deposited. While Wright and Barnett (2015a) suggested that the similarity with travertines textures not necessarily reflects a similar depositional environment but similar processes (such as rapid precipitation from high saturated solutions), Della Porta *et al*. (2017) did not exclude the possibility of the presence of hydrothermal travertines in the middle of these reservoirs and, Souza *et al.* (2018) interpreted many of the Barra Velha carbonate rocks as travertine related deposits.

1.1 OBJECTIVES

The occurrence of a 2000-2500 m thick column of salt (Ariri Formation) superimposed on the reservoir, in addition to the low-density contrast between the strata, compromises the seismic imaging of these reservoirs. Therefore, looking at and analyzing the rock samples collected in the wells would be the most efficient way to characterize these reservoirs since seismic attributes, such as acoustic impedance, are of low usefulness in defining the geometry of small bodies and their faciological distribution. On the other hand, the quality of the seismic data is getting better, allowing a better definition of the positive

features of the pre-salt. The seismic data used in association with the structural data (mapped faults) is a handy tool to identify features of possible travertine origin (at least those with dimensions from a few tens to hundreds of meters and a few tens of meters thick >20 m).

Studying the travertines that occur intercalated with the Aptian carbonates of the Santos Basin Pre-Salt is crucial because it can provide valuable information about the environment and the geotectonic context of the place where they were deposited.

Since travertine deposits occur in very particular geotectonic environments (associated with large geological fault zones in regions of crustal extension), the main contribution of this work concerns the petrographic characterization of the travertines found intercalated with the carbonates of the Barra Velha Formation, from the Santos Basin and the interpretation of its depositional environment. Through the petrographic characterization, it is also possible to show the impacts of diagenesis on the quality of reservoirs

1.2 THESIS STRUCTURE

This MSc thesis comprises two introductory chapters: (1) an introduction detailing the motivations, objectives, and geological setting, and (2) a literature review on travertines since this is the main topic addressed in this research.

The research's analytical methods, results, discussions, and conclusions will be presented in Chapter 3, in the form of a manuscript of the scientific article: *"Petrographic characterization and isotopic signature of the Aptian travertines of the Santos Basin, southeastern Brazil."*

1.3 GEOLOGICAL SETTING AND STUDY AREA LOCATION

1.3.1 Santos Geologial Setting

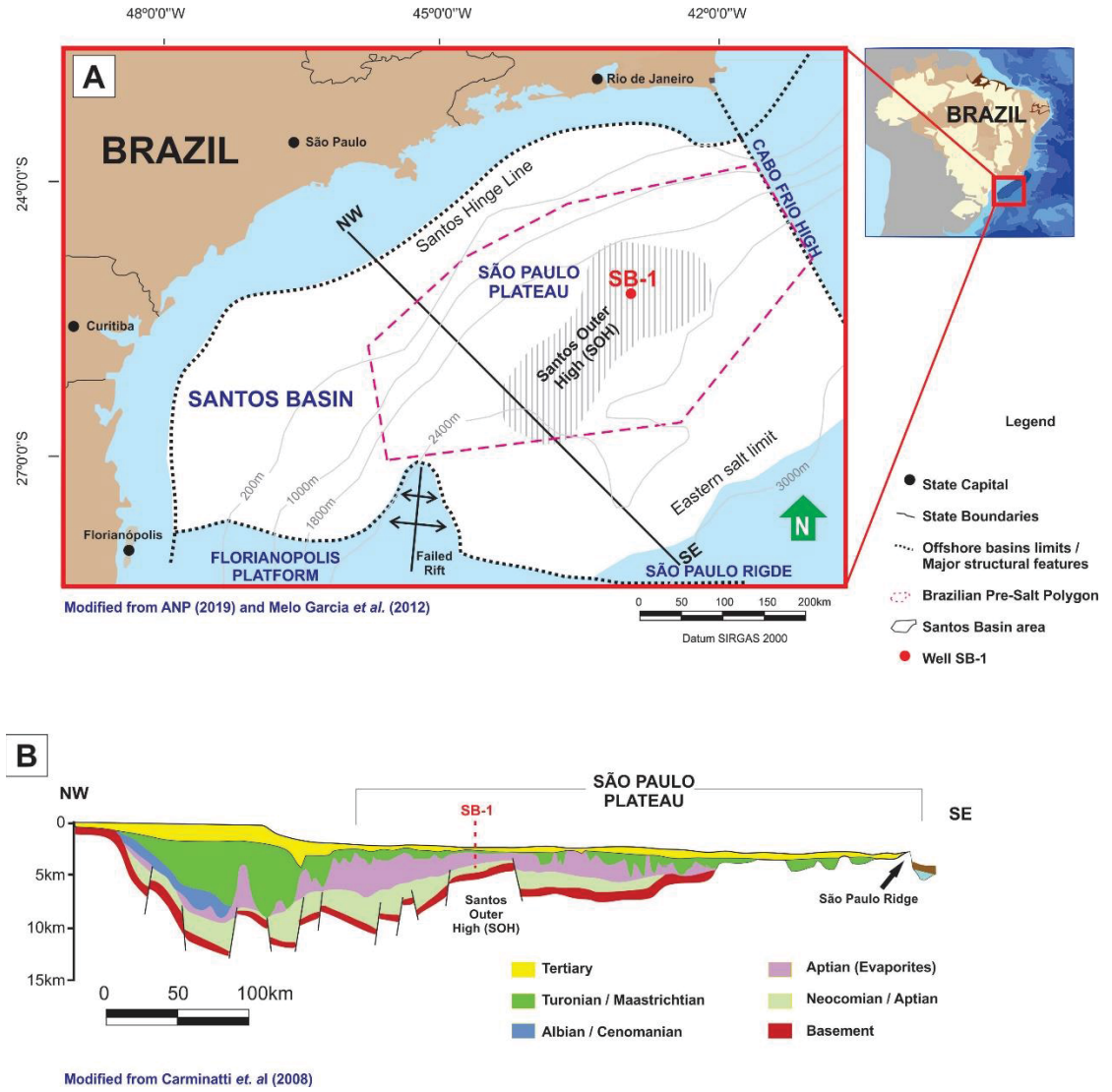

Figure 1 - Location map of the Santos Basin. A) Location map of Santos Basin with emphasis on the Santos Outer High (SOH - hatched polygon) with the location of the well SB-1 examined in this study (Modified from ANP, 2019 and Melo Garcia et al., 2012). B) Geological cross-section NW-SE.-

The Santos Basin is located on the southeastern Brazilian continental margin and extends from Cabo Frio to Florianopolis in about 350.000 km^2. Water level ranges from 150 m to almost 3000 m. The basin's exploratory potential has been recognized since the 1960's with the acquisition of the first seismic data. The first wildcat well was drilled in 1971 in shallow-water areas.

The Merluza turbidite field was the first discovery in 1979, followed by other fields in oolitic limestones in water around 300 meters (Carminatti et al., 2008).

In the early 2000s, technological advances allowed Petrobras to begin its exploratory efforts to drill in deep and ultra-deep waters areas that culminated in the discovering of the giant Tupi Field in 2006. This discovery opened a new frontier in Brazilian oil exploration. The unusual genesis and diagenetic history of the Pre-Salt lacustrine carbonate rocks attracted oil companies and became focus of debates in the geoscience community worldwide.

The northeast limit of the basin is the Cabo Frio High that separates Santos and Campos Basins. The Southwest limit is the Florianopolis Plateau separating the Santos Basin from the Pelotas Basin. Another two structures are important: the Santos Hinge Line to the west, which marks the west limit of the evaporitic sequence (Ariri Formation), and the São Paulo Ridge that makes the east limit. In the central portion of the São Paulo Plateau there is an unusual shallow region notice when the base of the evaporates is mapped. This area is nominated Santos Outer/External High (SOH). The Brazillian Pre-Salt hydrocarbon fields are located in SOH and therefore, our area of interest.

The tectonostratigraphic evolution of the Santos Basin, like all sedimentary basins in the Brazilian east coast (and their counterparts in southwest Africa) is related to the breakup of Western Gondwana when South America separated from Africa, and the South Atlantic Ocean began to open (Cainelli and Mohriak, 1999).

As a result of the continental rifting and seafloor spreading since the Late Jurassic, the Santos Basin was filled with three mega sequences: Rift, Post-Rift, and Drift (Moreira et al., 2007). Pereira & Feijo (1994) had already observed three sequences in previous works on the lithostratigraphy of the basin. The basement of the Santos Basin is composed of Precambrian metamorphic rocks of the Camburiu Formation. This tholeiitic flood basalt formed during the early stages of rifting in the Early Cretaceous has been dated by Mizusaki et al. (1992). It is responsible for heralding the beginning of the rifting in the southernmost part of the South American Plate. Extrusive and intrusive igneous activity occurred in this region, from the time of rifting up to the time of the evaporate deposition. Isotopic data suggests at least three

phases of igneous activity occurred: one at 113 Ma, another at 118 Ma, and the oldest 130 Ma (correlative to the Parana basalts). Camboriu, Piçarras, and Itapema formations are part of the Neocominan-Barremian Continental Rift Mega sequence. The rift phase is associated with the synthetic and antithetic faults forming several grabens and half-grabens filled by fluvial-deltaic sediments, with polymytic sandstones overlying volcanic rocks in the proximal regions. In the deeper portions occur dark shales and Mg-silicate clays from Piçarras Formation. The Piçarras Formation comprises sedimentation from the initial stage of rifting until the maximum tectonic activity. The Itapema Formation, on the other hand, represents the principal stage of the rifting phase, when the main faults significantly reduced their activity. This formation comprises another important reservoir: the bivalve coquinas deposits from Pre-Salt. Besides, there are still wackestones, packstones, carbonatic shales, and dark shales (Pereira and Macedo, 1990; Pereira and Feijó, 1994; Cainelli and Mohriak, 1999; Moreira et al., 2007).

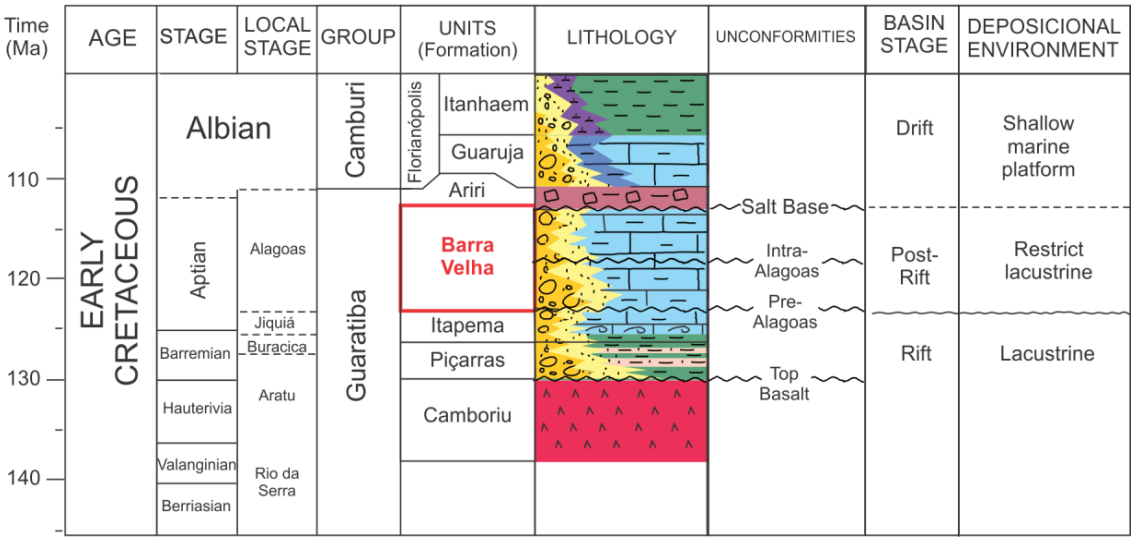

Figure 2 - Santos Basin stratigraphic chart (Modified from Moreira et al.; 2007)

The Neoaptian Post-rift Megasequence starts with the Barra Velha Formation made up of siliciclastic sediments along the basin margins (alluvial fans), carbonate sediments in the deeper portions and ends with evaporates (Ariri Formation). This megasequence lies within the Brazilian Alagoas Stage. The reservoirs are mainly lacustrine, shaped in a very stressful environment

with the deposition of microbialites, stromatolites, spherulites, dolomitized or not, laminites and shales in the distal regions. There are also grainstones and packstones composed mainly by fragments of stromatolites, microbiolites and spherulites (Cainelli and Mohriak, 1999; Moreira et al., 2007; Terra et al., 2009).

Finally, the basin evolved into a passive-margin allowing the deposition of the Drift Megasequence (Albian to Miocene age), which contains the largest Brazilian hydrocarbon production and reserves. This mega sequence is divided into a Restricted Marine Sequence (dominated by the shallow-marine carbonatic platform of the Guarujá Formation) and an Open Marine Sequence (made up of deep-water sediments of the Itanhaém Formation).

This study focuses on data from the SB-1 well (

Figure 1) located in Santos Outer High (SOH). 127 samples from a carbonatic core in the upper portion of the Barra Velha Formation were analyzed for geochemical and isotopic composition, and 40 thin sections were examined for petrography.

1.3.2 Barra Velha Formation

Ever since the first wells were drilled and described, several geological models and facies classification have been proposed for the carbonates of the Barra Velha Formation. They are usually based on petrographic, textural, and mineralogical observations (Dias, 2005; Falcão, 2015; Wright and Barnett, 2015, 2017; Muniz and Bosence, 2015; Herlinger et al., 2017; Fetter et al., 2018; Sartorato, 2018; Souza et al., 2018; Farias et al., 2019; Lima and De Ros, 2019; Gomes et al., 2020). In common, almost all emphasize the unusual character of these rocks.

Wright & Barnett (2015) described these unconventional carbonate reservoirs of the Barra Velha Formation as carbonates precipitated in an alkaline lake environment, similar to those found in the East African Rift, discarded the marine origin. The $^{87}Sr/^{88}Sr$ data provided by Tedeschi (2017) also supports this idea. Pietzsch et al. (2018) applied a paleo reconstruction of the Central South Atlantic segment based on Torsvik et al. (2009) to compare

the areas of Santos, Campos, and Espirito Santo basins during early Aptian and the size of modern-day Lake Tanganyika in the African Rift to show how a modern rift lake could be embedded within the Pre-Salt area (Figure 3).

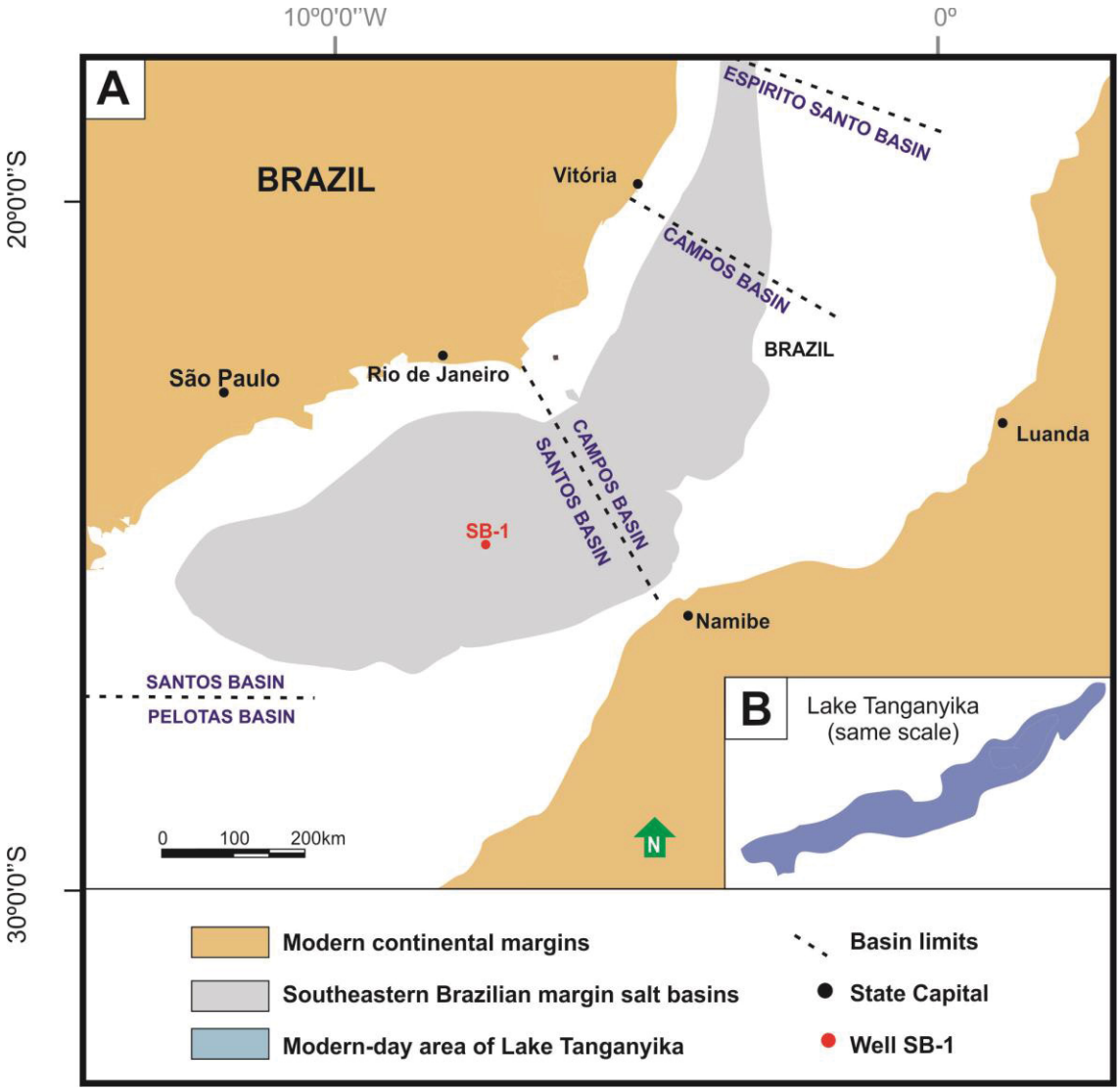

Figure 3 - Paleo reconstruction of the Central South Atlantic segment during the Aptian. A) Outline of the salt basins of Campos, Santos, and Esplrito Santo is shown in gray with the position of offshore Petrobras well SB-1. B) Area corresponding to the Lake Tanganyika (in blue) (the largest modern-day rift lake in the world, after the Baikal in Siberia), rotated and projected to scale with the map for size comparison (modified from Pieztch et al., 2018).

Wright & Barnett (2015) proposed a cyclic distribution for Barra Velha carbonates evolving the lake chemistry in the control facies development. For them, these typical cyclothems comprise three main components: mud laminated carbonates, spherulites with evidence of Mg-silicates, and calcitic

shrubs-like growths, all of them typically non-ferroan and inclusion-rich. Other authors also recognized high-frequency cycles (Dias, 2005; Muniz and Bosence, 2015; Wright and Tosca, 2016; Artagão, 2018; Sartorato, 2018; Farias et al., 2019; Lima and De Ros, 2019; Gomes et al., 2020). There is agreement over the presence of ciclicity, but the last authors suggest that in fact there are other types of a basic cycle with different facies associations, not only one typical cyclothem as proposed by Wright & Barnett (2015).

It is also a consensus that such challenging reservoirs need further studies, especially regarding the lacking of modern-day analogs and their biotic or abiotic origin.

2 TRAVERTINES

Travertines have been extensively quarried since Ancient Times; some quarries in Italy have been in operation for over 2.000 years. The Colosseum, hundreds of fountains in Rome, the St. Peter´s Basilica in the Vatican, the Basilique du Sacre Coeur in Paris are some examples of magnificent old buildings ramped up with this rock. Because travertines were the most desired material by ancient Roman architects, the first occidental studies related to this type of rock were not related to the geology itself but to the distribution of the material, its continuity, and commercial quality (Blake, 1947 apud Chafetz and Folk, 1984; Pentecost, 2005).

The Greek geographer and historian Strabo (c. 20 B.C., apud Pentecost, 2005) cited the ‘‘petrifying’’ hot waters of Hierapolis, Turkey. However, even before that, in the 4th Century B.C., travertines were recognized and described in a Chinese Cave (Needham, 1954 apud Pentecost, 2005).

The word travertine originates from *lapis Tiburtinus or lapis Travertinus;* a Roman building stone that originated from volcanic spring deposits in Bagni di Tivoli, Italy, a town 26 km east of Rome. Somehow the word *Tiburtinus* or *Tivertino* (ancient name of Tivoli during the Roman Empire) was corrupted and became in Italian *travertino* (Pentecost and Viles, 1994; Pentecost, 2005).

Even if you have never visited these historical places in person, if you type ‘’Tivoli’’ or ‘’Hierapolis’’ in Google Maps or Google Earth you will be surprised at how easy it is to recognize large white areas around these cities where the travertine quarries are located. Isn't it amazing that we are still looking for and exploring the same type of rock used to build the Colosseum and Hierapolis centuries ago?

Although we still use travertines as a building material, in the last decades, countless other perspectives and new frontiers, especially from the scientific point of view, are emerging and creating new areas.

‘‘*Thirty years after the carbonate petrological characterizations of Chafetz and Folk (1984), travertines and tufas provide a new frontier for future carbonate research. Innovative new research fields are now pushing the frontiers back and revealing unexpected clues, not only to crystal precipitation*

and early diagenetic processes, but also to past climatic, tectonic and hydrological regimes and even to the origins of life''

(Capezzuoli et al., 2014)

More than 2000 years have passed since the heyday of the Roman empire; there is still no universal classification or consensual definition in the literature on the term ‘‘travertine’’. Polemic nomenclature, as well as a faciologic, environmental and genetic classifications and discussions about the influence or participation of bacteria in the deposition process have generated many controversies. For this reason, dozens articles have been proposed in recent decades.

Most definitions emphasize the chemistry and the temperature of the water, while others point to the hydrogeological cycle, the inorganic versus organic deposition, climate change, or even the rate of evaporation as leading factors in the process of travertine precipitation (Chafetz and Folk, 1984; Guo and Riding, 1998; Pentecost, 2005; Jones and Renaut, 2010; Capezzuoli et al., 2014).

Chafetz and Folk (1984) defined travertine as a ‘‘freshwater’’ carbonate deposited by both inorganic and organic precipitation from springs. For them, physical-chemical conditions are the primary mechanism of precipitation near the spring, while organic processes become increasingly more important distally. Close to hot water springs (depending on temperature, pH, sulfur content), bacteria are the only ones that grow and reproduce in this harsh environment.

According to Capezzuoli et al. (2014), for years the term ‘‘travertine’’ was used indiscriminately to describe all kind of crystalline freshwater carbonates.

In this study we will adopt the following definition proposed by Guo and Riding, (1998):

‘‘Travertines are limestones that form where hot ground waters, rich in calcium and bicarbonate, emerge at springs. Carbon dioxide outgassing results in rapid precipitation and the resulting deposits are both locally restricted and internally complex.’’

The rapid precipitation of travertine deposits results from the loss of the carbon dioxide from the carbonated-rich water. The explanation to this loss is the result of either or both: (a) degassing during the fluid drop pressure (when the carbonated-rich water emerge on the surface from their depth and turbulent flow, the pressure goes down, the carbon dioxide is lost to the atmosphere and the calcium carbonate is precipitated); (b) bacterial and algal activity extracts carbon dioxide from the waters (Chafetz and Folk, 1984; Ford and Pedley, 1996; Guo and Riding, 1998).

Travertines are capable of forming positive reliefs of lithified rock with a growth rate of 200 mm/year, but these deposition rates and the ability to create relief vary from place to place through time and landscape evolution (Pentecost, 2005).

The importance of studying these rocks increased in the last 20 years when scientists realized that continental freshwater carbonates (both tufa and travertines are included in this group) can be used as proxy indicator of climate changes and an opportunity to reconstruct ecosystems. While tufas reveal more information about the precipitation rate, microbiological fauna and vegetation, travertines, on the other hand, bring in addition to paleoenvironmental information, data on carbon dioxide emissions in the past and important information about the region's tectonism (Capezzuoli et al., 2014).

Another important usage is related with paleo-seismic history, earthquake prediction and hazard reduction programs. Because travertines are mostly occurring in step-over zones and these areas act as barriers to fault propagation, they are considered good indicators of tectonic activity (Hancock et al., 1999).

A new economic significance came to light when, in the middle of the year 2000, giant hydrocarbon reserves were discovered in the sag-rift section of the Santos Basin, in southeastern Brazilian margin. Because these reservoirs were described by Wright and Barnett (2015) as highly alkaline lacustrine deposits, analogous to the lakes found in the East African Rift where microbialites and hydrothermal vents coexist, the possible occurrence of hydrothermal travertines was not excluded by Della Porta et al. (2017).

2.1 TECTONIC ASPECTOS OF TRAVERTINES

The presence of travertines is preferentially associated with extensional tectonic systems (e.g. Aegean Region in Greece and Turkey, the northern Apennines in Italy and the Basin Mountains Range Province in the USA). These regions offer the perfect conditions for circulation and ascension of fluids to the surface (water thermal upwelling), through failed and fractured substrate. Most deposits accumulate within 1-2km to active fault traces, always in the hang walls of normal faults or step-over zones (relay ramps) between two faults. So far there are no reports of travertines in active thrusts (Hancock et al., 1999).

The relation between travertines and tectonics is so close that Hancock et al. (1999) strongly recommended the use of the term ‘‘travitonics’’ . Although they do not claim the credit for introducing the neologism, the idea of the article was to emphasize the importance of this deposits as a tool to study neotectonic attributes.

Recent improvements in earthquake dynamics simulations are capable of simulate long-term seismicity within topologically realistic fault models. Paleo-seismic studies, historical data and records of the most recent earthquakes provide critical information to validate forecast models, for they must reproduce the seismicity patterns of the region of interest (Uysal et al., 2007).

Wherever travertines are datable by U-series method, it is possible to constrain fissure generation related to seismic evolution in prehistoric times and calculate time-averaged dilation and lateral propagation rates for individual fissures (Uysal et al., 2007). Furthermore, it is possible to correlate these seismic events with peaks of hydrothermal activity (reported as changes in well levels and spring flows) that occur for a period of 6-12 months after earthquakes faulting or deglaciation periods when the amount of groundwater is greater than the average (Muir-Wood and King, 1993).

2.2 TRAVERTINES DEPOSICIONAL ENVIRONMENTS

Depositional and morphological classifications of travertines have been proposed by several authors (Chafetz and Folk, 1984; Pentecost and Viles, 1994; Guo and Riding, 1998; Capezzuoli et al., 2014).

Chafetz and Folk (1984) divided the travertine deposits into five major categories based on the morphology of the deposits in central Italy and Central-West U.S.: (1) waterfall or cascade, (2) lake-fill, (3) sloping mound, (4) terraced mound and (5) fissure ridge. Guo and Riding (1998), recognized three depositional systems: (a) Slope Depositional System; (b) Downslope Depression and (c) Reed Mound Depositional System. These depositional environments were recognized in Rapolano Terme (Italy), grouped into lithotype combinations and subdivided into six sub-environments described in the following items 2.2.1 to 2.2.8 (Figure 4).

Capezzuoli et al. (2014), in turn, proposed a classification focused on the distance from the spring. They named *proximal* region the vent itself and the area very close to it, the *intermediate* would be the slope environments (with or without terraces) and, the distal portions that encompass all deposits forming low relief topography where the water temperature in near-ambient and ground water is mixed with rain water.

2.2.1 Vents (Spring Mounds and Fissure Ridges)

Proximal environment, according to Capezzuoli et al. (2014), corresponds to the vent itself and the region very close to it (=vent slope). The macro-morphologies of these springs are represented by two end-member types: circular springs mounds and fissure ridges (Figure 6). Vent development will be determined by the local relief (that is driven by the rheology of the underlying materials and structural settings, both reflection of the local tectonic). For example, fissure-ridges are formed in brittle-fracturing bedrock exposed at the surface, while isolated structures such as cones, pinnacles, towers and

mounds are generally aligned and form where fissures underlie unconsolidated lake-bottom sediments (Altunel and Hancock, 1993; Brogi et al., 2014).

Travertine spring mounds occur in two situations: (1) emergent spring mounds consists of a dome form by a travertine deposit with a concave slope surrounding the hot spring orifice; (2) submerged spring mound which occurs in saline lakes.

The first type has many expressive examples in the world, one of the largest is that at Homestead Utah measuring 20 m in height (Figure 6). The second type is the submerged mound with occur in saline lakes. These result from the mixing of Ca-rich water spring water with saline, carbonated-rich lake water leading to immediate precipitation of calcium carbonate. Where the cones, towers and pinnacles are aligned they reflect the underlain control by fractures. The results are spectacular and good examples of this case are the towers and pinnacles morphologies from Mono and Pyramid Lakes in U.S. and, Lake Abbe in the West African Rift, Ethiopia (Pentecost and Viles, 1994; Pentecost, 2005; Capezzuoli et al., 2014).

Fissure ridges, on the other hand, result from build-ups around spring orifices along fractures (joints and faults). They represent the conduits for the upwelling hydrothermal fluids and range from about 100 to 2000 m long, 5 to 400 m wide and 1 to 20 m high. The morphology of the fissure ridge depends on how fast is the water flux: slow rates generate relatively more high but narrow deposits, while rapidly flows tend to build more spread out fissure ridges (Bargar, 1978; Altunel and Hancock, 1993; Pentecost and Viles, 1994; Hancock et al., 1999; Brogi et al., 2014).

Both banded and bedded travertines are characterized by millimeter to centimeter scale laminated crystalline crusts (cc) of acicular, dendritic, fibrous or prismatic calcite/aragonite crystals grown in syntaxial continuity. In the central portion of the ridge structure crystalline crusts form vertical or sub vertical banded layers or veins entirely organic precipitated, while several depositional units of horizontal to sub horizontal bedded travertine occur in the flanks of the ridge (Bargar, 1978; Altunel and Hancock, 1993; Hancock et al., 1999; Özkul et al., 2002; Brogi et al., 2014; Figure 4 and Figure 6).

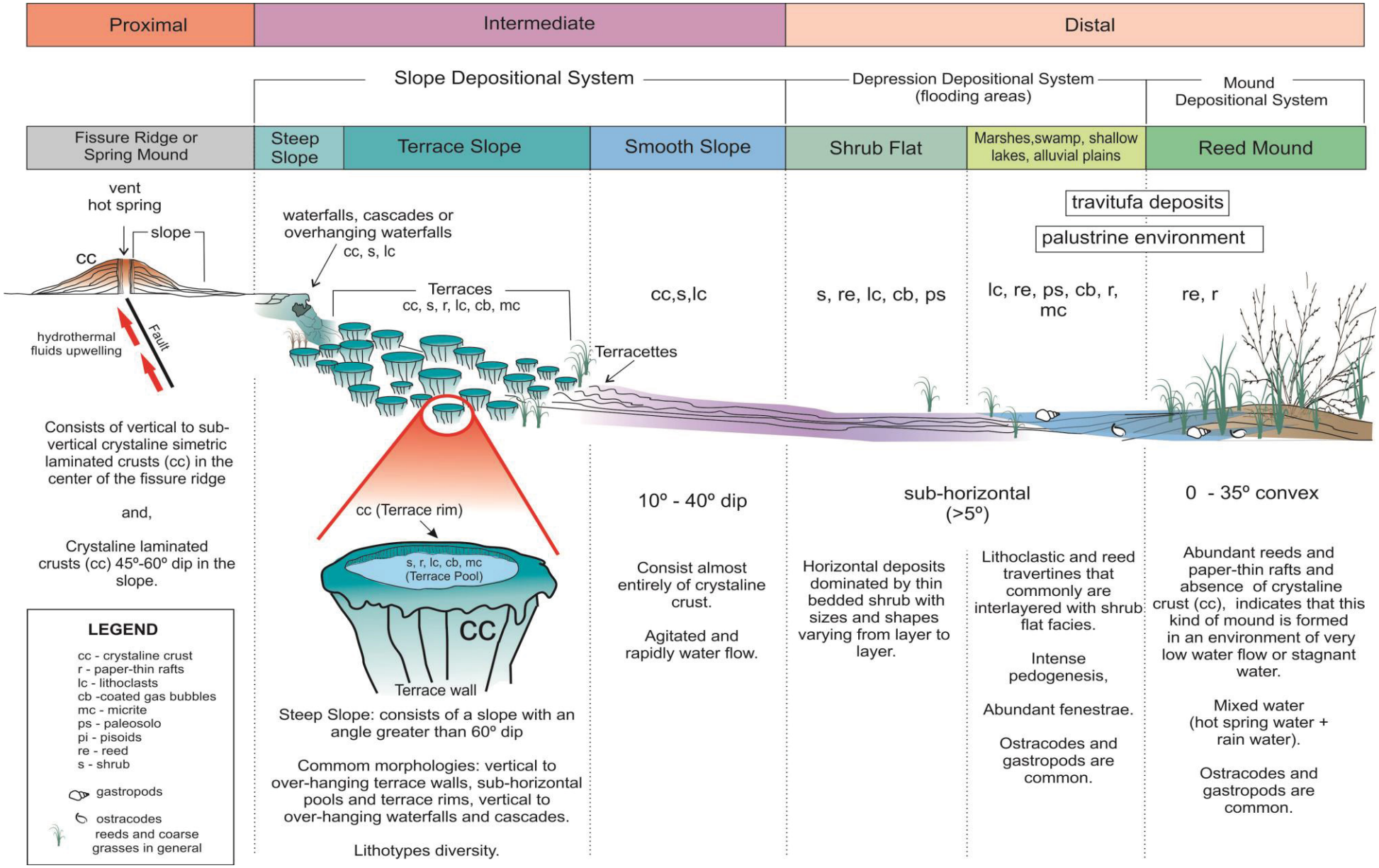

Figure 4 -Travertines depositional systems and facies (Based on Chafetz and Folk, 1984; Guo and Riding, 1998; Özkul et al., 2002; Brogi et al., 2014; Mors et al., 2019)

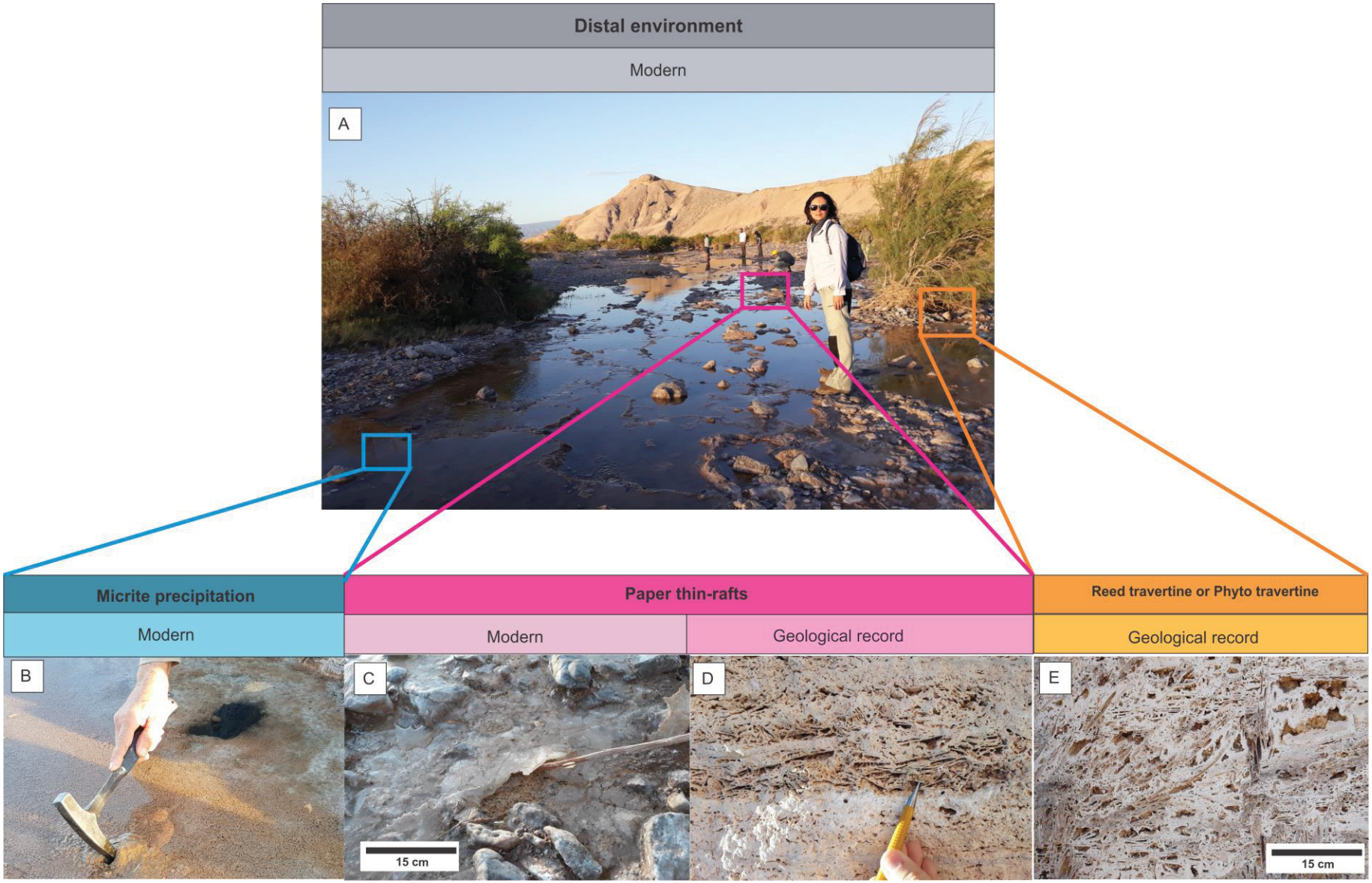

Figure 5 - Palustrine environment (swamp) around the city of San Juan (Argentina), modern and geological records (main features).

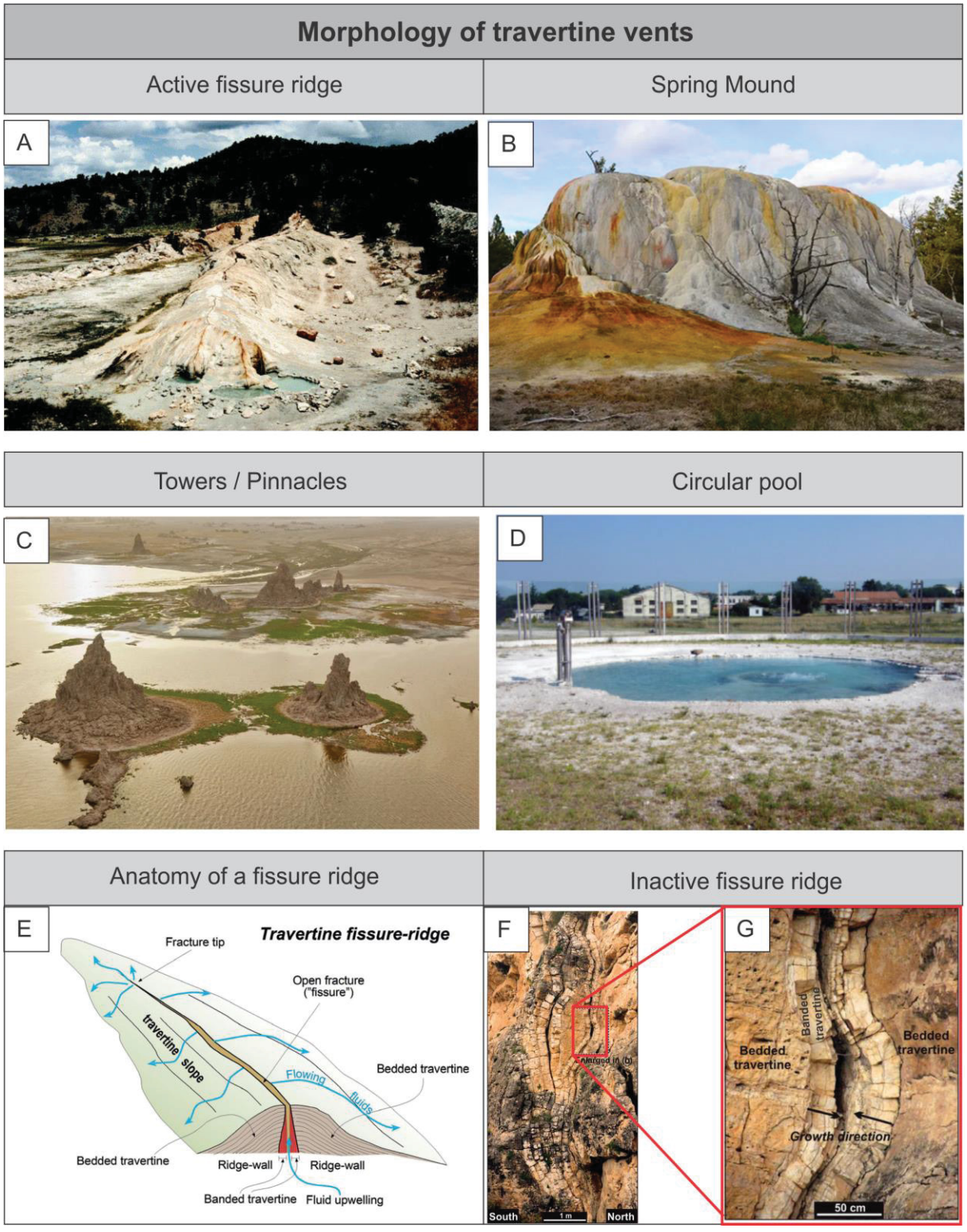

Figure 6- Morphology of travertine vents. A) Typical fissure-ridge from which the hot carbonate-rich waters flow. Note the whale-back form. Bridgeport travertine deposit, California (Hancock et al., 1999); B) Orange Spring in Mammoth Hot Spring, Yellowstone Nacional Park (www.yellowstonepark.com); C) Travertine towers in Lake Abbe, Afar Depression, Ethiopia-Djibouti border (George Steinmetz for National Geographic); D) Bullicane Spring, a low relief, circular mound with bubbling pool in Viterbo, Italy (Capezzuoli et al., 2014); E) Schematic illustration of the anatomy of a travertine fissure-ridge (Brogi et al., 2014); F) Example of banded and bedded travertine of the Çukurbağ fissure-ridge (Pamukkale, Turkey); G) Detail of F.

2.2.2 Terrace Slope (Guo & Riding, 1998)

Consist of a sequence of flat-floored shallow pools that receive water from the spring above. It is what Chafetz and Folk (1984) called ‘’Terraced Mounds’’, Warwick (1950) called rimstone, and Bargar (1978) named terracettes. Travertine forms a raised rim around each pool, due to the precipitation of calcium carbonate as the water flows over the edge to the vertical terrace wall until it reaches the next terrace below. The rims are made up of a dense crystalline crust (cc) that confined the water inside the pool and rapidly translated to the diverse pool facies (Figure 4).

In Rapolano Terme quarry, Guo and Riding (1998) observed that terrace slopes can reach up to 15 m thick and 200 m in length. Terrace walls vary from several centimeters to 2 m and consist basically of a crystalline crust (cc). Terrace pools are decimeters to meters in size and can cover a wide variety of facies, being shrubs (s) the major component, followed by lithoclasts (lc), pisoids (pi), micritic (m), paper-thin raft (pr), coated gas bubble (gb).

The presence of crystalline crust (cc) indicates agitated and rapidly flowing water (turbulent flow), which means more degassing and consequently more calcium carbonate precipitation (Chafetz and Folk, 1984; Guo and Riding, 1998).

Terraces slopes are among the most beautiful, famous and spectacular geologic views in the world and Mammoth Hot Springs in Yellowstone (Wyoming, USA) and Pamukkale in western Turkey are the most spectacular modern analogs to these systems.

2.2.3 Smooth Slope (Guo and Riding, 1998)

Smooth slope is non-terrace, high angle surface with dips of 10º-40º (Figure 7). They consist almost entirely of crystalline crust (cc) made up of well-developed feather-crystals oriented perpendicular to the surface in decametric layers.

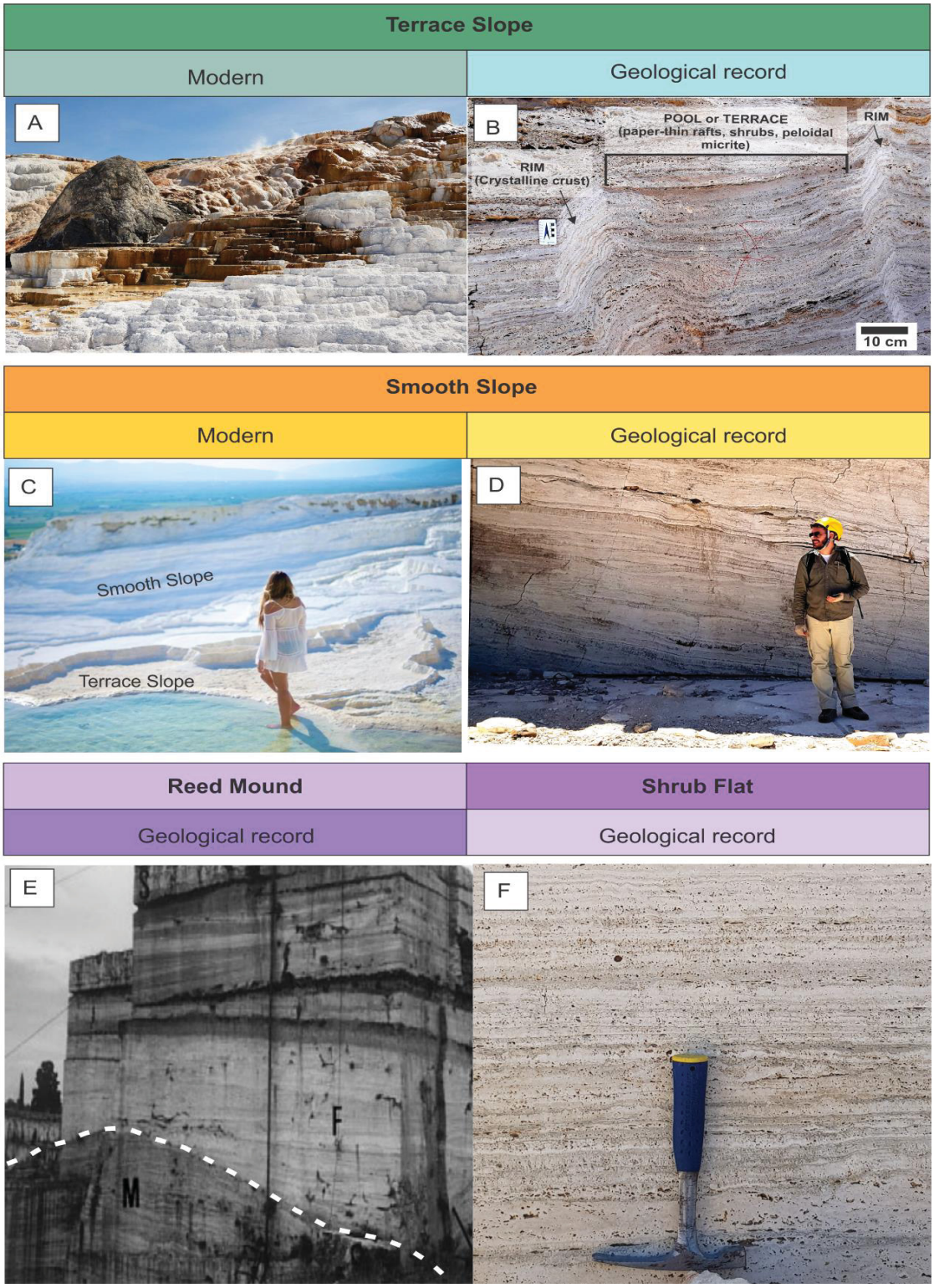

Figure 7 - Examples of modern and geological records of travertines around the world. A) Travertine terraces at Mammoth Hot Springs, Yellowstone National Park, 2016 (Frank Schulenburg/Wikipedia); B) Geological record of terrace slope (rimmed pools or terraces) in a quarry wall in La Laja, San Juan, Argentina; C) Smooth slope view from the terrace slope in Pamukkale, Turkey (www.viatur.com); D) Geological record of a smooth slope in a quarry wall in La Laja, San Juan, Argentina; E) Mound Facies (M), overlain by Shrub Flat Facies (F) in Cava la Chiusa, Italy (Guo and Riding, 1998); F) Horizontal layers dominated by thin bedded shrubs in a quarry wall in La Laja, San Juan, Argentina.

Both Terrace Slope and Smooth Slope could have abundant crystalline crusts (cc) which indicates agitated and rapidly flowing water, like in Italy. The absence of terraces could be explained by the reduced surface roughness. Guo and Riding (1998), advocated that the terrace formation does not require a pre-existing steep slope, but can develop from a horizontal or gently surface depending mainly on water turbulence, velocity and surface roughness.

Under laminar flow (which is the case in the smooth slope), water shears horizontally, parallel to the direction of the flow, leading to the formation of parallel layers (cc). In the event of a new pulse of water from the hot spring, the laminar flow can be replaced by a turbulent flow. This input, could locally result in increased flow velocity, increased degassing, and consequently rapidly calcium carbonate precipitation, which in turn causes an increase in surface roughness. If this is the case, the initiation of terrace development process could start.

2.2.4 Waterfall

Waterfall define vertical falls that consist predominantly of crystalline crust (cc), and resemble terrace walls but in larger scale. The initial layers can be traced continuously from top to the base of the waterfall. Exposure and abrasion are common and result in erosion, local collapse and accumulation of fragments (lithoclastic deposits) at the foot of the cliff (Pentecost and Viles, 1994; Guo and Riding, 1998)

Although Waterfall and Cascade facies were observed in Italian, North America and Andean travertines (Chafetz and Folk, 1984; Guo and Riding, 1998; Mors et al., 2019), these kind of deposits are very characteristic of cold water tufas (Pedley, 1990) and, seems less common and much more scarce in hot spring travertines (Guo and Riding, 1998).

2.2.5 Reed Mound (Guo and Riding, 1998)

The Reed Mound is an interleaved complex of lenticular units with convex surfaces that slope (0-35º). In Rapolano Terme these mounds are up to 10m thick and 200m in length. Reed (r) facies is the major component (about 60%), and coated bubble (cb) and paper-thin raft (pr) are common. Reed cavities can contain brown iron-rich sediment with ostracodes and gastropods. The presence of paper-thin rafts in the space between the stems and, the absence of crystalline crust (cc) point to an ambient of very slow water flux or stagnant water ambient. Supply from the hot spring water in this region is limited and flow seems to be erratic often covering only partially the surface or filling small depressions. This scenario could explain the deposit´s architecture with complex interbedded units, with the common presence of overlaps and merges with one other. It is likely that spring water on the mounds was diluted by rain and ground water that emerges near to the bases of the hill slopes. Locally, mounds crests are eroded, karstified and, overlain palaeosols.

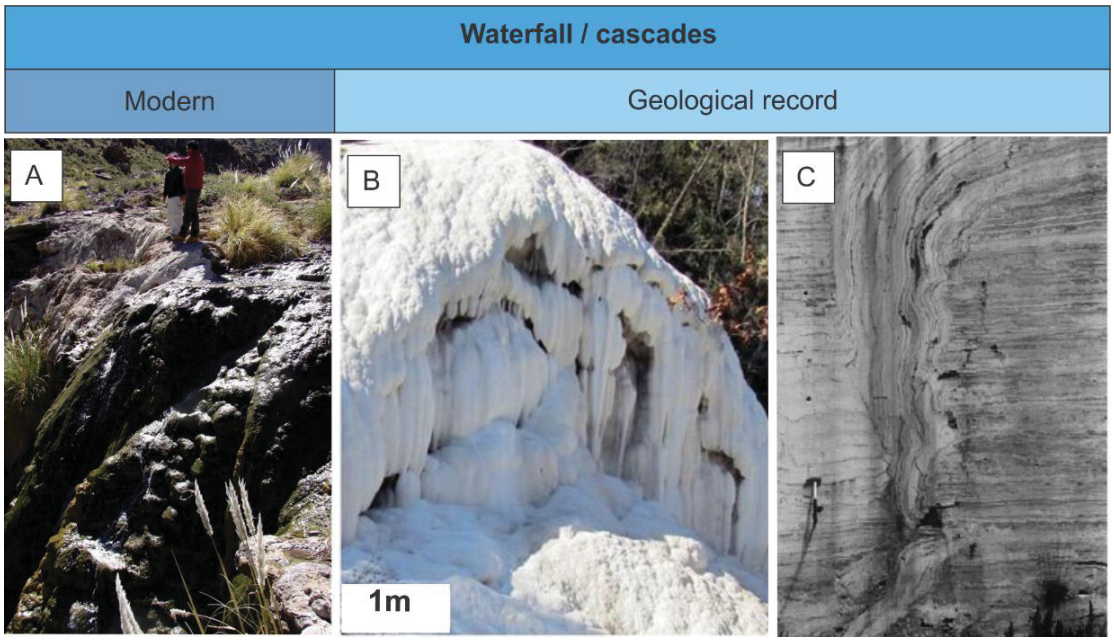

Figure 8 - Examples do waterfall depositional environment. A) Waterfall at the Las Vizcachas creek with development of botryoids on its surface in Puna plateau, Catamarca, Argentina (Mors et al., 2019); B) Quaternary thermogene travertine deposits with waterfall morphology, central Italy (Della Porta, 2015); C) Waterfall facies in Cava Campo Muri, Rapolano Terme, Italy (Guo and Riding, 1998).

2.2.6 Self-built channels (Bean 1971 *apud* travitonics)

It is a term used to describe a self-built channel, with a narrow shape with 0.5-3.0 m in wide and up to 10 m high, similar to an aqueduct that distribute carbonated-rich waters to lower ground within the Pamukkale area. The walls of this ‘‘petrified’’ channels are the result of the continuos deposition of calcium carbonate from a turbulent flow (Hancock et al., 1999).

2.3 CONTROLS ON TRAVERTINE PRECIPITATION

For Guo and Riding (1998) water chemistry directly influenced by temperature would be the main responsible for the control in the precipitation of these deposits. This observation made by Chafetz and Folk (1984) who believed that travertines deposits are the result of both organic and inorganic processes: inorganic processes are dominant close the spring where the water is ‘‘energetically’’ degassing; while organic processes are becoming more important downstream as the water usually cools down and the environment becomes less harsh. The chemistry of the water, more than its temperature, will determine what organisms are living, or not, near the spring orifice. Such explanation lies in the fact that besides the calcium bicarbonate, the water emerges with other solutes, like sulfur, for example, and in many situations the chemistry of the water is considered poisonous for many macro-organisms (plants and trees).

An end-member scheme for the travertine precipitation would start close to spring orifice with predominance of inorganically precipitates and absence of living organisms, as the conditions become milder bacteria would be the first to appear, followed by cyanobacteria and finally plants, as the temperature approaches to the surface conditions macrophytes (mosses and grasses) and gastropods tend to become more common. As we can see Guo and Riding (1998) were not the first to suspect the importance of bacteria in this process, but perhaps they were the first to identify and recognize the bacteria influence in textures and lithified structures of ancient carbonates, by comparing them with the textural structures of today's travertines in Italy, Idaho, and in the Yellowstone National Park. In this same article,

they presented the hypothesis that shrubs represent accumulations formed in the summer, while the intercalated thin clay deposits would be winter deposits.

Besides the organic or inorganic precipitation and the chemistry and temperature of the water, the final deposit will result of many others variables, such as the amount of CO_2 dissolved in the water, the local relief, pH, salinity and light intensity (Chafetz and Folk, 1984; Guo and Riding, 1998). In the amount of CO_2 dissolved in the water for example, (if there are no changes in others variables), the higher the concentration of dissolved HCO_3 in solution, the greater the amount of $CaCO_3$ precipitated, due to degassing.

According to Pentecost (2005), four chemical processes are responsible for the generation of almost all travertines in the world, and the vast majority of them are formed by the degassing of groundwater rich in carbon dioxide containing more than 2 mmol L-1 (c. 80 ppm) of calcium (only the first one will be detailed as follow). The water's ability to precipitate travertines through this first reaction (Eq 1) is produced when carbon dioxide dissolved in groundwater (carbonic acid) reacts with carbonate rocks and forms a solution containing calcium ions and bicarbonate (bicarbonate of calcium).

$$CaCO_3 + CO_2 + H_2O <=> Ca^{2+} + 2(HCO_3)^- \qquad \text{(Eq 1)}$$

Thus, for Pentecost (2005), Eq. 1 represents the reversible chemical reaction responsible for the formation of most precipitated travertine deposits in the world.

The rapid precipitation of travertine deposits results from the loss of the carbon dioxide from the carbonated-rich water. The explanation to this loss is the result of either or both: (a) degassing during the fluid drop pressure (when the carbonated-rich water emerge on the surface from their depth and turbulent flow, the pressure goes down, the carbon dioxide is lost to the atmosphere and the calcium carbonate is precipitated); (b) bacterial and algal activity extracts carbon dioxide from the waters (Chafetz and Folk, 1984; Ford and Pedley, 1996; Guo and Riding, 1998).

High concentrations of carbon dioxide are capable of dissolving large volume of carbonate.

2.4 STABLE ISOTOPES OF TRAVERTINES

The interpretation of isotopic signatures in travertines, especially oxygen and carbon, provide important information about the physical chemical conditions of the precipitation, the influence of metabolic process and, especially about the carbon dioxide source. In favorable circumstances oxygen isotope provides information on the temperature at which deposition precipited. Carbon and Oxygen isotope signals in some relatively closed shallow-water carbonates systems have moderate preservation potencial. While Carbon may be preserved, oxygen isotope are commonly altered. Other elements such as hydrogen, strontium and sulphur can also provide information on the parent rock, provenance of solutes and, magmatic contributions of volatiles such as S and CO_2 (Flugel, 2004; Pentecost, 2005).

2.4.1 Carbon dioxide sources (CO_2)

For limestones, fractionations of the isotopes of carbon and the oxygen are the most interesting, because they are the chemical elements that form carbon dioxide molecules. The carbon dioxide (CO_2) that is essential for travertine precipitation can be derived from many sources, but the most common include:

- *Decarbonation of limestones*: in both, contact and regional metamorphism areas, baking carbonate sediments in the presence of clays and other minerals is a common process, and leads to liberation of carbon dioxide. This can occur at temperatures ranging from 100-800ºC and depths of up to 5 km. (Cathelineau et al 1989). Sano (1996), reported in a Japanese site, that decarbonation was responsible for up to 90% of deep carbon source.

- *Mantle degassing/Magmatic generator*: carbon dioxide is a common magma constituent and as magma rises, pressure reduction leads to outgassing. Some of the carbon dioxide gas reached the Earth´s surface, but large amounts can be dissolved under high hydrostatic pressures into circulating groundwater and dissolve large volumes of calcium carbonate at depth, providing highly concentrated bicarbonate solutions. This case will be encouraged in the presence of deep faults in

regions of crustal extension. It is important to notice that CO_2 is often accompanied by ^3He, thought to be present in the upper mantle (Piperov et al 1998).

- *Heated Organic matter*: many oil fields have a cap of gas containing 1-5% vol carbon dioxide. Its origin is not clear but some possible explanations include thermally-generated sources. Hutcheon et al. (1990) advocate that the calcite destruction at temperatures between 70º and 220ºC may be responsible for production of large quantities of CO_2, particularly in sand and shales with high carbonate content. This could be an explanation for carbon dioxide occurs with methane in coal deposits (Eq. 2.2) and also resulting from the interaction between methane and ferric oxide (hematite; Eq. 2.3). Decarboxylation of organic acids occurs between 200-300ºC, but can begin in low temperatures (100ºC) due to the cleavage of the weak C-COOH bond. But few travertines seem to be associated with such process (Pentecost, 2005).

- ‘‘*Organomox” waters*: significant oxidation of buried (non-soil) organic matter might occur in low temperaures (0-30ºC) and is conceivable that large quantities of carbon dioxide could be released by this process. It is worth mentioning that this is different from the thermal generation process mentioned before, and an example of this case would be the Plitvice travertine (Croatia), whose origin of carbon dioxide is possibly associated with a peat deposit (Srdoc et al., 1983; Pentecost, 2005).

Other carbon dioxide sources include sulphate reduction by bacteria (carbon dioxide is formed in anaerobic waters and sediments by bacteria, especially the sulphate-reducers); acetate fermentation by methanogenic bacteria and, by oxidation of pyrite spontaneous combustion (Pentecost, 2005).

Decarbonation, mantle degassing and CO_2 from heated organic matter are considered ‘‘thermogene’’ sources because their carbon dioxide originates from thermal process within or even below the Earth´s crust. It is important to note that thermogene source waters are not necessarily hot, although this is frequently the case, the term is applying to the source rather than the exit temperature of the water (Pentecost, 2005).

2.4.2 Carbon Isotopes

The modern Vienna Peddee Standard (VPCB), taken from the marine limestone is defined as zero, and carbon isotopes ratios are measure relative to this. Carbon in gaseous, dissolved and solid state may diverge considerable from zero. Atmospheric CO_2, for example, currently has $\delta^{13}C$ value about -7‰, thus depleted in the heavier isotope. Carbon dioxide species fractionations are better defined than oxygen isotopes, since they do not have the problem with the exchanged Oxygen between the water molecules and oxygen from dissolved carbon dioxide.

About the main sources of carbon dioxide and their $\delta^{13}C$ signature, marine limestones $\delta^{13}C$ is about 0‰, soil zone CO_2 is about -15‰ and, magmatic carbon around -7‰ (all depleted in ^{13}C).

Like oxygen, the carbon isotope composition and their associated waters changes downstream. As the evasion of carbon dioxide progress, the lighter molecules are preferentially lost, leaving the solution enriched in ^{13}C as the water moves away from the source (Pentecost, 2005).

2.4.3 Oxygen Isotopes

For the oxygen, the internacional standard is based on the Vienna Standard mean ocean water (VSMOW), but for carbonates VPDB is more convenient, and there is no problem since the values are interchangeable.

Compared to carbon, the oxygen isotopic composition is less straightforward. Although the exchanges that occur between the oxygen of the water molecules and oxygen from dissolved carbon dioxide complicates the interpretation of $\delta\ ^{18}O$ values in carbonates, there is a reasonable agreement that this ratio can be used to estimate paleo temperature and rates of evaporation where the equilibrium between the water and the carbonate oxygen is establish.

2.4.4 Geochemical classification

A geochemical classification based on the carrier CO_2 was proposed by Pentecost (1993). This proposal separates the travertines into two groups according to the origin of the carbon dioxide. The distinction between them is based on the source of the carbon dioxide responsible for the travertine precipitation. Final isotopic composition of the travertine deposit are the main tool to identify the origin and the interaction of carbon dioxide with underground rocks and fluids, on its way until the carbonate is precipitated on the surface (Pentecost, 1993, 2005; Pentecost and Viles, 1994).

2.4.4.1 Thermogene travertine

The first group is called by Pentecost (1993, 2005) thermogene or thermal. This group embraces travertines formed due to CO_2 and other fluids that have a deep origin, they were also referred as ‘‘endogene’’ travertines by Crossey et al., (2006) and ‘‘hypogean’’ by Teboul et al. (2016). Water responsible for these deposits are usually hot and present $\delta^{13}C$ range between -4 and +8‰. This range reflects the heavier carbon released from decomposing marine limestones caused by metamorphism (decarbonation), hydrolysis and oxidation of reduced carbon, but significantly CO_2 contributions come straight from the upper mantle in areas of volcanic activity can result in the deposition of travertines depleted in ^{13}C. This travertines have a more restricted distribution, being located mostly in areas of recent volcanic activity (Pentecost and Viles, 1994). This group often contains some meteoric carrier, but the bulk of carbon dioxide originates from thermal process within or even below the Earth´s crust. Mantle generated carbon dioxide, often under pressure and with high concentrations are capable of dissolve large volumes of rock in a geothermal circuit. Their dissolved inorganic carbon contend (DIC) and dissolved calcium are 10-100 mmol L^{-1} (400-4000 ppm as HCO_3) and 2-20 mmol L^{-1} (80-800 ppm as CO_3) respectively, two to ten times higher than meteogene sources (Pentecost, 2005).

Thermogene travertines are displaced in a range between -1‰ and +10‰, with a mean of +4.3‰. These values reflect straight the non-soil-zone carbon sources, including water-rock interactions on the way through the spring and also the enrichments in travertine formation during rapid CO_2 evasion. In most cases the carbon dioxide is believe to originate from decarbonation reactions caused by contact or regional metamorphism or magmatic.

2.4.4.2 Meteogene travertine

For Pentecost (1993, 2005), meteogene travertines are those whose carrier CO2 has ‘‘shallow’’ origin from the soil-zone and epigean atmosphere. This carbon dioxide is regarded as meteoric in origin, since all terrestrial vegetation fixes carbon from atmosphere and the soil atmosphere is by far the most important contributor of carbonic acid leading to limestone dissolution and CO_2 enrichment of groundwaters (Pentecost and Viles, 1994; Pentecost, 2005). There were also named as ‘‘epigenic’’ (Crossey et al., 2006) and ‘‘epigean’’ (Teboul et al., 2016). These travertines are the most common and widely distributed. They occur typically in cold water springs in regions underlain by limestones or evaporates (gypsum). Their dissolved inorganic carbon content (DIC) and dissolved calcium rarely exceeds 8 mmol L^{-1} (480 ppm as HCO3) and 4 mmol L^{-1} (160 ppm as Ca). A distribution of $\delta^{13}C$ for all travertines was summarized by Pentecost (2005) and it is shown in Figure 9. For meteogene travertines, the mode -10‰, with mean - 7.0‰, reflects the depleted ^{13}C of soil CO_2, a phenomenon that has been observed since earliest investigations by Craig (1983, apud Pentecost, 2005).

Lake travertines have $\delta^{13}C$ values significantly heavier than those meteogene stream deposits. The aqueous CO_2 phase frequently approaches atmospheric equilibrium proving carbonate precipitate of $\delta^{13}C$ ~ +4‰, probably influenced by photosynthetic enrichment, evaporation and effects might also occur as a result of methanogenesis in lake sediments (Ferreri and Stanzione 1978, Casanova and Hilarie-Marcel 1992 Turner and Fritz, 1983). In saline lakes,

evaporation may lead to considerable enrichment in ^{13}C, with values up +16.5‰ have been reported (Stiller et al 1985).

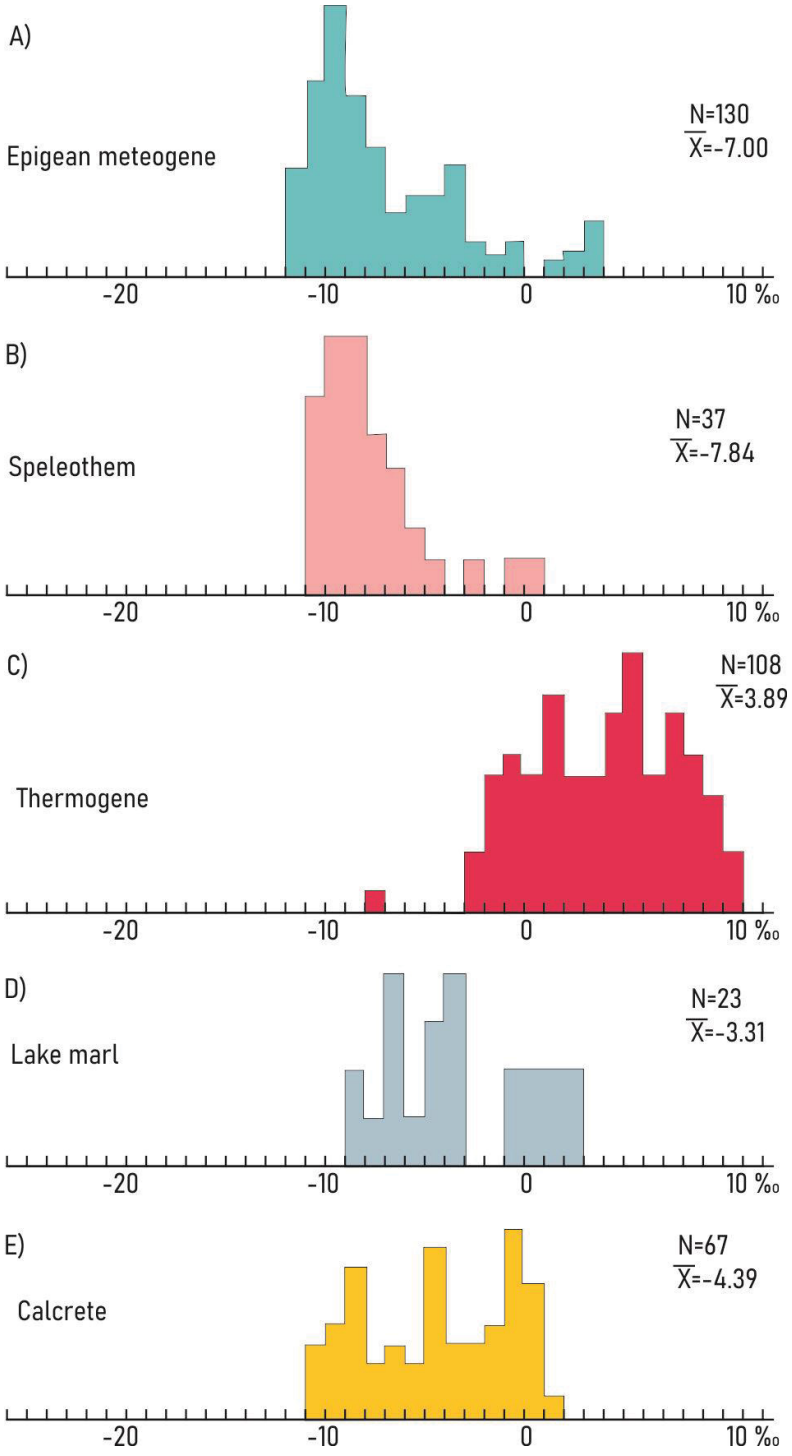

Figure 9 - Distribution of $\delta^{13}C$ (PDB, ‰) of travertine and others carbonates based upon site and sample means. A) Epigean meteogene; B) Speleothem; C) Thermogene; D) lacustrine marl; E) calcrete (modified from Pentecost, 2005).

2.4.4.3 Thermometeogene travertine

It is important to distinguish thermogene travertines from those formed by hot meteogene waters resulting from deep circulation. Occasionally, meteoric waters infiltrate the soil and percolate underlying limestones or evaporates (gypsum) through fractures and faults. These waters become heated, rise and emerge as hydrothermal vents. These deposits were considered by Pentecost (2005) a sub division of meteogene travertines and named as thermometeogene travertines. They usually possess low CO_2 levels derived from soils, with only meteoric carrier and, are invariably depleted with ^{13}C, with no thermal source of CO_2.

2.5 TRAVERTINES VERSUS TUFAS

Pentecost (2005) argued that the term tufa was not needed because ‘’travertine’’ should be applied to all continental limestones that have formed around groundwater seepages, springs, and along streams and rivers.

At present, there is little consensus on use of the terms: both tufas and travertines are continental ‘‘freshwater’’ limestones deposited in springs from waters that are saturated or supersaturated with calcium and bicarbonate. When the precipitating water is hydrothermal (hot) in origin we named ‘‘travertine’’, while the term ‘‘tufa’’ is reserved for cool or ambient freshwater deposits rich in microphytes and macrohytes, leaves and wood tissue preserved on the longer term as molds and casts formed by an early cement of spar and/or micrite (Pedley, 1990; Ford and Pedley, 1996; Guo and Riding, 1998; Jones and Renaut, 2010).

The difference between tufas and travertines are not always clear, especially when the two deposits occur intercalated in the field or when the cool water precipitants represent the distal part of the deposit. When this happened and the water had already cooled enough to permit the growth of macrophytes, microphytes and the presence of small vertebrates the complications arise, since the result is a proximal travertine and a distal tufa deposit and the boundaries between them are unclear. In this sense, we can interpret tufas and travertines as endmembers of the

same continuum. Although there are some complications, they can be distinguished from each other by their origin that is reflected in their textures, sedimentary facies, geometry of the bodies (Capezzuoli et al., 2014).

However, there are a group of tufas characterized by a typical hydrochemical signature indicative of ambient temperature precipitation from cooled, deeply cycled (geothermal) waters that are more difficult to interpret. They are generally encountered in the peripheral sectors of geothermal fields, Capezzuoli et al. (2014) suggested the term ‘travitufa’ in order to distinguish them from regular tufas.

Travertines are characterized by high depositional rates, regular bedding, low porosity and permeability and an inorganic crystalline fabric. Bacteria and cyanophytes are the only organisms found in typical travertines since extreme environmental conditions such as high temperatures, high rates of deposition and alkaline pH to not allow the growth of plants (macrophytes). They also have a strong connection with tectonics as emphasized in Chapter 2.1, while tufa deposits occur in a wide range of environments, not necessarily linked to tectonically active areas. (Capezzuoli et al., 2014).

In contrast, the term tufa should be reserve to continental carbonates typical of karstic areas, deposit commonly near cascades, waterfalls or dispersed lakes. Tufa deposits range in thickness from several centimeters to tens of meters. Produced from ambient (cool) temperature water and characterized by high porosity. The remarkable feature of these deposits is the common presence of the preserving structure of objects on which it was originally deposited (leaves, wood tissue, macrophytes plants, microphytes and invertebrates), preserved on the longer term as molds and casts formed by an early cement of spar and/or micrite (Srdoc et al., 1983; Pedley, 1990).

Both, tufa and travertines can be used as proxy indicator of climate changes and an opportunity to reconstruct ecosystems. Because the environmental conditions in which tufas precipitate are very stringent, they are an useful tool in paleo climatic studies providing data about the precipitation rate, microbiological fauna, climate, vegetation and, biologic factors; while travertines can tell a lot about the region's tectonism, and are considered a proxy for natural past CO_2 output in the atmosphere (Srdoc et al., 1983; Kampman et al., 2012; Capezzuoli et al., 2014; Janssens et al., 2020).

Another difference lies in the macro-morphology of the depositional systems. While travertines precipitate frequently around thermal springs forming circular mounds, linear fissure-ridges, pinnacles or towers; tufas forms as the ambient temperature water flows (like a river) from the resurgence point, or multiple resurgence points usually in karstic regions (Capezzuoli et al., 2014).

When looking to the present tufa they are always related to persistently high-water tables, extensive ground cover by macrophytes and moderate levels of $CaCO_3$ in the groundwater. The tufa growth appears to be retarded by cold conditions and semi-arid regions are incapable of sustaining the high-water table necessary for a continuous discharge. The ideal temperature and humidity conditions are typically found in regions of temperate climate and therefore with a very limited environmental window, which has great value in paleoenvironmental interpretation studies (Pedley, 1990).

Table 1 - Main characteristics of travertine and tufa (Capezzuoli et al., 2014).

	Travertine	Tufa
Depositional processes	Dominantly abiotic	Dominantly biotic
HCO_3^- content (mmol/l)	>7	<6
$\delta^{13}C$ (PDB‰)	−1 to +10	<0
DIC (mmol/l)	>10	<8
Water temperature	Thermal, generally higher than 30°C	Ambient, generally lower than 20°C
Mineralogy	Calcite, aragonite	Calcite
Depositional rate	Higher (cm to m/year)	Lower (mm to cm/year)
Fabric	Mainly regularly bedded to fine laminated	Mainly poorly bedded
Crystal calcite size	Macro (dendritic, bladed or acicular) to micritic crystals	Dominantly micritic to microsparitic crystals
Primary porosity	Generally low (less than 30%)	Generally high (over 40%)
Biological content	Low (bacteria and cyanophytes)	Very high (micro to macrophytes)
Depositional morphologies	Multi-symmetrical bodies (mounds, ridges and slopes)	Axial-symmetrical bodies (cascade, dams and barrages)
Distinctive lithofacies	Coated bubbles, shrubs	Phytoherms
Hydrological setting	Regular, generally permanent flow	Variable, rainfall-dependent flow
Climatic control on deposition	Less dependent	Strictly dependent
Anthropogenic influence on deposition	Scarcely influenced	Deeply influenced
Tectonic relation	Always present	Often absent

2.6 MODERN TRAVERTINES *VERSUS* GEOLOGICAL RECORD

Although travertines are quite lithified compared to other surface rocks, as they are terrestrial deposits with very limited and isolated occurrence, they are easily eroded and have a low potential for preservation in the geological record (Hancock et al., 1999). With a few exceptions (e.g. basins with high subsidence rates or in arid zones), freshwater carbonates are prone to rapidly erosion and that is the main reason why these deposits are often preserved in Quaternary but are rare in older geological times (Capezzuoli et al., 2014). Besides, Pedley (1990) also attributes the absence of depositional models as part of the imperfection in recognize older records.

Although modern analogs show the macro morphology, only eroded and quarried walls reveal the internal structures and give us the whole picture of the travertine system (Guo and Riding, 1998).

3 RESULTS

Manuscript to be submitted at Marine and Petroleum Geology on 2022.

3.1 ABSTRACT

The study of travertine carbonates gained both geological and economic significance after de discovery of gigantic hydrocarbon reserves in the Aptian section of the Santos Basin. Known as the Pre-Salt, located in the southeastern Brazilian coast, the unconventional carbonate reservoirs of the Barra Velha and Macabu Formations are currently responsible for half of the Brazilian oil production. Since the first drilled and described wells, many geological models and facies classifications have been proposed. In common, almost all emphasized the unusual character of these rocks precipitated in an alkaline lacustrine environment, similar to those found in the East African Rift. This study highlights one specific well drilled in Santos Basin Outer High, in which rock samples were collected, analyzed, and suggested the occurrence of travertine facies. Thin section petrography, scanning electron microscopy, and stable isotopes analyses were integrated to unravel these peculiar rocks' origin and depositional environment. Macroscopic descriptions and detailed petrography revealed features typically found in travertine systems, such as strongly banded carbonates with high inclinations angles, calcite crusts, rafts, and micro-karst features. At the same time, $\delta^{13}C$ positive values and some mineral phases commonly precipitated by hydrothermal systems in carbonate deposits such as pyrite, barite, and bitumen point out to a post deposition of travertines history. Travertine precipitation and the alterations processed later indicate a complex and heterogeneous diagenetic history of these rocks, both associated with hydrothermal fluids carried through the fault and fracture systems that act in the Santos during the opening of the Atlantic Ocean but in different geological times. The combined data set provides clear evidence of travertines' presence in Pre-Salt and hydrotermal post-depositional alterations. The latter one, likely associated with Late Cretaceous or Paleogene magmatic activity that controlled creation, dissolution, and obliteration of the porosity in Pre-Salt reservoirs.

3.2 INTRODUCTION

Since the first wells drilled and described in the Aptian section of Santos and Campos Basin (known as the Pre-Salt section) and its counterpart in the Kwanza Basin of Angola, many geological models, and facies classification have been proposed. They were usually based on petrographic, textural, and mineralogical observations (Dias, 2005; Muniz and Bosence, 2015; Wright and Barnett, 2015, 2017; Herlinger et al., 2017; Pietzsch et al., 2018; Souza et al., 2018; Farias et al., 2019; Lima and De Ros, 2019; Gomes et al., 2020).

The macroscopic similarity observed between the porous types described in outcrops of travertine systems in different regions of the world and those observed in the sampled rocks in Santos Basin Pre-Salt is striking and motivated the search for analogs that could help in understanding the genesis and the paleoenvironmental context in which these reservoir rocks were deposited. While Wright & Barnett (2015) suggested that the similarity with travertines textures not necessarily reflects a similar depositional environment but similar processes (such rapid precipitation from high saturated solutions), Della Porta et al. (2017) did not exclude the possibility of the presence of hydrothermal travertines in the middle of these reservoirs and, Souza et al. (2018) interpreted many of the Barra Velha carbonate rocks as travertine related deposits.

Sartorato (2018) observed that the occurrence of a 2000-2500m thick column of salt (Ariri Formation) superimposed on the reservoir, in addition to the low-density contrast between the strata, compromises the seismic imaging of these reservoirs.

Therefore, looking at and analyzing the rock samples collected in the wells would be the most efficient way to characterize these reservoirs since seismic attributes, such as acoustic impedance, are of low usefulness in defining the geometry of small bodies and their faciological distribution.

Studying the travertines that occur intercalated with the Aptian carbonates of the Santos Basin Pre-Salt is crucial because it can provide valuable information about the palaeo-environment, geotectonic context and depositional model.

Since travertine deposits occur in very particular geotectonic environments (associated with large geological fault zones in regions of crustal extension), the main contribution of this work concerns on petrographic characterization of the

travertines found intercalated with the carbonates of the Barra Velha Formation from the Santos Basin and the interpretation of its depositional environment.

3.2.1 Geological setting

Santos Basin is located on the southeastern Brazilian continental margin and extends from Cabo Frio to Florianopolis in an area of about 350.000 km^2. It lies from depths from 150 m to almost 3000 m b.s.l. The exploratory potential of the basin has been recognized since the sixties with the acquisition of the first seismic data. The first wildcat well was drilled in 1971 in shallow-water areas. The Merluza turbidite field was the first discovery in 1979, followed by other fields of oolitic limestones in the water depth around 300 meters (Carminatti et al., 2008).

In the early 2000s, technological advances allowed Petrobras to begin its exploratory efforts to drill in deep and ultra-deep waters areas that culminated in the discovery of the giant Tupi Field in 2006. This discovery opened a new frontier in oil exploration. The unusual genesis and diagenetic history of the Pre-Salt lacustrine carbonate rocks attracted oil companies and became the focus of debates in the geoscience community around the world.

The northeast limit of the basin is the Cabo Frio High that separates Santos from Campos Basin. The Southwest limit is the Florianopolis Plateau, which separates it from Pelotas Basin (Pereira and Macedo, 1990). Another two structures are important: the Santos Hinge Line to the west, which marks the west limit of the evaporitic sequence (Ariri Formation), and the São Paulo Ridge that makes the east limit. In the central portion of the São Paulo Plateau, there is an unusual shallow region notice when the base of the evaporates are mapped. This area is nominated Santos Outer High (SOH). Brazillian Pre-Salt hydrocarbon fields are located in SOH and, therefore, our area of interest (Carminatti et al., 2008; Gomes et al., 2009).

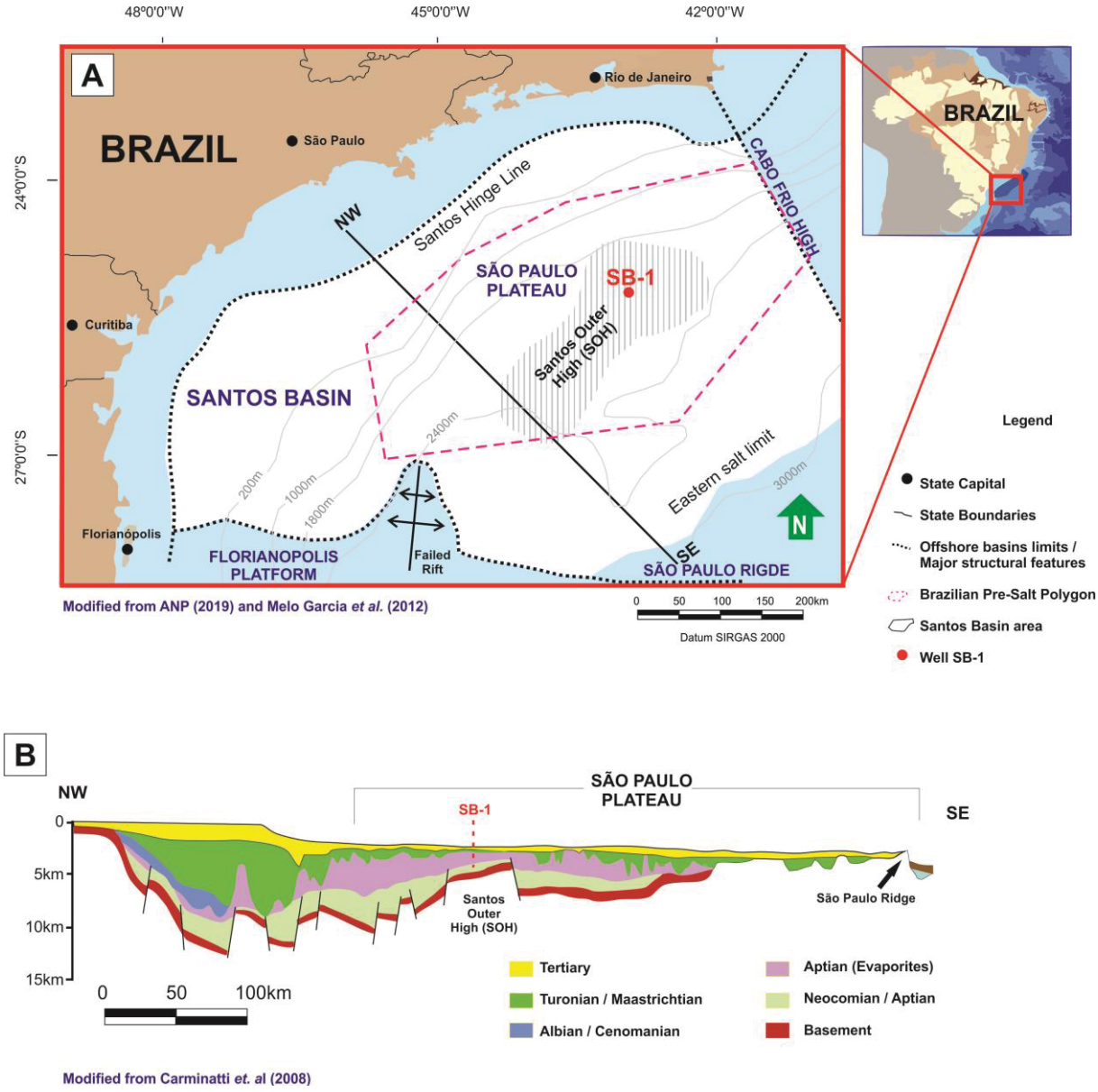

Figure 10 - Location map of the Santos Basin. A) Location map of Santos Basin with emphasis on the Santos Outer High (SOH - hatched polygon) and the location of the well SB-1 (Modified from ANP, 2019 and Melo Garcia et al., 2012). B) Geologial cross-section NW-SE.

The tectonostratigraphic evolution of the Santos Basin, like all sedimentary basins in the Brazilian east coast (and their counterparts in southwest Africa), is related to the breakup of Western Gondwana when South America separated from Africa and the South Atlantic Ocean began to open (Cainelli and Mohriak, 1999).

As a result of continental rifting and seafloor spreading that began in the Late Jurassic, the Santos Basin was filled with three super or mega sequences: Rift, Post-Rift, and Drift (Figure 11; Moreira et al., 2007). Pereira and Feijo (1994) had already

observed three sequences in previous works on the lithostratigraphy of the basin. The basement of the Santos Basin is composed of Precambrian metamorphic rocks of Camburiu Formation. It is responsible for heralding the beginning of the rifting in the southernmost part of the South American Plate. Extrusive and intrusive igneous activity occurred in this region, from the time of rifting up to the time of the evaporate deposition. Isotopic data suggests at least three phases of igneous activity occurred: one at 113 Ma, another at 118 Ma, and the oldest 130 Ma (correlative to the Parana basalts). Camboriu, Piçarras, and Itapema formations are part of the Neocominan-Barremian Continental Rift Mega sequence. The rift phase is associated with the synthetic and antithetic faults forming several grabens and half-grabens filled with fluvial-deltaic sediments. That is why overlying the volcanic rocks occur in the basin margins polymitic sandstones and in the deeper portions the dark shales and Mg-silicate clays from Piçarras Formation. This formation comprises sedimentation from the initial stage of rifting until the maximum tectonic activity. Itapema Formation, on the other hand, represents the final stages of the rifting when the main faults significantly reduce their activity. This formation comprises another important reservoir of Pre-Salt play: the bioclastic deposits called coquinas, besides that there are still wackestones, packstones, carbonatic shales and, dark shales (Pereira and Macedo, 1990; Pereira and Feijo, 1994; Moreira et al., 2007, Cainelli and Mohriak, 1999).

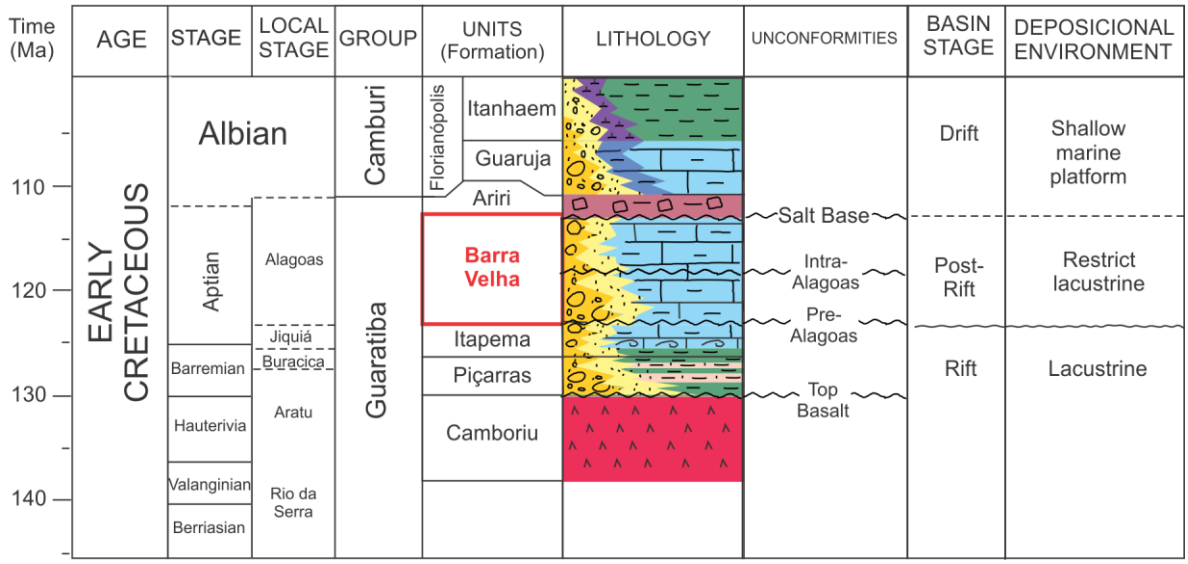

Figure 11 - Santos Basin lithostratigraphic chart (Modified from Moreira et al.; 2007)

The Post-rift Neoaptian Megasequence starts with the Barra Velha Formation, which is made up of siliciclastic sediments along the basin margins (alluvial fans), carbonate sediments in the deeper portions and ends with evaporates (Ariri Formation). This mega sequence lies within the Brazilian Alagoas Stage. Their reservoirs are mainly lacustrine, shaped in a very stressful environment with the deposition of microbiolites, stromatholites, spherulites, dolomitized or not, laminites and shales in the distal regions. Grainstones and packstones composed of fragments of stromatholites, microbialites and also spherulites occur (Cainelli and Mohriak, 1999, Moreira et al., 2007, Terra et al., 2010).

Finally, the basin evolved to a passive margin that allows the deposition of the Drift mega sequence (Albian to Miocene age), which contains many of the Brazilian hydrocarbon production and reserves. This mega sequence is divided into a Restricted Marine Sequence (dominated by the shallow-marine carbonatic platform of Guarujá Formation) and Open Marine Sequence (made up of deep-water sediments of the Itanhaém Formation).

3.2.2 Barra Velha Travertines

Wright & Barnett (2015) discarded the marine origin and described these unconventional reservoirs of the Barra Velha Formation as carbonates precipitated within alkaline lake environment, similar to those found in the East African Rift. The $^{87}Sr/^{88}Sr$ data provided by Tedeschi (2017) also supports this idea. Pietzsch et al. (2018) used a palaeoreconstruction of the Central South Atlantic segment based on Torsvik et al. (2009) to compare the areas of Santos, Campos, and Espirito Santo Basin during early Aptian and the size of modern-day Lake Tanganyika in the African Rift to show how a modern rift lake could be embedded within the Pre-salt area.

Wright & Barnett (2015) proposed a cyclic distribution for Barra Velha carbonates evolving the lake chemistry in the control facies development. For them, these typical cyclothems comprise three main components: mud laminated carbonates, spherulites with evidence of Mg-silicates, and calcitic shrubs-like growths, all of them typically non-ferroan and inclusion-rich. Other authors also recognized high-frequency cycles (Dias, 2005; Muniz and Bosence, 2015; Wright and Tosca, 2016; Artagão, 2018; Sartorato, 2018; Farias et al., 2019; Lima and De Ros,

2019; Gomes et al., 2020). There is agreement over the presence of them, however the last authors suggest that, in fact, there are other types of basic cycle with different facies associations, not only one typical cyclothem as proposed by Wright & Barnett (2015). It is also a consensus by many authors that these challenging reservoirs need further studies because remain doubts especially regarding the lacking of modern analogs and its biotic or abiotic origin.

The macroscopic similarity observed between the porous types described in outcrops of travertine systems in different regions of the world and those observed in the sampled rocks in Santos Basin Pre-Salt is striking and motivated the search for analogs improve the understanding of the genesis and the paleoenvironmental context in which they were these reservoir rocks were deposited. While Wright & Barnett (2015) suggested that the similarity with travertines textures not necessarily reflects a similar depositional environment but similar processes (such a rapid precipitation from highly saturated solutions), Della Porta et al. (2017) did not exclude the possibility of the presence of hydrothermal travertines in the middle of these reservoirs and, Souza et al. (2018) interpreted many of the Barra Velha Formation carbonate rocks as travertine related deposits.

This study aimed to characterize the rocks cored in the SB-1 well, located in the Santos Basin Outer High, compare them with the rocks classically described in the Brazilian Pre-salt by previous authors (Dias, 2005; Muniz and Bosence, 2015; Liechoscki de Paula Faria et al., 2017; Arienti et al., 2018; Artagão, 2018; Sartorato, 2018; Farias et al., 2019; Lima and De Ros, 2019; Gomes et al., 2020) and conclude whether or not they can be classified as travertines.

Travertines have been extensively quarried since Ancient times. Some quarries in Italy have been in operation for over 2.000 years. More than 2000 years have passed since the heyday of the Roman empire; there is still no consensual definition in the literature on the term ‘‘ travertine ’’. Polemic nomenclature, as well as a faciologic, environmental and genetic classifications and discussions about the influence or participation of bacteria in the deposition process have generated many controversies. For this reason, dozens of articles have been proposed in recent decades.

Most definitions emphasize the chemistry and the temperature of the water, while others point to the hydrogeological cycle, the inorganic versus organic deposition, climate change, or even the rate of evaporation as leading factors in the

process of travertine precipitation (Chafetz and Folk, 1984; Guo and Riding, 1998; Pentecost, 2005; Capezzuoli et al., 2014).

Chafetz and Folk (1984) defined *travertine* as a ‘‘freshwater’’carbonate deposited by both inorganic and organic precipitation from springs. For them, physical-chemical conditions are the main mechanism of precipitation near the springs, while organic processes become increasingly more important distally. Close to hot water spring (depending on temperature, pH, sulfur content), bacteria are the only ones that then grow and reproduce in this harsh environment.

According to Capezzuoli et al. (2014), the term ‘‘travertine’’ was used indiscriminately to describe all kinds of crystalline freshwater carbonates.

In this study, we will adopt the following definition proposed by Guo and Riding (1998):

‘‘Travertines are limestones that form where hot ground waters, rich in calcium and bicarbonate, emerge at springs. Carbon dioxide outgassing results in rapid precipitation, and the resulting deposits are both locally restricted and internally complex.’’

The rapid precipitation of travertine deposits results from the loss of carbon dioxide from the carbonated-rich water. The explanation for this loss is the result of either or both: (a) degassing during the fluid drop pressure (when the carbonated-rich water emerges on the surface from their depth and turbulent flow, CO_2 the pressure goes down, the carbon dioxide is lost to the atmosphere and the calcium carbonate is precipitated); (b) bacterial and algal activity extracts carbon dioxide from the waters (Chafetz and Folk, 1984; Ford and Pedley, 1996; Guo and Riding, 1998).

The importance of studying these rocks increased in the last 20 years when scientists realized that continental freshwater carbonates (both tufa and travertines are included in this group) could be used as a proxy indicator of climate changes and an opportunity to reconstruct ecosystems. While tufas reveal more information about the precipitation rate, microbiological fauna, and vegetation, travertines, on the other hand, bring in addition to paleoenvironmental information, data on carbon dioxide emissions in the past, and important information about the region's tectonism (Capezzuoli et al., 2014).

A new economic significance came to light when, in the middle of the year 2000, giant hydrocarbon reserves were discovered in the sag-rift section of the Santos Basin, on the southeastern Brazilian margin. Because these reservoirs were described by Wright and Barnett (2015) as highly alkaline lacustrine deposits, analogous to the lakes found in the East African Rift where microbialites and hydrothermal vents coexist, the possible occurrence of hydrothermal travertines was not excluded by Della Porta et al. (2017).

The presence of travertines is preferentially associated with extensional tectonic systems (e.g., Aegean Region in Greece and Turkey, the northern Apennines in Italy, and the Basin Mountains Range Province in the USA). These regions offer the perfect conditions for circulation and ascension of fluids to the surface (water thermal upwelling) through failed and fractured substrate. Most deposits accumulate within 1-2 km to active fault traces, always in the hang walls of normal faults or step-over zones (relay ramps) between two faults. So far, there are no reports of travertines in active thrusts (Hancock et al., 1999).

The relation between travertines and tectonics is so close that Hancock et al. (1999) strongly recommended the use of the term ‘‘travitonics’’ . Although they do not claim the credit for introducing the neologism, the idea of the article was to emphasize the importance of this deposits as a tool to study neotectonic attributes.

Depositional and morphological classifications of travertines have been proposed by several authors (Chafetz and Folk, 1984; Pentecost and Viles, 1994; Guo and Riding, 1998; Capezzuoli et al., 2014).

Chafetz and Folk (1984) divided the travertine deposits into five major categories based on the morphology of the deposits in central Italy and Central-West U.S.: (1) waterfall or cascade, (2) lake-fill, (3) sloping mound, (4) Terraced mound and (5) fissure ridge. Guo and Riding (1998), recognized three depositional systems: (a) Slope Depositional System; (b) Downslope Depression and (c) Reed Mound Depositional System. These depositional environments were recognized in Rapolano Terme (Italy), grouped into lithotype combinations and subdivided into six sub-environments.

Capezzuoli et al. (2014), in turn, proposed a classification focused on the distance from the spring. They named proximal region the vent itself and the area very close to it, the intermediate would be the slope environments (with or without terraces) and, the distal portions that encompass all deposits forming low relief

topography where the water temperature in near-ambient and ground water is mixed with rain water.

For Guo and Riding (1998) water chemistry directly influenced by temperature would be the main responsible for the control in the generation of these deposits. This observation had already been made by Chafetz and Folk (1984) who believed that travertines deposits are the result of both organic and inorganic process: inorganic process are dominant close the spring where the water is ‘‘energetically’’ degassing; while organic process are becoming more important downstream as the water usually cools down and the environment becomes less harsh. For them, the chemistry of the water more than temperature will determined which organisms are living or not near the spring orifice, this explanation lies in the fact that besides the calcium bicarbonate, the water emerges with other solutes, like sulfur, for example, and in many situations the chemistry of the water is considered poisonous for many macro-organisms (plants and trees).

An end-member scheme for the travertine precipitation would start close to spring orifice with predominance of inorganically precipitates and absence of living organisms, as the conditions become milder bacteria would be the first to appear, followed by blue and green algae and finally plants, as the temperature approaches to the surface conditions macrophytes (mosses and grasses) and gastropods tend to become more common. As we can see Guo and Riding (1998) were not the first to suspect the importance of bacteria in this process, but perhaps they were the first to identify and recognize the bacterias in textures and lithified structures of ancient carbonates by comparing them with the textural structures of today's Italian travertines, Idaho and Yellowstone. In this same article, they presented the hypothesis that shrubs represent accumulations formed in the summer, while the thin clay deposits that are intercalated with them would be winter deposits.

Besides the organic or inorganic precipitation and the chemistry and temperature of the water, the deposit will be the result of many others variables such as the amount of CO_2 dissolved in the water, the local relief, pH, salinity and light intensity (Chafetz and Folk, 1984; Guo and Riding, 1998). The amount of CO_2 dissolved in the water for example, (if there is no changes in others variables) the higher the concentration of dissolved HCO_3 that can be maintained in solution, the greater the amount of $CaCO_3$ that can be precipitated due to degassing.

According to Pentecost (2005), four chemical processes are responsible for the generation of almost all travertines in the world, and the vast majority of them are formed by the degassing of groundwater rich in carbon dioxide containing> 2 mmol L-1 (c. 80 ppm) of calcium (only the first one will be detailed as follow). The water's ability to precipitate travertines through this first reaction (Eq 1) is produced when carbon dioxide dissolved in groundwater (carbonic acid) 'attacks'' carbonate rocks and forms a solution containing calcium ions and bicarbonate (bicarbonate of calcium).

$$CaCO_3 + CO_2 + H_2O <=> Ca^{2+} + 2(HCO_3)^- \qquad \text{(Eq 1)}$$

Equation 1 represents the reversible chemical reaction responsible for the formation of most precipitated travertine deposits in the world.

3.3 ANALYTICAL METHODS

This paper focuses on data from SB-1 well located in the horst structure of the Santos Outer High (Figure 10). The core available come from the upper section of the Barra Velha Formation above the Intra-Alagoas Unconformity. For this study, 83 m of carbonatic core (#1 to #6) and 41 thin sections were available (Figure 12). Standard-thickness thin sections were prepared from blue epoxy resin-impregnated. Staining with Alizarin red-S and potassium ferrocyanide solution was applied in some thin sections to differenciate the carbonate minerals as outlined by Dickson (1965). All thin sections were examined by petrographic Zeiss microscope between uncrossed (//P) and crossed polarizers (XP) at Petrobras Research Center (CENPES) in Rio de Janeiro and at the Mineral and Rock Analysis Laboratory of the Federal University of Parana (UFPR).

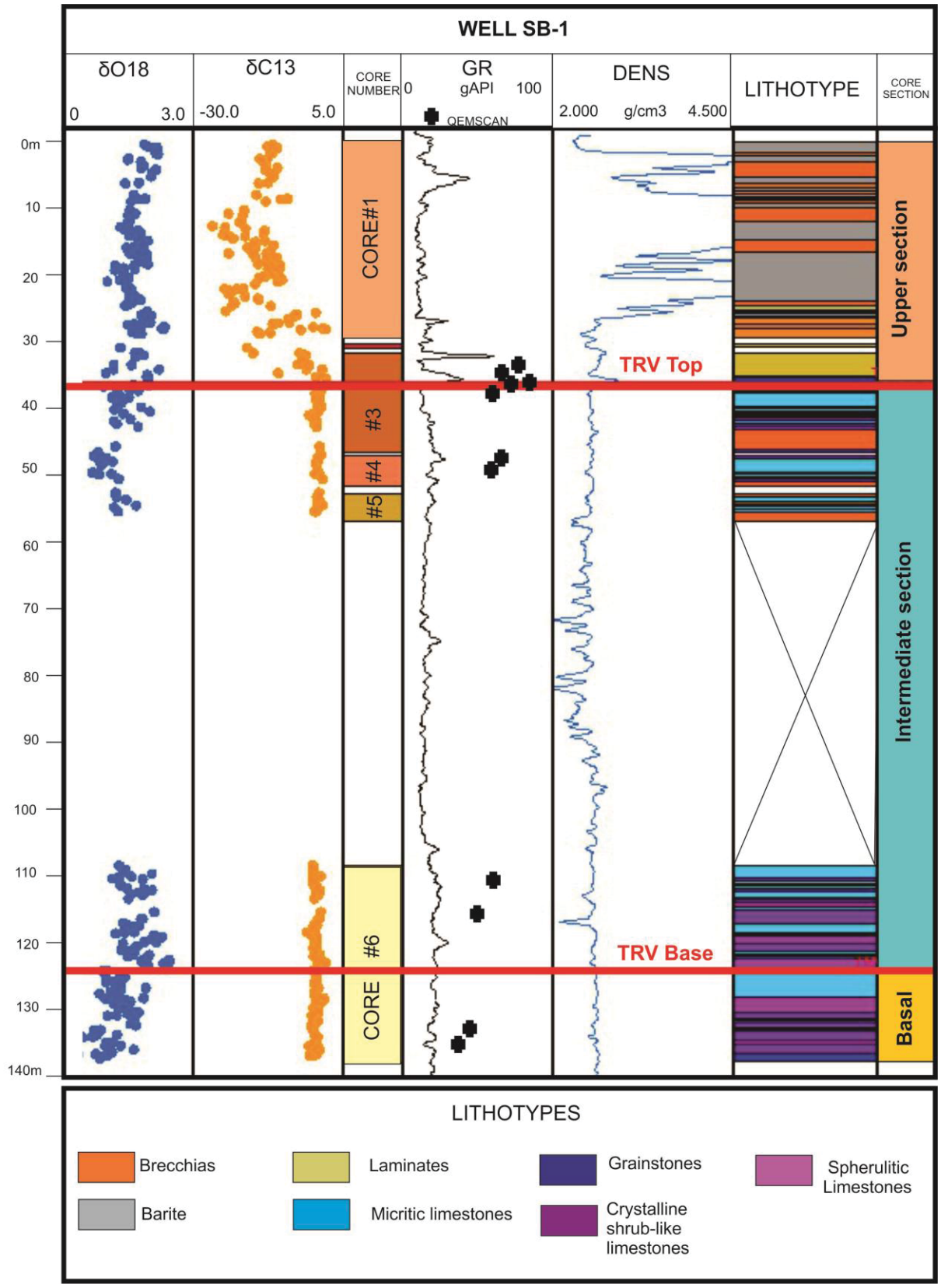

Figure 12 - Stratigraphic logs of well SB-1 at Santos Basin. $\delta^{18}O$ and $\delta^{13}C$: samples analysed for oxygen and carbon isotopes, core sampling and positioning, GR: gamma ray curve and thin sections analysed for QEMSCAN; DENS: Density curve, facies description. TRV T: top of travertine interval; TRV B: base of travertine interval.

Carbon and Oxygen isotopes analyses were performed on 240 bulk rock samples derived from core plugs of SB-1 well (Figure 12). The samples were analyzed ‘online’ using an IRMS Thermo Scientific Delta XL Advantage coupled to a Gasbench II device in the University of São Paulo (USP) Lab. In addition, 33 samples (~100mg) of selected carbonate phases were obtained for carbon and oxygen isotopes punctual analyses from 12 thin sections (120 µm-thick) by reaction with 100% H_3PO_4 at 70 °C in the Isotope Lab of Petrobras Research Center (CENPES) using a Thermo Scientific Delta V Isotope Ratio Mass Spectrometer, coupled to a Gasbench II unit. All data were reported relative to Vienna Pee Dee Belemnite (VPDB) international standard in per mil units (‰). The isotopic values encountered represent a deviation in parts per mil of a sample in relation to the reference material NBS-19 (TS-Limestone), yiellding results better than ±0.09 ‰ for $\delta^{13}C$ and ±0.10 ‰ for $\delta\ ^{18}O$.

In addition, 11 petrographic thin sections were selected for automated mineralogical distribution mapping using QEMSCAN 650 (FEI) equipment with two EDS/Bruker detectors. These mineralogical maps show the spatial distribution of mineral phases and the relationship between them; their abundance was quantified as area percentages or percentage of mass (considering the theoretical density of minerals). Quantities lower than 0.01% were ignored.

3.4 RESULTS

Although 83 m were available for the analysis, we focused on cores #3 to #6, where the travertine section was recognized. This specific interval corresponds to approximately 37 m.

3.4.1 Lithotypes classification

As emphasized by Jones and Renaut (2010), $CaCO_3$ precipitation in springs produces a vast array of crystal forms that range from micrite and equant spar, to large crystalline crusts and complex dendrite crystals.

Names and characteristic features of the main lithotypes of well SB-1 are listed and illustrated in this chapter. As stressed by Claes et al. (2015), that similar fabrics can occur in different lithotypes; for example, peloidal micrite is typical for peloidal lithotypes but is also one´s of the main fabrics of micritic dendrites.

Microcrystalline calcite (micrite) is a very common constituent in travertine deposits (Jones and Renaut, 2010; Özkul et al., 2013; Claes et al., 2015). Although the term micrite is still a point of discussion in several debates, the term coined by Folk (1959) refers to carbonate of mud grade. Micrite is a component of carbonate rocks that can occur as a matrix, as cement, or as peloids. It can be generated by chemical precipitation, disaggregation of peloids, or micritization (Flugel, 2004). It is used here in a sense, according to Jones (1989), as a synonym for calcitic particles smaller than 4 μm, without genetic connotation.

Regarding the macroscopic description, the whole core can be divided into three distinct intervals (Figure 12 and Figure 13). The basal section studied corresponds to the lower portion of core#6, which is composed of an intercalation of peloid micritic limestones (MCT-pe) with predominant spherulitic crystalline limestones, crystalline shrub-like crusts and intraclastic grainstones. It is the only one of the three sections in which ostracods up to 1mm in length have been described.

The intermediate portion encompasses the upper half of core #6, cores #4 and #5 in its entirety, and the base of core #3. This range contains at its top an abrupt contact between the intraclastic grainstone composed of carbonate fragments (rounded carbonate grains) without apparent organization under the calcitic crust with an angle of approximately 40º. This contact is the top of the travertine in well SB-1. This intermediate portion of the core contains the rocks of most interest in this study.

The distribution of the lithotypes of this section can be observed in Figure 14. On the macro-scale, the intermediate is the portion of the core that reveal features typically found in travertine systems, such as strongly banded carbonates with high inclinations angles, calcite crusts, rafts, and micro-karst features. In the well SB-1 these crusts can be formed by lithotypes MCT-pe, CCL-sh, CCL-ef ou MCC (Figure 14 and Figure 15).

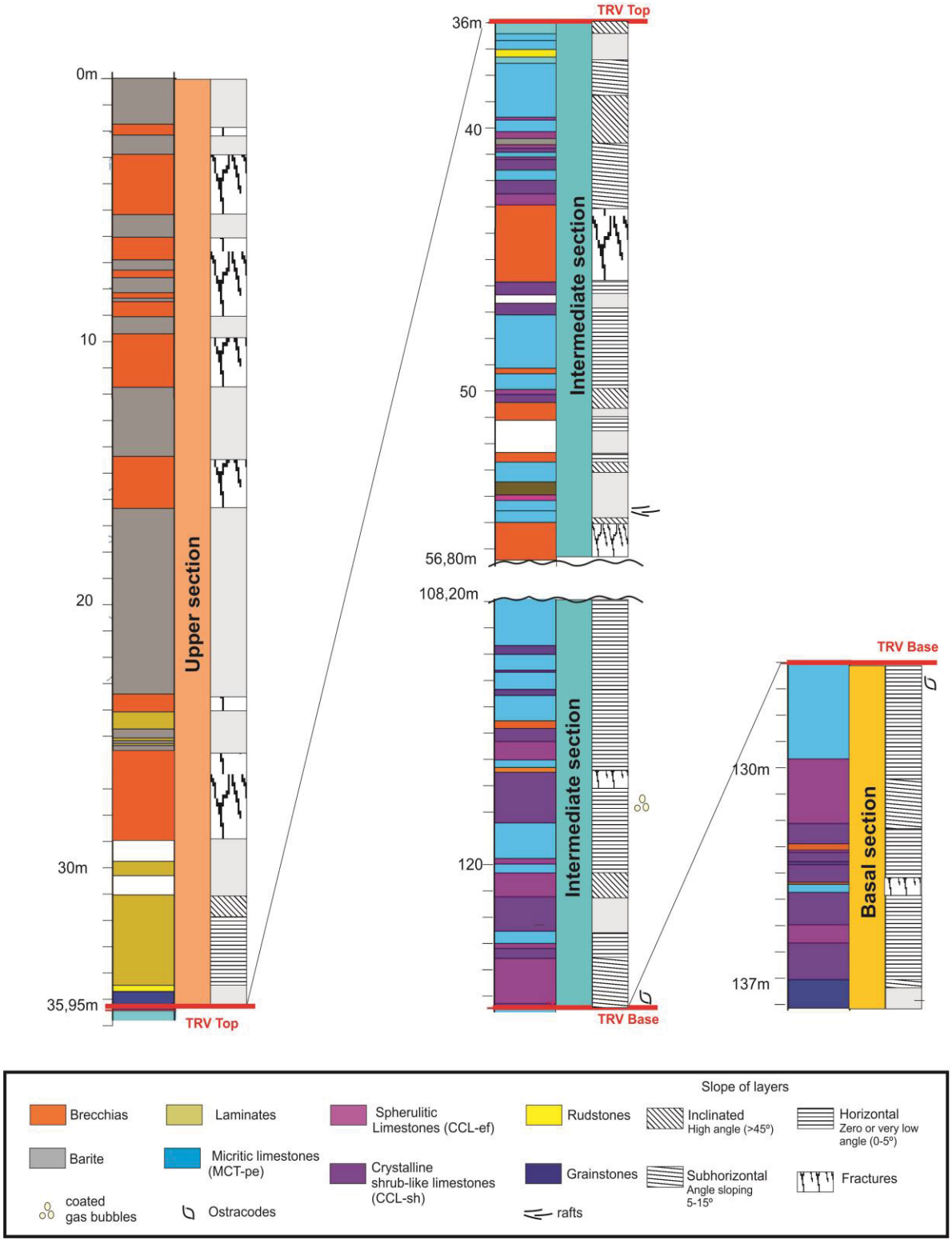

Figure 13 – Detailed stratigraphic lithological columm from well SB-1 of the Barra Velha Formation (sag phase) at Santos Basin.

The upper part that encompassing the rest of core #3 and cores #1 and #2 is characterized by a very significant textural change compared to the intermediate interval and basal sections. These intervals are intensely brecciated, fractured, and baritized, and in most cases, it is no longer possible to identify the original lithotype (Figure 13 and Figure 15).

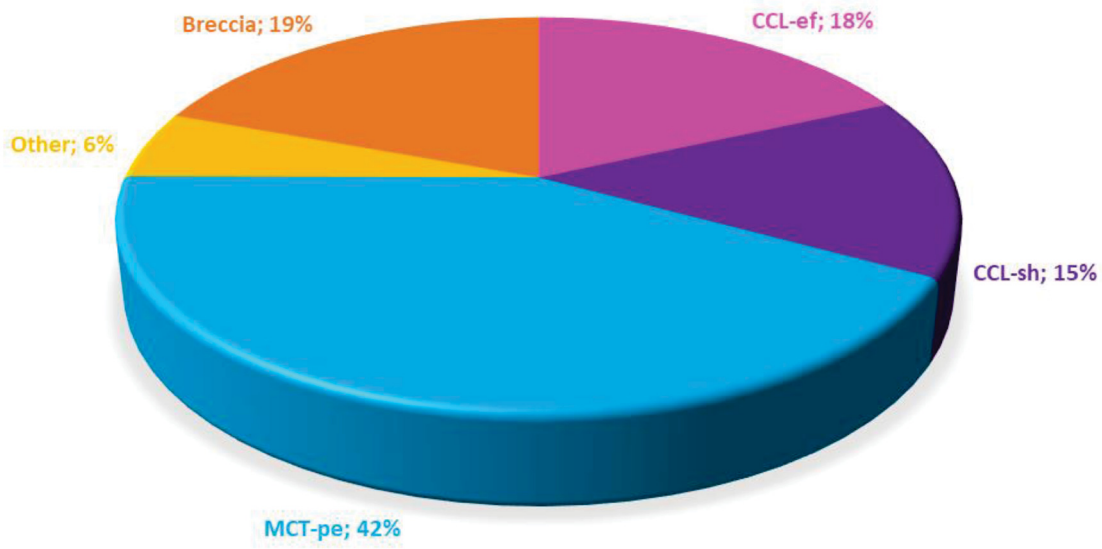

Figure 14 - Lithotypes distribution in the intermediate section of well SB-1 (travertine interval). MCT-pe: lithotype composed of aggregates of microcrystalline calcite (peloidal micrite); Crystalline Spherulite Limestone (CCL-ef); Crystalline Shrub-like Arborescent Limestones (CCL-sh); breccias, and others represent microcrystalline crusts, rafts, bubbles, microcrystalline peloidal limestones, intraclastic rudstones.

According to macroscopic description and petrography, 42% of the rocks described in the intermediate section are microcrystalline clotted limestones (MCT-pe). This lithotype is composed of aggregates of microcrystalline calcite (micrite), which are presented in well-defined crusts that vary between 0.5 and 3 cm in thickness. The inclination of the crusts varies from sub-horizontal to 45 degrees (Figure 14). Crystalline Spherulite Limestone (CCL-ef) represents 18% of the described rocks; Crystalline Shrub-like Arborescent Limestones (CCL-sh), similar to fascicular-optic calcite with a fan-shaped structure, represent 15%. Breccias represent 19% of the intermediate section, and microcrystalline crusts, rafts, bubbles,

microcrystalline peloidal limestones, intraclastic rudstones represent the remaining 6%.

The rocks from well SB-1 were divided into 2 groups according to their fabrics: (a) The microcrystalline lithotypes and (b) crystalline fabrics (Table 2).

Table 2 - Lithotypes interpreted for the intermediate section of well SB-1

FABRICS	ACRONYMS	LITHOTYPE
MICROCRYSTALLINE FABRICS	MCL-pe	Microcrystalline Peloidal Limestone
	MCT-pe	Microcrystalline Clotted Limestone or Clotted Peloidal Limestone
	MCL-de	Micritic or Microcrystalline Dendrite Limestone
	MCC	Micritic or Microcrystalline calcite crust
	MCL-r	Rafts ou Paper thin-rafts
CRYSTALLINE FABRICS	CCL-ef	Crystalline Spherulite Limestone
	CCL-sh	Crystalline Shrub-like Limestone

3.4.1.1 Micritic peloidal limestone (MCL-pe)

The constituents of micritic peloidal limestone are aggregates of non–translucent dark tiny spheroids of carbonate (50 to 200 μm), usually covered by micro-spar or spar crystals. The spar (bladed, tooth dog, or scalenohedral) is present within almost every pore. Commonly the peloids are amalgamated. The visually estimated porosity varies from 5 to 10%. Pore types are vugular and interpeloidal, not exceeding 1mm. Often the porosity follows lamination and resembles fenestral porosity, hence ‘‘pseudo-fenestral porosity’’ (Figure 18).

3.4.1.2 Clotted Peloidal Limestone (MCT-pe)

Clotted Peloidal Limestone is the main lithofacies of the intermediate section and represents 42% of this interval.

The constituents of clotted peloidal limestone are aggregates of dark microcrystalline calcite, as well as the micritic peloidal limestone. However, unlike the previous facies, on micro-scale aggregates are not spheroids that can be individualized. They are aggregates formed by the amalgamation of the peloids, giving the rock a lumpy structure with a coagulated aspect. They are also usually covered by micrite, micro-spar or spar crystals. The spar (bladed and tooth dog) is present within almost every pore. Porosity is vugular and pseudo-fenestral and could reach up to 6mm. The visually estimated porosity is about 15-20%.

In general, MCT-pe occurs with bedded aspect throughout the entire intermediate section (Figure 13). For MCT-pe these centimeter bedded (1-10 cm) may be horizontal, subhorizontal, and even reach greater inclinations close to 45 degrees.

3.4.1.3 Micritic Dendrite Limestone (MCL-de)

The constituents of micritic dendrite limestone are a dark micritic ‘‘branching elongated structure’’, composed of peloidal micritic aggregate. Dendrites are structures that contain multiple branches starting from the same point, with their height larger than their width (Claes et al., 2015; Erthal et al., 2017). According to Claes et al. (2015), secondary branches are uncommon, this is also true in SB-1 well. On micro-scale was possible to observe that dendrites are formed mainly of aggregates and peloids 0.1 to 3mm in size and, individual branches vary from 0.2 to 1.5mm. The branching structure is oriented perpendicular to the substrate. The visually estimated porosity is about 10%-15%. Pore types are inter-dendrite and intra-dendrite microporosity. Dendrites are usually coated by sparry calcite, including scalenohedral (Figure 16).

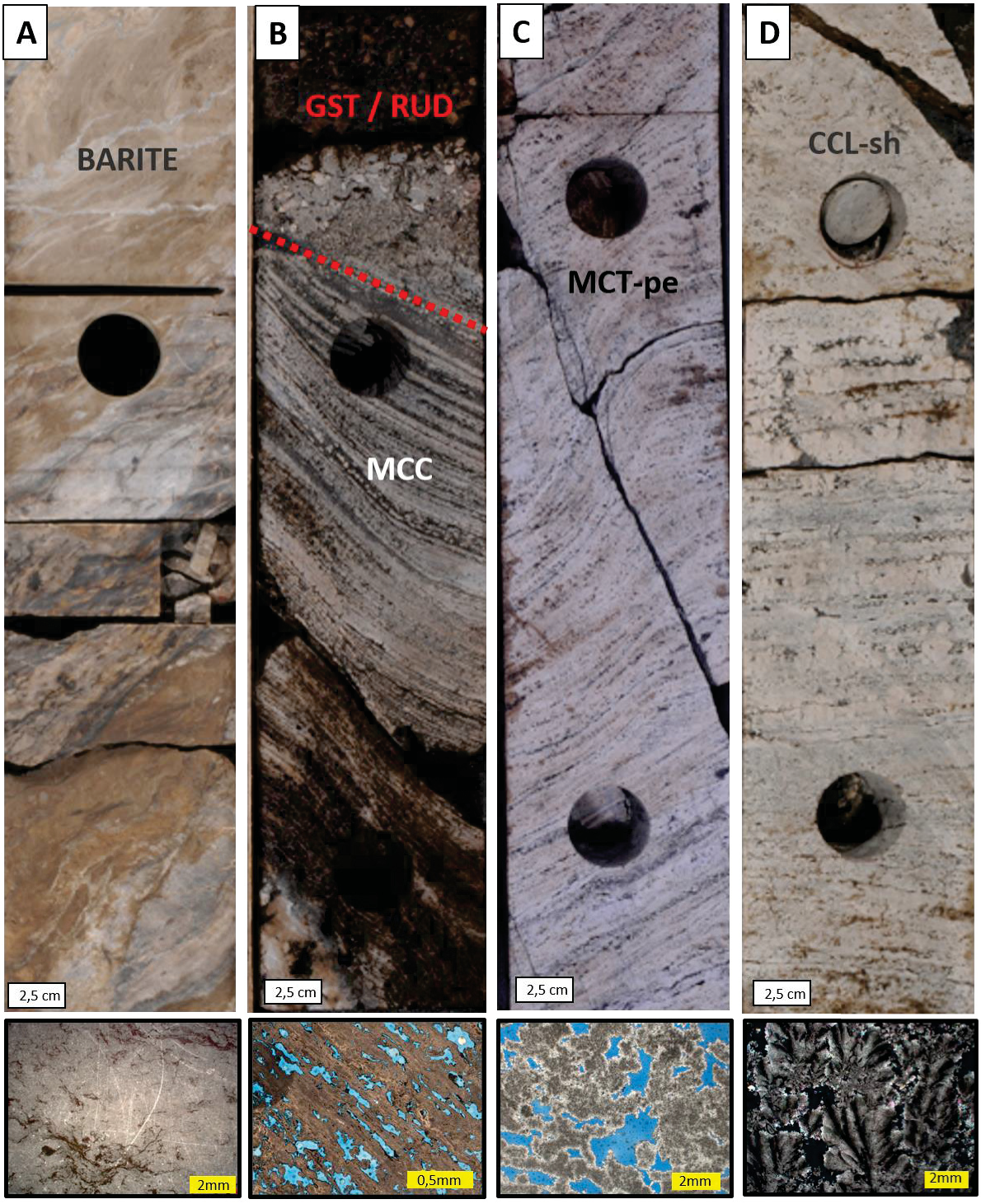

Figure 15 – Macroscopic features of the core SB-1, and their corresponding microphotography below . A) Photo of the barite that occurs at the upper section of core#1; B) dashed red line represents the contact between the grainstone that overlaps the travertine interval, the lithotype below the dashed red line is an example of MCC (microcrystalline calcite crust) represented in the thin section below; C) Crustiform Clottted peloidal limestone (MCT-pe); D) Subhorizontal crusts of Crystalline Arborescent Limestone (CCL-sh).

3.4.1.4 Microcrystalline Calcitic Crust (MCC)

Thin micritic calcite crusts approximately 2mm thick constitute the microcrystalline limestone described in well SB-1. This lithotype occurs exclusively at the beginning of the intermediate section and corresponds to the crusts with the highest inclinations observed for this well (about 45 degrees). On the micro-scale, parallel layers of micrite with an average thickness of 1mm were described. The porosity is fenestral and relatively high (~20%).

The high angle of inclination of these layers suggests that they were formed in a slope-type environment (possibly smooth slope), where the water enriched in calcium bicarbonate flows quickly due to the slope, increasing the rate of degasing and resulting the rapid precipitation of calcite (Figure 4 and Figure 17).

3.4.1.5 Crystalline Shrub-like Limestone (CCl-sh)

Crystalline Shrub-like Limestone (CCl-sh) from SB-1 are mainly characterized by their branching shrub-like structure. On macro scale are formed by bedforms distinguished from a sequence of crystalline shrub crusts that can be between 0.5 cm and 2 cm thick; 0,5 cm on average. They can be horizontal to subhorizontal with inclinations of up to 10º (Figure 15).

On micro-scale, they usually have a feather or fan shape that forms fascicular calcite crusts of crystalline fabric. Morphologically they resemble small shrubs with radial-fibrous and ondulose extinction under crossed polarized nichols. They are milimeter size (5-25mm high and 1.5 to 5mm width). The branching structure is oriented perpendicular to the substrate.

According to Erthal et al. (2017), the shrub ‘‘branching structure’’ can have many morphologies the height much larger than their width characterize dendriform shrubs; arborescent shrubs also show an elongated vertical grow form, with their height larger than width, but branches are absent or are under development; arbustiform also have they preferential vertical growth, but their height is shorter than their width in a ratio of 1:2 (H/W). Dendriform and arborescent shrubs morphologies were described in SB-1, the last one is the most common (Figure 16).

The visually estimated porosity is about 5%-10%. Pore types are inter-particle (inter-shrub), intra-crystalline microporosity, and vugular. Dendrites are usually coated by sparry calcite, including scalenohedral type.

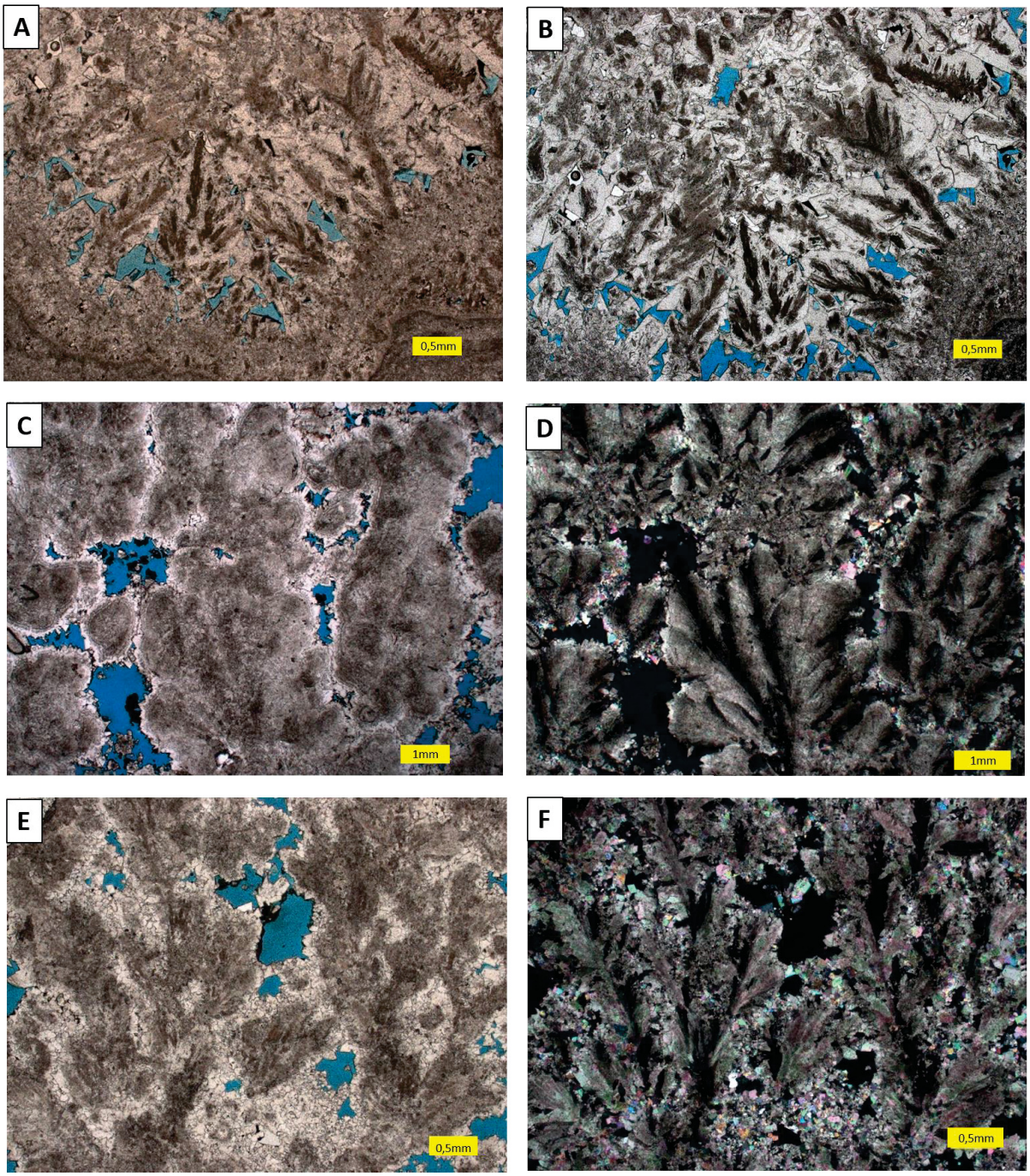

Figure 16 – Photomicrograph of shrub morphologies described in well SB-1 (imagens pairs are PPL and XP). A and B) Micritic Dendrite Limestone; C and D) Arborescent Limestone; E and F) Crystalline Dendrite Limestone.

3.4.1.6 Crystalline Spherulitic Limestone (CCL-ef)

Crystalline Spherulitic Limestone (CCL-ef) lithotype refers to the limestone composed by small spherical to sub-spherical calcite aggregates with symmetrical fibro-radial extinction under the optical microscope.

On the macro-scale, Crystalline Spherulitic Limestone (CCL-ef) is banded. These bands are commonly horizontal, can reach up to 40 cm thick, and occur predominantly in the basal section and lower portions of the intermediate section.

In thin sections, these small spheres were called calcite spherulites. The diameter of these spherulites ranges between 0.1mm to 4mm (generally less than 2mm); in rare cases, they reach up to 5mm (Figure 17). Some spherulites are a mix: they look like a spherulite but grow preferentially in one direction made them asymmetric. These are probably a transitional form between spherulitic and fascicular/arborescent forms (Lima and De Ros, 2019).

The porosity of CCL-ef is inter-particle. The nuclei of the spherulites are usually formed by microcrystalline calcite, but not rarely this core seems to have been replaced by silica or dolomite. This is not a surprise, although the spherulites seem to be well preserved in well SB-1, process of dissolution, dolomitization and recrystalization of these nucleis had already been described by Pietzsch et al., (2018); Farias et al., (2019); Lima and De Ros, (2019); Gomes et al., (2020).

3.4.1.7 Grainstones/Rudstones (GST/RUD)

Grainstones and rudstones occur at 3 intervals in well SB-1: (1) the most significant grainstone is a 70 cm thick interval separating the upper section from the intermediate section, defining the top of the travertine facies with an erosive contact (Figure 13 and Figure 15). The clasts are rounded and sub-rounded, ranging from 0.5-1mm, but can reach up to 2mm (medium to very coarse sand). They present punctual contacts, very thin irregular micritic coatings, and predominantly inter-granular porosity. In some clasts, it is possible to observe that there was an internal dissolution. Although part of this generated porosity was filled by dolomite, it is still possible to observe clasts with intraparticle porosity. As cement is practically absent, porosity is very high (15-25%).

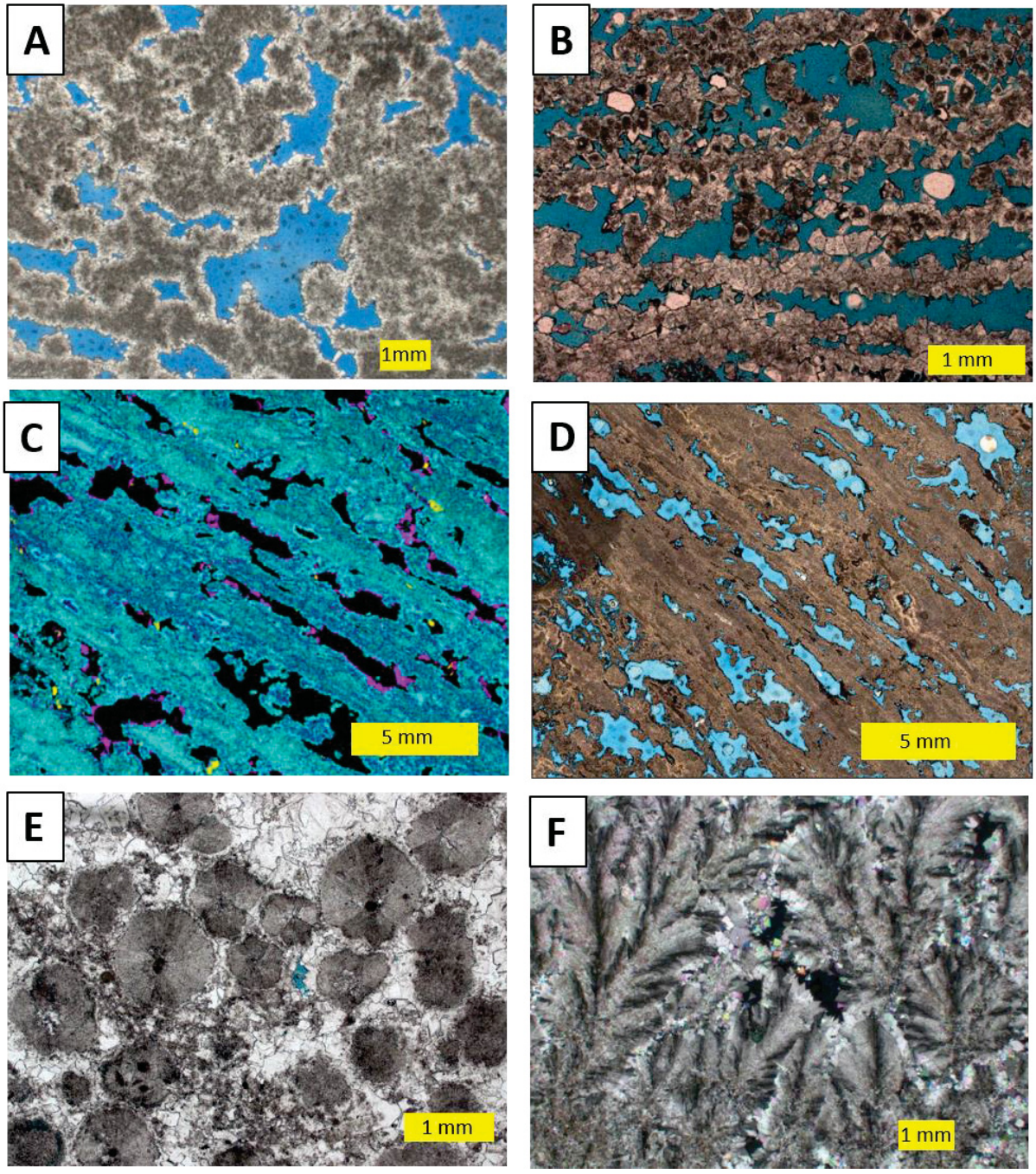

Figure 17 - Lithotypes described in well SB-1. A) Microcrystalline Clotted Limestone (MCT-pe); B) Rafts (CCL-r); C) QEMSCAN image of Microcrystalline Calcitic Crusts (MCC); Microcrystalline calcite (light-blue), dolomite (dark-blue); carbon rich material (pink); quartz (yellow). D) MCC composed by microcrystalline calcite (micrite); E) Crystalline Limestone composed by spherulites (CCL-ef) and; F) Crystalline Shrub-like Limestone (CCL-sh) under crossed polarized nichols.

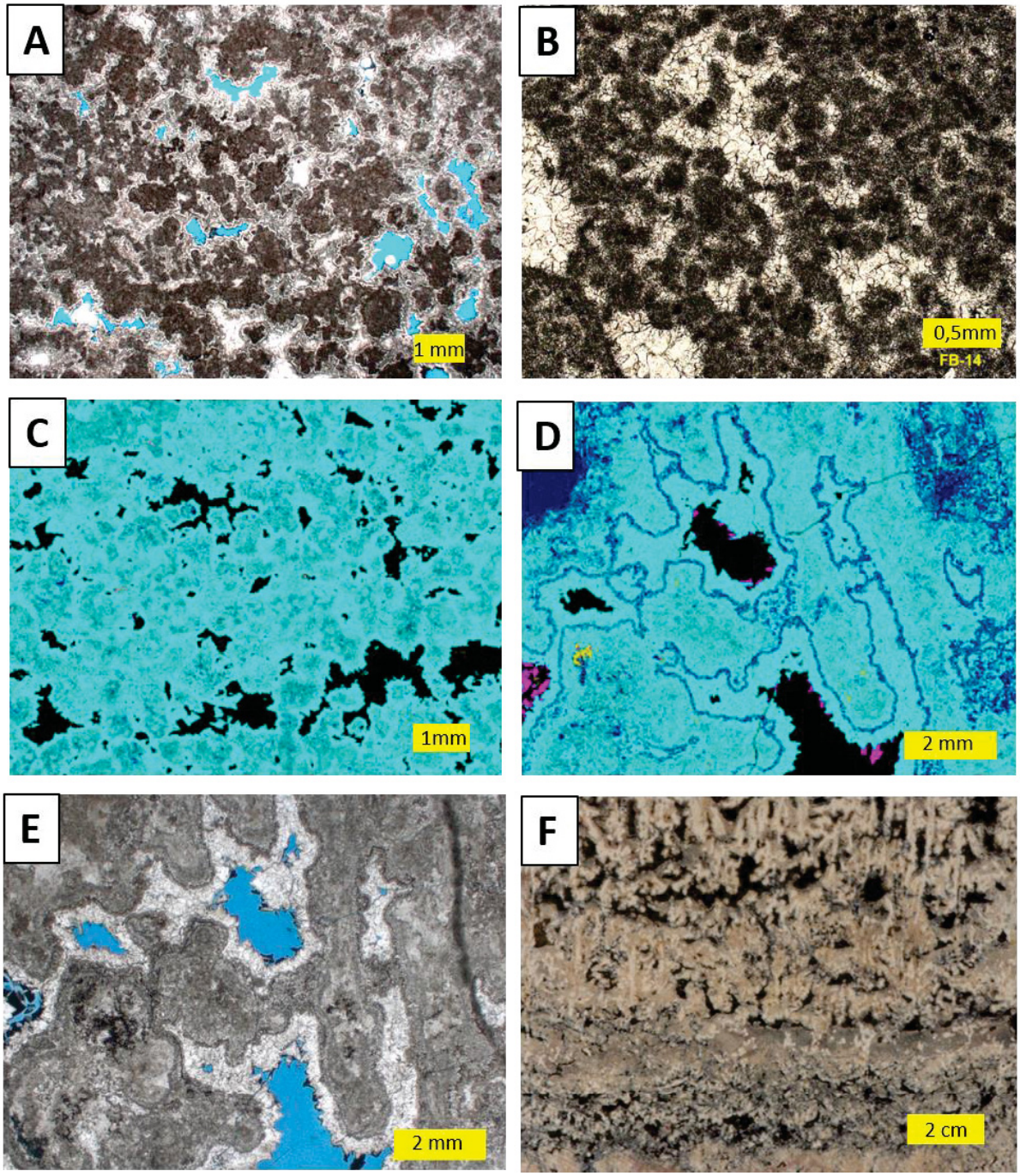

Figure 18 – Photomicrograph and QEMSCAN images of SB-1 compared to others travertines around the world. A) Peloidal limestone from SB-1 (MCL-pe); B) Peloidal limestone from a Turkish travertine deposit; C) QEMSCAN image of the MCL-pe: 0-1% MgO microcrystalline calcite (light blue), 4-7% MgO microcrystalline calcite (light gray); D) QEMSCAN image of Microcrystalline Clotted Limestone (MCT-pe) with microkarst features. Microcrystalline calcite (light-blue), dolomite (dark-blue); carbon rich material (pink); and quartz (yellow). E) Photomicrograph of detail of microkarst features from SB-1. F) Microcrystalline Clotted Limestone (MCT-pe) with microkarst features on macro-scale.

The second interval is 50 cm thick rudstone composed of sub-angled pebble up to 1 cm in diameter and larger rounded pebbles (>15 cm) surrounded by a matrix of coarse to very coarse sand.

The last interval is a sloping layer of approximately 2 cm thick with coarse sand clasts and a medium sand matrix.

All grainstones and rudstones from well SB-1 are composed of CCL-sh and CCL-ef limestone fragments, being intraclastic grainstones and rudstones, with inter-particle and intra-particle porosity.

The rounding of clasts indicates the longevity and type of events associated with the rework. Rounded and sub-rounded clasts like the one at the top of travertine (1) need more time and must be associated with more than one rework phase. Forming them needs a continuous water flow, which could be from the travertine system itself. This water is responsible for bringing clasts from topographically higher portions to low areas (depressions).

The most angular clasts (2 and 3) are probably associated with wetter periods that caused an increase in water flow and even sudden outflows capable of bringing clasts from higher areas to lower portions in a short period, thus not allowing a high degree of rounding.

Falcão (2015) observed that the presence of reworked facies reflects the some subaerial conditions to which these rocks were subjected, making them more susceptible to erosion.

Although Chafetz and Folk (1984) and Pentecost and Viles (1994) have described travertines frequently undergo erosion containing a significant proportion of clastic material, in SB-1 this proportion is very small and almost insignificant.

3.4.1.8 Rafts and coated gas bubbles

Rafts or paper thin-rafts are very delicate, laminated, and brittle sub-horizontal structures formed by aligned crystalline plates of calcite. Depending on the organization of the plates, these structures can lead to very high porosities, which is what happens in the rafts of the SB-1 well. According to Claes et al. (2015), cementation is two-fold: reduce de pore space but also strengthens their structure promoting pore preservation.

In the samples available rafts are very rare ocorring only in one specific interval of 25 centimeters. On microscopic scale the individual plates are approximately 0.3mm thick and the pore space between the plates vary from 0.3 to 0.6 mm (Figure 17). They are formed by dirty-looking micritic peloids, and have overgrowth of syntax calcite as already noted by Falcão (2015).

The interpretation is that these calcitic plates are formed in regions where the speed of water flow decreases, becoming calmer. The water that is saturated in Calcium stays stagnant in pools or puddles, and very delicate calcite layers begin to form. When the puddle dries up or occurs, an increase in water flow speed, or as the films get thicker and heavier, they tend to break and sink, being deposited (Figure 7; Bargar 1978; Guo and Riding 1998).

Coated gas bubbles occur in sub-horizontal bands in one interval of well SB-1 (Figure 19). Carbonate coating of gas bubbles is typical of travertine systems, and they may be generated by microbial activity or by stream/CO_2, produced by turbulence, pressure release, or shallow boiling. These bubbles were probably formed very near the sediment-water interface and go upward. Surface tension allows sufficient time for incipient lithification. Coated gas bubble preservation is only possible when they were trapped and in stagnant conditions of water bodies (Chafetz and Folk, 1984; Guo and Riding, 1998; Capezzuoli et al., 2014; Della Porta et al., 2017).

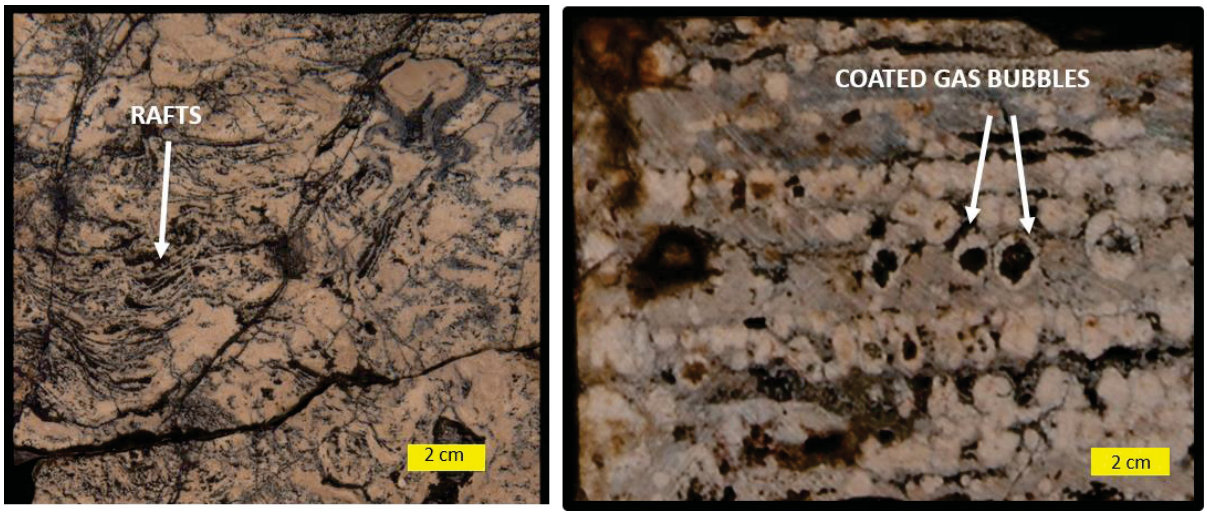

Figure 19 – Macroscopic features of paper thin rafts and coated gas bublles in SB-1 well.

3.4.1.9 Breccias

The breccias described in SB-1 are rocks fragmented at different levels that can be classified as fault breccias. Its composition is usually monomitic, which means that the fragments consist exclusively of travertine composition, usually floating in a peloid micritic matrix (when it is present). The clasts are millimeter to centimeter-sized and vary from angular to sub-angular, and the matrix is conglomerate/coarse sand to medium size.

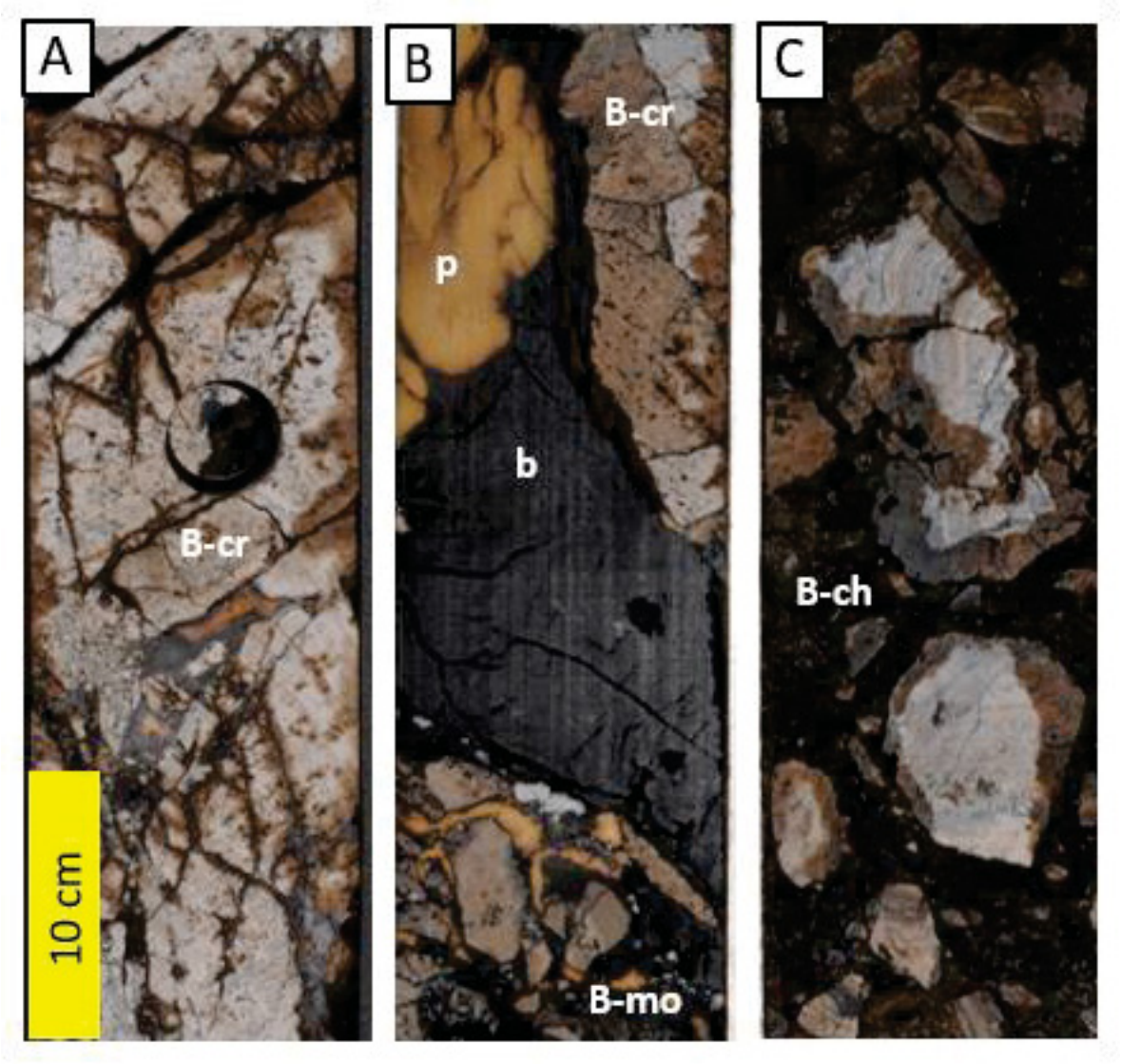

Figure 20 – Brecchias from SB-1. A) Crackle breccia (B-cr) with faults filled by oil and solid bitumen; B) Crackle (B-cr) and mosaic breccia (Bmo) fractures and pores filled with solid bitumen (b) and paraffin (p); C) Chaotic breccia (B-ch).

In SB-1, three types were recognized according to the classification proposed by Woodcock and Mort (2008) depending on how the clasts fit together: (1) crackle, (2) mosaic, and (3) chaotic breccia.

Figure 20 exemplifies some types of breccias found in well SB-1. Crackle breccias have clasts separated by thin seams of cement or matrix. The clasts are little rotated with respect to each other (Figure 20A). Clasts in mosaic breccias show more separation and rotation but still show some fitting to adjacent clasts (Figure 20A and Figure 20B). In chaotic breccias (Figure 20C), clasts are more strongly rotated and have lost any geometric fit to formerly adjacent clasts.

The porosity of the breccia depends on the nature and degree of brecciation. In addition to the secondary porosity of fractures, due to the peloid and micritic matrix, some interpeloidal porosity is expected in some of them.

3.4.1.10 Porosity and diagenesis

The interparticle (interpeloidal), vugular, and pseudo-fenestral are the most common porosity types for MCT-pe and MCL-pe. Usually, the micritic peloids are coated by a fine calcite rim, and the pores are not fully filled by a cement of any kind. Besides calcite, they can also be filled in a smaller proportion by dolomite and bitumen; rarely by strontianite, Sr-barite, apatite, fluorite, and pyrite.

In Crystalline Calcitic Shrub-like Limestone (CCL-sh), the main pore types that occur are primary growth-framework and inter-crystalline. Secondarily occur calcite dissolution and vugular porosity. The most commom diagenetic phases that replace preexisting constituents and fill the porosity in this lithotype are a fine to prismatic calcite rim, scalenohedral calcite, fine to mosaic quatz, dolomite, barite and bitumen.

The pores of Crystalline Spherulite Limestone (CCL-ef) are filled with fine to macrocrystalline calcite mosaic in the intermediate section. Vugs can also be filled in a smaller proportion by dolomite, pytite and bitumen. In the basal section, the most common cement in this lithotype is the macrocrystalline quartz.

Fracture and breccia porosity types are relatively more important in the upper section, although fractures can be identified in the whole core. The fractures apertures range from millimetric to centimetric and from partial to fully cemented. They are usually filled with macrocrystalline calcite, exhibiting beautiful mosaic

calcite, barite, anhydrite, pyrite, and dolomite. In the upper section is commom to find vugs filled with pyrite, barite, bitumen, macrocrystalline quartz, and anhydrite.

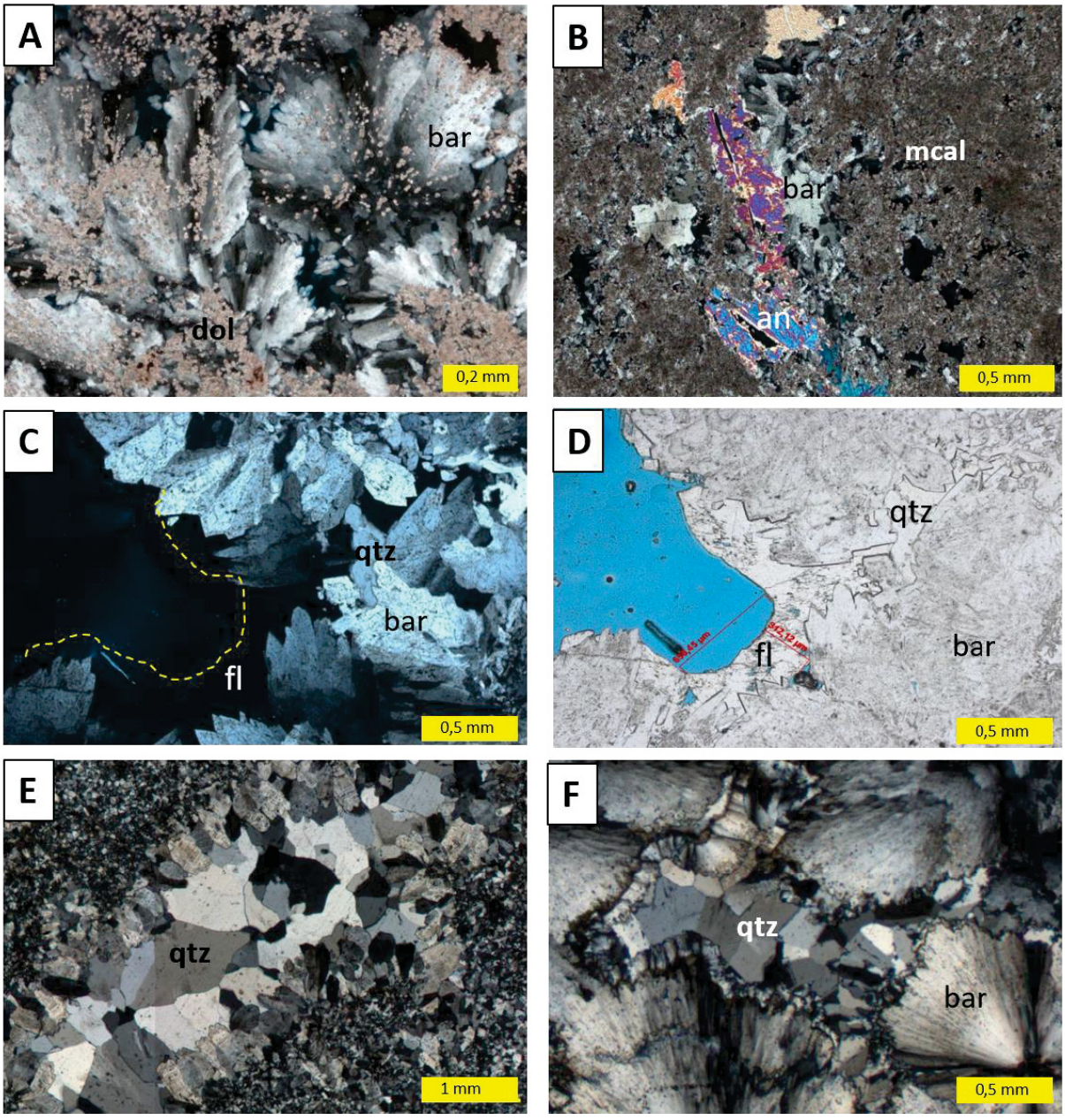

Figure 21 – Exotic paragenesis observed in the well SB-1. A) Feathering barite (bar) replacing dolomite (dol) matrix in upper section; B) Anhydrite (an) and barite (bar) filling pore of the upper section of SB-1; C and D) barite (bar), fluorite (fl) and quatz (qtz) filling pore with cross and non crossed polarizers; E) quartz mosaic filling pore, and D) macrocrystalline quartz filling pore after barite (bar).

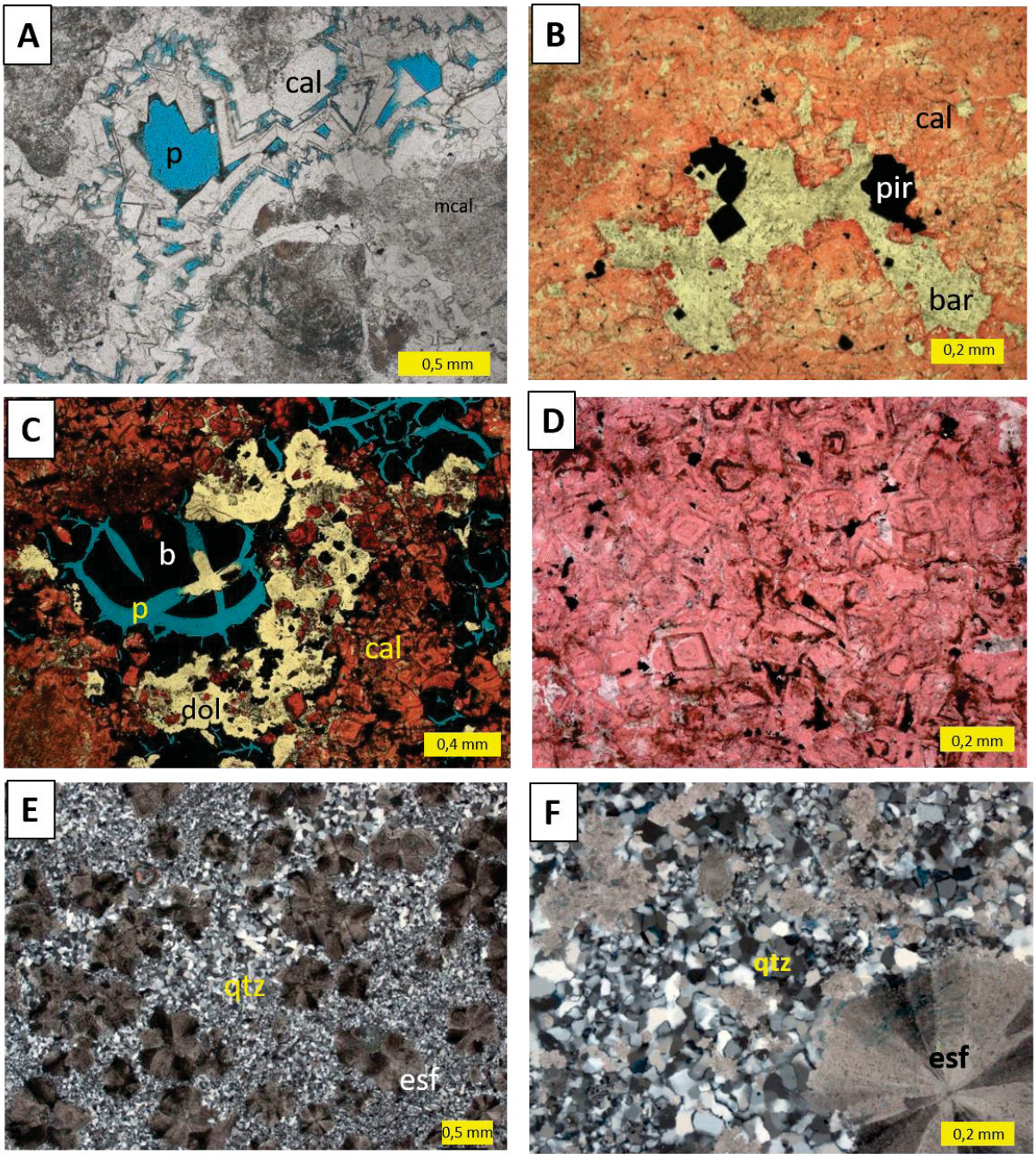

Figure 22 – Photomicrographs highlighting main diagenetic features. A) macrocrystalline escalenohedral calcite cement (cal) filling a vugular pore (p), note the intracristalline porosity caused the dissolution of some calcite phases; B) Pyrite (pir) and barite (bar) filling vugular pore in intermediate core section; C) bitumen (b), dolomite (dol), and calcite (cal) that replaced dolomite filling vugular pore (p) in intermediate core section; D) Detail of calcite with blocky habit testifying a domite dissolution phase replaced by calcite; E and F) Calcite spherulites exhibiting quartz matrix.

Table 3 – Paragenetic sequence interpreted for travertine facies from well SB-1.

Travertine facies (MCT-pe, MMC, CCL-sh)			
Paragenetic events	**Syndepos**	**Eodiagenesis**	**Mesodiagenesis/Hidrotermal**
Peloidal micrite			
Microcrystalline calcitic crust			
Fascicular calcite (shrubs)			
Calcite rim			
Calcite escalenohedral cement			
Calcite dissolution			
Microcrystalline dolomite			
Pore-filling saddle-dolomite			
Pore-filling macrocrystalline calcite			
Pore-filling quartz micro/macrocrystalline			
Pore-filling pyrite			
Pore-filling fluorite			
Pore-filling barite			
Pore-filling bitumen			

3.4.2 Qemscan analysis

The Qemscan data indicate that the most abundant mineral in thin section is calcite, covering an average of 74.30% of the analyzed area of the thin section, followed by quartz (average of 9.24%), and by dolomite (4.31%). Other minerals were also identified in quantities below 1%, they are: micas (Al micas + illite + smectites), pyrite, barite, carbon rich material (bitumen), goyazite, fluorite, Sr-barite, celestite, apatite, K-felspar, anhydrite, and stroncianite. The results obtained in QEMSCAN analyses are shown in Appendix 1.

Calcite in turn can be divided into 4 categories, according to its MgO content: Calcite 1 (0 to 1% MgO); Calcite 2 (1 to 4% MgO); Calcite 3 (4 to 7% MgO); Calcite 4 (7 to 10% MgO).

QEMSCAN analyzes, in addition to mineralogy, provided us with essential data regarding the 2D porosity of the rock obtained from de thin section. The most porous lithotype found in SB-1 is the GST that occurs at the base of the upper section with 26.14%, and the least porous is the silicified CCL-ef found in the basal section (1.87%).

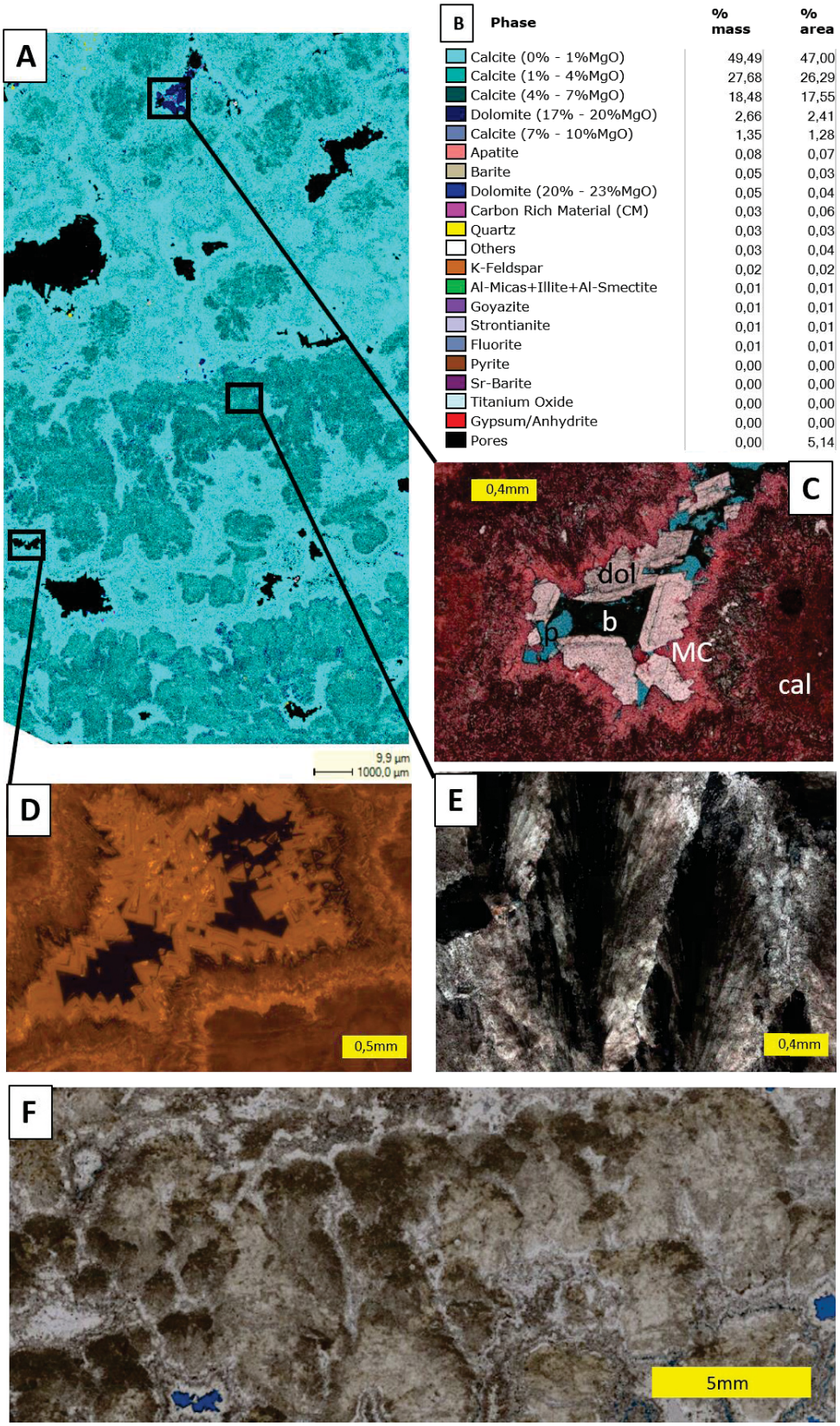

Figure 23 – Photomicrographs showing some aspects of CCL-sh. A and B) QEMSCAN results; C) pore cements filled with dolomite (dol), bitumen (b), microcrystalline calcite (cal), macro crystalline calcite (MC), and pore (p); D) Cathodoluminescence image showing zoned calcite cementation; E) cross-polarized view of fibrous calcite crystals with radiating extinction ans vertical crystals orientation; F) detail of shrubs under uncrossed polarizers.

3.4.3 Oxygen and Carbon Isotopes

The interpretation of isotopic signatures in travertines, especially oxygen and carbon, provides important information about the physical-chemical conditions of the precipitation, the influence of metabolic process, and, especially about the carbon dioxide source. In favorable circumstances, oxygen isotope provides information on the temperature at which deposition occurred. Carbon and oxygen isotope signals in some shallow-water carbonates in relatively closed systems have moderate preservation potential. Carbon may be preserved, oxygen isotope is commonly altered. Other elements such as hydrogen, strontium, and sulphur can also provide information on the parent rock, the provenance of solutes and, magmatic contributions of volatiles such as S and CO_2 (Flugel, 2004; Pentecost, 2005).

The range of bulk $\delta^{13}C$ values for all analyzed carbonates is quite wide, varying between -25.64‰ and 1.38‰ . If were consider the $\delta^{13}C$ range values only for the travertine section (intermediate) is relatively narrow, varying between -4.52‰ and 1.38‰ (Figure 25). The range of $\delta^{13}C$ for three different carbonate phases are: 1) -2.49 to 2.62‰ for syngenetic fascicular calcite (CCL-sh); 2) 0.49 to 2.25‰ for micritic calcite crust (MCC) , and 3) -0.76 to 0.68‰ for peloidal micrite (MCT-pe).

In contrast to the $\delta^{13}C$, the bulk $\delta^{18}O$ values from the analyzed carbonates show a narrow variation range varying between -3.92‰ to 1.52‰ (Figure 25). The averages per core section show significant differences, as shown in table 3. The range of $\delta^{18}O$ for three different carbonate phases are: 1) -2.32 to 0.73‰ for syngenetic fascicular calcite (CCL-sh); 2) -1.55 to 0.22 ‰ for micritic calcite crust (MCC) , and 3) -5.77 to 0.48‰ for peloidal micrite (MCT-pe).

Table 4 - $\delta^{18}O$ - $\delta^{13}C$ Mean per core section of SB-1 (for bulk samples)

	$\delta^{18}O$ Mean (‰ VPDB)	$\delta^{18}O$ Range (‰ VPDB)	$\delta^{13}C$ Mean (‰ VPDB)	$\delta^{13}C$ Range (‰ VPDB)
Upper section	-0.44	-2.27 – 1.23	-12.95	-25.64 – 0.75
Intermediate section	-1.20	-3.92 – 1.52	-1.37	-3.16 – 0.87
Basal section	-2.00	-2.90 – -0.62	-2.31	-4.79 - -0.71

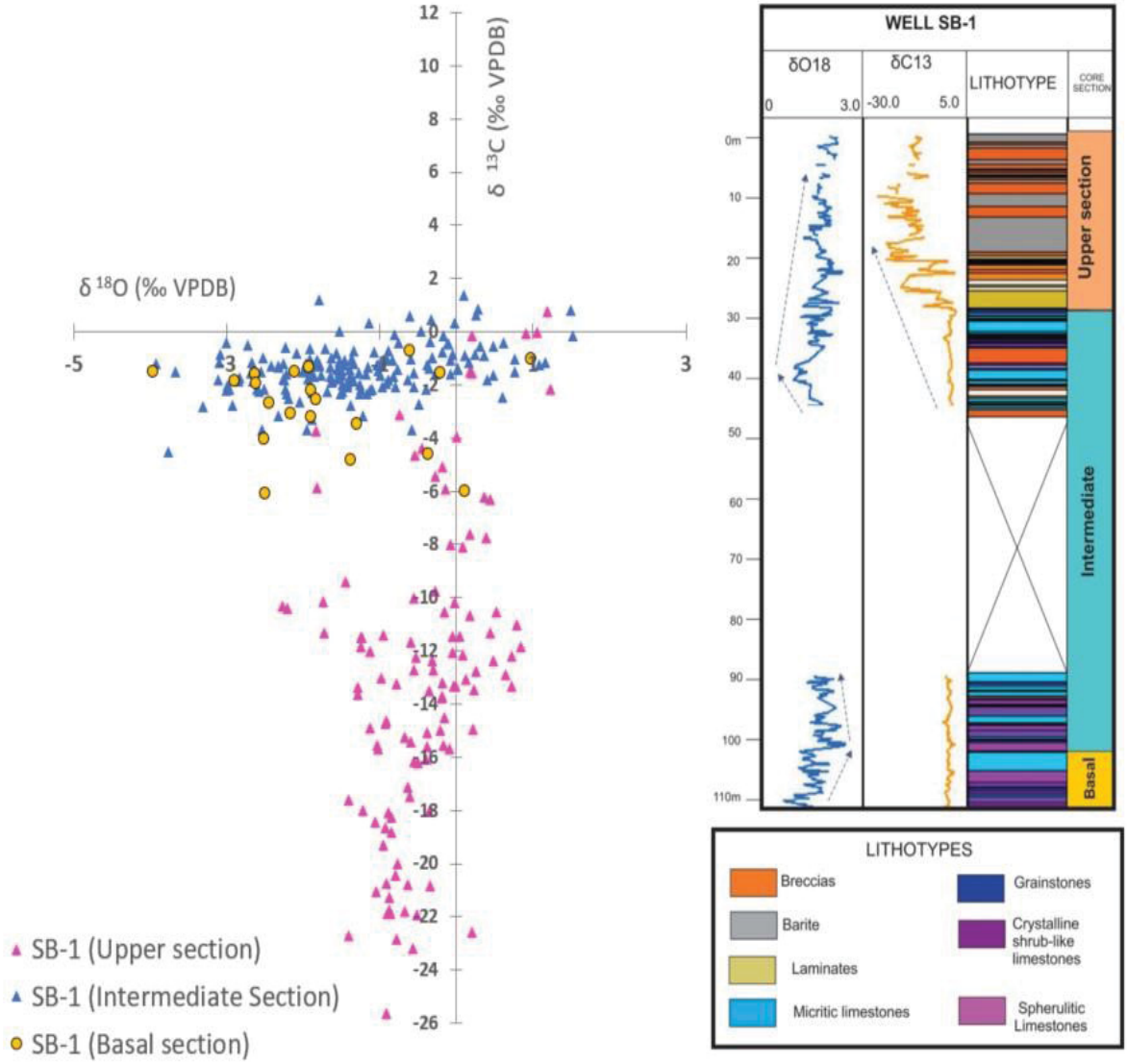

Figure 24 - $\delta^{18}O$ - $\delta^{13}C$ cross-plot of bulk samples per core section, and values plotted vertically along the stratigraphic section of SB-1.

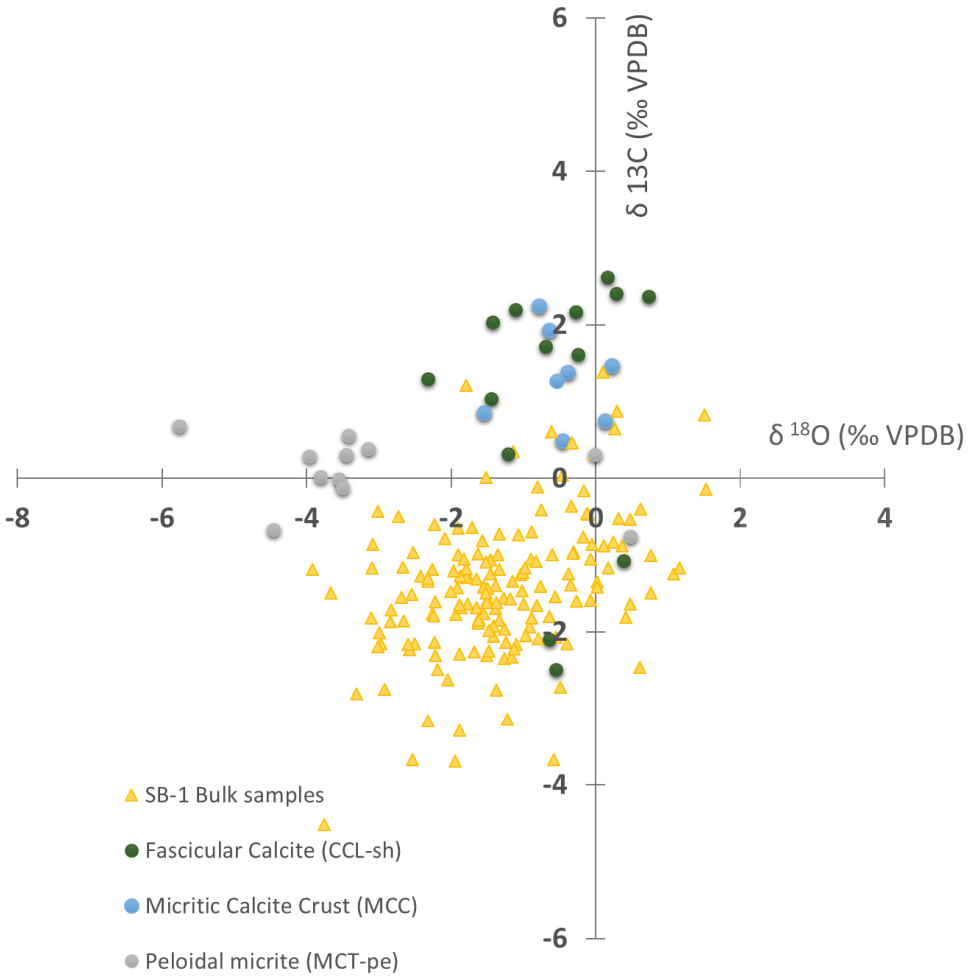

Figure 25 - $\delta^{18}O$ - $\delta^{13}C$ cross-plot of intermediate core section. Bulk samples (yellow triangules), and values by selected lithotypes CCL-sh (green circles), MCC (light blue circles), and MCT-pe (grey circles).

3.5 DISCUSSION

Regarding the macroscopic description, the whole core can be divided into three distinct intervals (Figure 12 and Figure 13):

(I) The basal section composed of an intercalation of peloidal micritic limestones with predominant spherulitic crystalline limestones, crystalline shrub-like crusts and grainstones. The basal section has been interpreted as lacustrine, mostly due to the similarity of the

spherulitic limestone (CCL-ef) with the spherulites described in literature as typical lacustrine spherulites in the Pre-Salt of Santos and Campos Basin (Pietzsch et al., 2018; Farias et al., 2019; Lima and De Ros, 2019; Gomes et al., 2020). It is the only one of the three sections in which ostracods up to 1 mm in length have been described. On the contrary to the intermediate section, where most of the rocks are cemented by calcite, rocks in the basal section are cemented by silica and dolomite, as commonly seen in the spherulites of the Pre-Salt. From the top of this section onwards, the travertine system begins to be installed.

(II) The intermediate portion of the core contains the rocks which is most interest in this study. Compared to the basal section, the most significant change concerns in texture: the crystalline fabrics changes into a microcrystalline where a clotted texture predominates. In addition, ostracodes are absent here in the intermediate section. The crust-like appearance becomes more evident in this section. Cementation by quartz and dolomite, common in the basal section, gives place to calcite cement (bladed, prismatic fringes, dog-tooth, and scalenohedral types). Another significant change between the basal and intermediate sections concerns oxygen isotopes. There is a notable change in the boundary basal-intermediate sections: Oxigen becomes slightly positive, suggesting a more evaporative environment supporting the idea of the onset of a travertine system outbidding a lacustrine system – at least in the area of the SB-1 well. This interval also contains at its top the abrupt contact between a grainstone/rudstone composed of carbonate particles (rounded carbonate grains) without apparent organization under a calcitic crust with an angle of approximately 40º. On the macro-scale, the intermediate is the portion of the core that contains more calcite crusts, similar to those in classic travertine systems.

(III) The upper part is characterized by a very significant textural change compared to the intermediate interval and basal sections. These intervals are intensely brecciated, fractured, and baritized, and in most cases, it is no longer possible to identify the original lithotype.

The petrographic analysis indicated a fundamental difference between the studied well and previous petrographic analysis reported in the literature in other wells from the same geologic unit (Barra Velha Formation): absence of some ‘‘typical’’ facies such as Mg-clay laminites with or without spherulites, composed macroscopically of alternate light and dark carbonate bands, wavy and/or crenulated, with various degrees of dolomitization and silicification.

In previous works where the Pre-Salt spherulitites were described, one of the hypotheses is that these calcite spheres are generated inside a sediment as eodiagenetic elements. In this case, the calcite spherulites occur replacing and displacing the pre-existing sediment (a laminated Mg-clay deposits, for example), suggesting that they grow in the middle of the sediment while unconsolidated in a very early stage of burial (Wright and Barnett, 2015; Wright and Tosca, 2016; Herlinger et al., 2017; Lima and De Ros, 2019; Gomes et al., 2020). Its precipitation would be associated with changes in water chemistry and hydrodynamic conditions, probably an increase in the concentration of calcium ions in the aqueous body possibly caused by an increment in the evaporation rate (Falcao, 2015; Pietzsch et al., 2018; Lima and De Ros, 2019; Gomes et al., 2020).

In some wells, it is still possible to see this preserved clay, which corroborates the theory that spherulites are eodiagenetic elements (Saller et al., 2016; Herlinger et al., 2017; Sartorato, 2018; Lima and De Ros, 2019; Gomes et al., 2020), but this is not the case in well SB-1, where Mg-clay was not observed. If this fine sediment exists, the hypothesis is that it had been dissolved. The spherulites of lithotype CCL-ef are coated by calcite fringes ou quartz mosaic. Falcão (2015) also raised the possibility that these spherulites may have originated within bodies of aqueous water, under a very shallow water layer (mm to cm thick), similar to what occurs in modern travertine environments such as Catamarca in Argentina and Mammoth Hot Springs in Yellowstone.

The main Pre-Salt reservoirs have been described as crusts made of coalescent aggregates of fibrous fascicular optic calcite similar to what Grotzinger and Knoll (1999) called ‘‘abiotic’’ stromatolites formed by the accretion of carbonate sediments through physical processes. For Chafetz and Guidry (1999), the crystal-ray shrubs from Barra Velha Formation are a product of abiotic precipitation related to CO_2 loss and evaporation characteristic of some travertine facies.

Another significative petrographic distinction concerns on cement types: in the SB-1 intermediate section predominates calcite fringes or calcitic mosaics; whereas in other Pre-Salt carbonates, predominate dolomite and silica as major cements (Saller et al., 2016; Sartorato, 2018; Farias et al., 2019; Lima and De Ros, 2019; Gomes et al., 2020). Silica phases occur in the basal section and can be identified especially in the CCI-ef, filling interparticle pores, and causing a significant reduction in porosity, in some cases so drastically as to be less than 2%.

Regarding the data obtained by QEMSCAN analyses, they also corroborate the division of the core into three sections, as can be seen in Figure 26. In the basal section, it is possible to observe the calcitic composition of the elements (spherulites) with their predominantly quartz cementation. In the intermediate section, the domain is essentially calcite with different proportions of MgO. In this interval, the thin sections analyzed by QEMSCAN showed to be composed of 74% calcite, on average. In the upper portion, the dominant mineralogy is quartz, dolomite, and barite. This data is very useful because, in addition to the percentage, it provides us images that allow us to observe how the minerals (especially those in small proportions, less than 1%) are distributed on the rock and also give us very clear information about pore shapes, percentage, rock textures, and pore filling.

The uppermost interval was not studied in detail in the present work. However, some aspects should be highlighted, such as the exotic paragenesis compared to a typical carbonate system (barite, anhydrite, Sr-barite, fluorite, pyrite, bitumen), intense fracturing, and brecciated intervals hindering the original lithology. Most likely, the brecciation and barite precipitation are related to hydrothermal fluids in a later diagenetic phase, as shown by petrographic analyses and corroborated by significant negative values both in oxygen and carbon isotopic data. Similar paragenesis was described in Pre-Salt carbonate reservoirs of the northern Campos Basin, and fluid inclusions with temperatures of 92-152ºC characterized a hydrothermal system chemically compared to those that form carbonate hosted Pb-Zn Mississipi Valey (MVT) and Irish-type deposits (Lima et al., 2020).

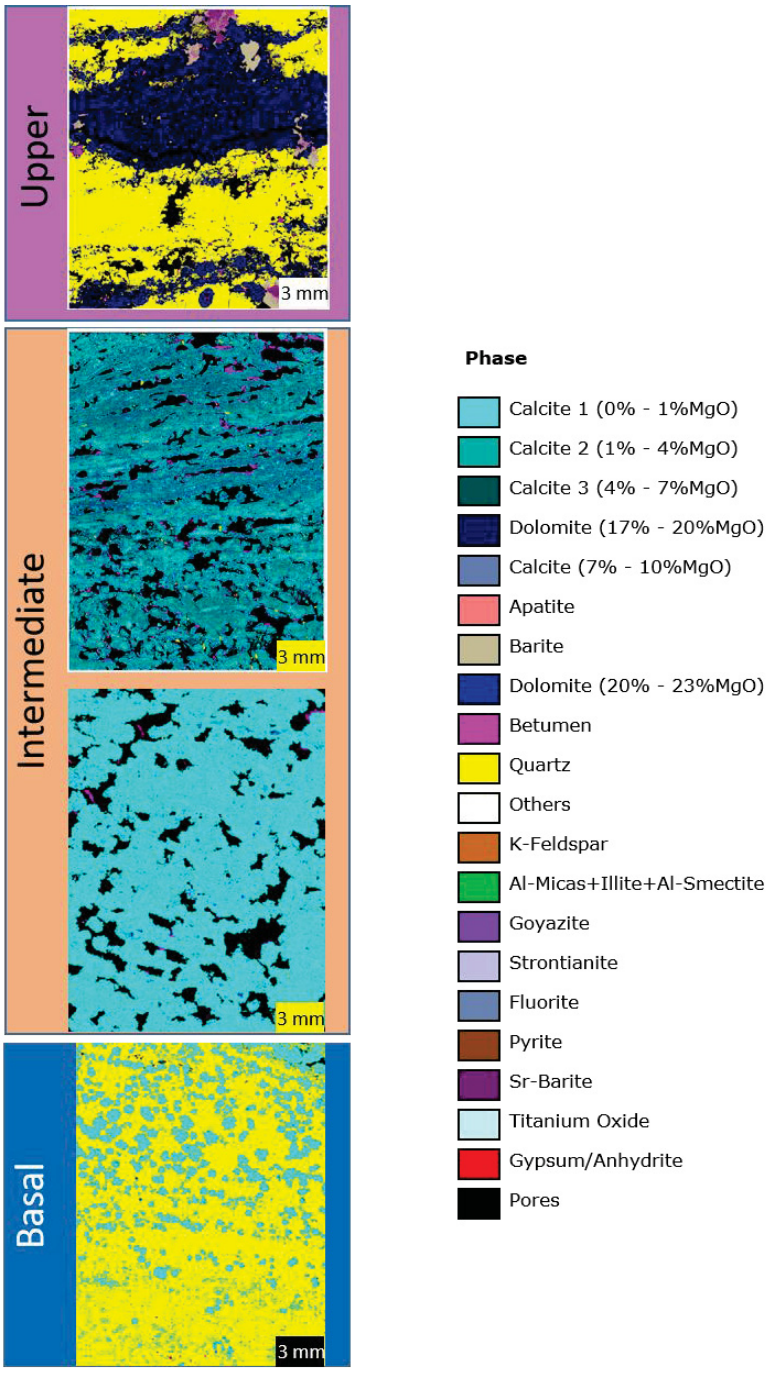

Figure 26- QEMSCAN results of 4 representative thin sections of SB-1. Upper section: characterized by an intensely brecciated and baritized interval where, in most cases, it is no longer possible to identify the original lithotype, commonly cemented by quartz (yellow), dolomite (dark blue), barite (gray) and Sr-barite (dark-purple). Intermediate section: predominates microcrystalline calcite fabrics, clotted peloidal textures, calcite crusts, and calcite cement. Basal: spherulitic crystalline limestone (CCL-ef) from basal section. On the contrary to the intermediate section, where most of the rocks are cemented by calcite, rocks in the basal section are cemented by silica (yellow) and dolomite (dark blue).

The Pre-Salt carbonate data from SB-1 show a bimodal distribution for $\delta^{13}C$ bulk samples (Figure 24, pink and blue triangles). The most negative values for $\delta^{13}C$ (between -5‰ to -25.64‰) correspond to the intensely fractured portion in the uppermost core section, where bitumen, dolomite, quartz, and barite cement predominates, with smaller proportion of pyrite, anhydrite, fluorite, and Sr-barite. These values are compatible with the $\delta^{13}C$ isotopic signature (between -22 to -26‰.) observed in rare mantle xenoliths from non-hotspot volcanoes (Deines, 2002).

For the intermediate section, the $\delta^{18}O$ values ranging from -4.52‰ to +1.38‰ VPDB, with $\delta^{13}C$ distribution between -3.92 and 1.52‰ VPDB, are related with classical travertine facies such as crystalline calcite crusts (MCC), microcrystalline peloidal clotted carbonates (MCT-pe), and arborescent limestones (CCL-sh), commonly present in cores 3, 4, 5, and 6. Such isotopic data is somewhat distinct from more evaporitic isotopic data as proposed by (Farias et al., 2019) for the Pre-Salt carbonates of the Santos Basin, but not so different from isotopic data of the carbonates described by Lima et al. (2020) in the Campos Basin.

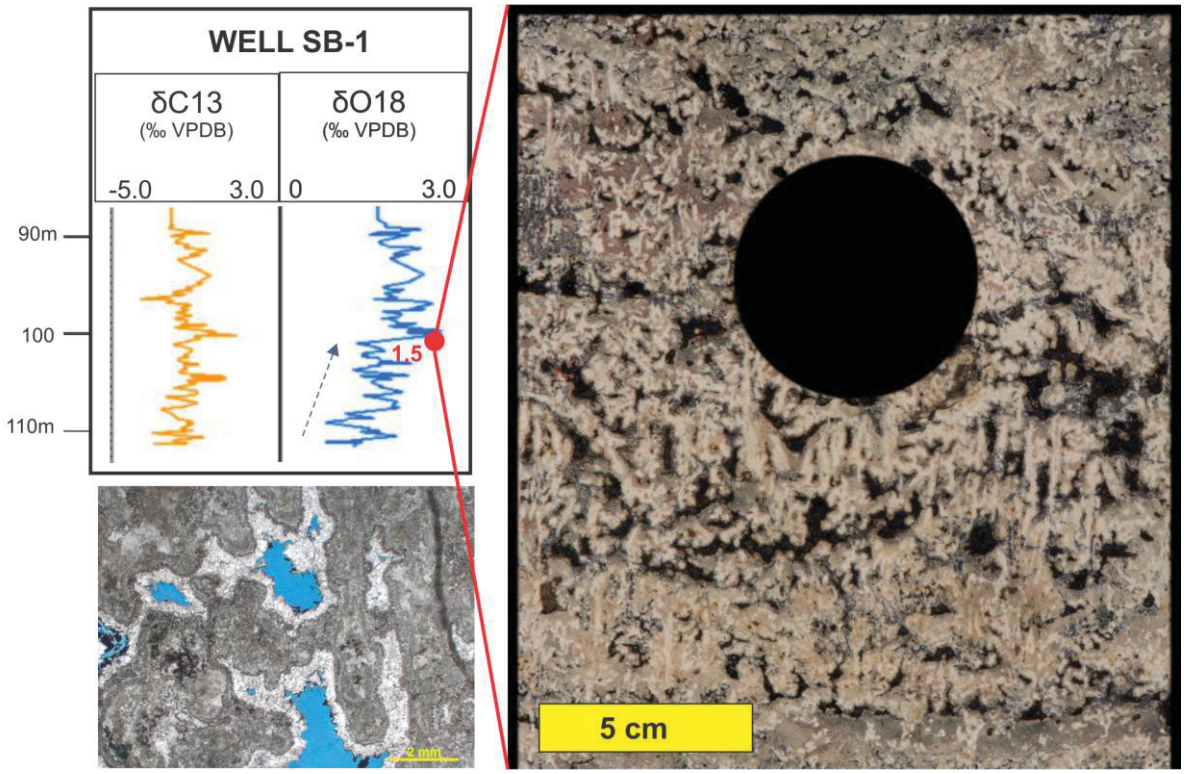

Figure 27 – Detail of micro-karst features on macro-scale and petrography. Isotope signature showing a positive peak, probably associated with a subareal environment or indicating a more evaporative system.

There is an interval that shows a significant positive $\delta^{18}O$ value in the intermediate section (Figure 27). Positive $\delta^{18}O$ values are typical from evaporative systems and can be used as indicative of evaporated endorheic saline lakes, common in closed basins within rift settings, such as in the East African rift lakes. $\delta^{18}O$ in lakes is positive because evaporation favors the escape of light isotope ^{16}O to the atmosphere. In closed systems, the water resides long times in the basin, allowing its isotopic signatures to be influenced by evaporation. In SB-1, this positive $\delta^{18}O$ peak occurs in the facies that presents microkarst features, which also corroborates for an interpretation of a more evaporative environment, probably subaerial (Figure 27).

When we look at $\delta^{18}O$ - $\delta^{13}C$ cross-plot (Figure 25), which shows the data from the punctual analysis of 3 distinct carbonate phases, it is possible to verify that the $\delta^{13}C$ values are more positive when compared to the bulk samples. The data displacement is also observed in the $\delta^{18}O$, in which the MCT-pe is more negative than the bulk samples. The highest $\delta^{13}C$ values and the lowest $\delta^{18}O$ observed represent the original carbon isotopic of the hydrothermal fluid that was responsible for travertine precipitation.

Comparing the bulk and punctual data of the intermediate interval, we notice that the original precipitated rock (travertine) underwent complex and heterogeneous diagenetic alterations throughout its history. At least one more post-diagenetic event, likely associated with Late Cretaceous or Paleogene magmatic activity, occurred. This event triggered fault reactivation and caused a new pulse of hydrothermal fluids, which controlled the creation, dissolution, and obliteration of the porosity in Pre-Salt reservoirs. This pulse drastically altered the rocks in the upper section of SB-1 core to the point of making them unrecognizable in some samples. The intermediate section may have been less affected by this hydrothermal pulse than the upper interval, which could explain the shift between the isotopic signature of the $\delta^{13}C$ collected punctually in the specific lithotypes and the bulk data. The result of $\delta^{13}C$ bulk signature would be, therefore, a mixture between the $\delta^{13}C$ of the original travertine with the signature of the hydrothermal fluid responsible for the baritization of the upper section and the precipitation of minerals typical of hydrothermal parageneses, such as pyrite, barite, Sr-barite, fluorite, anhydrite, goyazite, and bitumen.

The oxygen isotope from SB-1 well $\delta^{18}O$ values point to a deeper origin or a mixture with meteoric water, but purely surface meteoric water is excluded. Large-scale diagenetic alterations were described in SB-1 but mainly in the basal and upper sections. However, recrystallization has been observed especially in these sections and could imply a resetting of the depositional stable isotopic signature. It was considered that the main recrystallization phases are early diagenetic in the intermediate section, caused by the percolation of waters from the same system that originates the travertine rock, therefore not being able to fully reset isotopic signature.

Being the $\delta^{13}C$ signature, the result of the contribution of CO_2 in the precipitation process, the values that were observed especially in the upper section indicate a deeper origin, probably with mantellic contribution for the post depositional event. The negative values of $\delta^{13}C$ (between -5‰ to -25.64‰) found in SB-1 are compatible with the $\delta^{13}C$ isotopic signature (between -22 to -26‰.) observed in rare mantle xenoliths from non-hotspot volcanoes (Deines, 2002).

This hypothesis is also corroborated by He isotopes ($^3He/^4He$) measured from petroleum samples in the Santos Basin (Santos Neto et al., 2012). Helium molecules do not migrate alone from the mantle but together with CO_2 and other volatiles. When measuring this associated helium is possible to trace CO_2 origin. The high R/Ra up to 5.60 ($^3He/^4He$) measured by Santos Neto et al. (2012) suggest mantellic origin.

This mantellic source would be associated with the serpetinization of the upper mantle, occurring below areas with strongly thinned continental crust or even through direct mantle exhumation (Manatschal and Bernoulli, 1999; Zalán et al., 2011; Gamboa et al., 2019; Lima et al., 2020).

Another probable source of CO_2 that also explain the $\delta^{13}C$ values is related to the contribution of light carbon derived by organic matter alteration, microbiological activity, diagenetic processes, or by the interaction of the CO_2 with sediments with lighter isotopic composition, such as the rocks of the rift section of the Santos Basin.

Apparently, the breccias described in this well are of tectonic origin, associated with mapped seismic faults close to the well (Figure 28). Probably the same faults are responsible for carrying the hydrothermal fluid rich in CO_2 from which travertine precipitated. However, it is likely that these same faults have been reactivated at later times in geological history, serving as a conduit for hydrothermal fluids from other phases, likely associated with Late Cretaceous or Paleogene

magmatic activity that controlled creation, dissolution, and obliteration of the porosity in Pre-Salt reservoirs. The pathways for these hydrothermal fluids were probably the same deep fault system used for oil and CO_2 migration. The salt layer on top worked as seal rocks for both hydrocarbon and hydrothermal fluids.

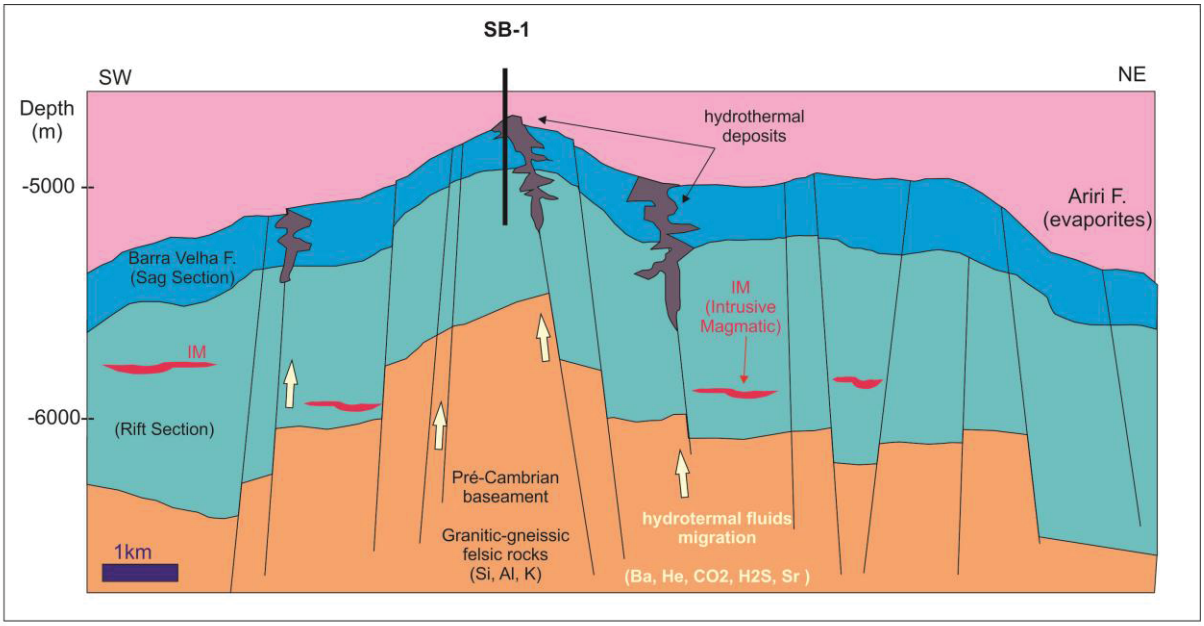

Figure 28 – Schematic section (SW-NE) with the location of SB-1 well and the representation of the fault-focused hydrothermal system that probably originate the travertine deposit and was the responsible form mixing hydrothermal fluids, water from de granitic-gneissic felsic basement, fluids from Rift Section and mantle.

3.6 CONCLUSIONS

Although many authors agree that shrubby fabrics resemble travertine (Wright and Barnett, 2015; Saller et al., 2016; Souza et al., 2018; Farias et al., 2019), most of the shrubby facies studied in the Santos Basin are not interpreted as travertine. However, for the studied interval in the present work, we believe otherwise. The 35 m of cored rock in well SB-1 is herein interpreted as travertine due to the following features:

1. Bedding with slopes greater than 40 degrees with convex features that are similar to those described in the Slope Depositional System of modern travertine systems;

2. Signature of stable isotopes $\delta^{13}C$ and $\delta^{18}O$ differentiated from other Pre-Salt rocks;
3. Micro karst features that resemble subaerial environments associated with $\delta^{18}O$ evaporative signatures;
4. Presence of paper thin-rafts and coated gas bubbles;
5. Petrographic features significantly different from those described in other Pre-Salt wells, such as predominantly calcite cement instead of silica or dolomite, presence of scalenohedral calcite, absence or rare eodiagenetic dolomite in thin sections.

The predominance of calcite cement (instead of silica and dolomite) and the absence of some typical Pre-Salt lithotypes such as laminites and laminated Mg clay deposits also indicate that the diagenetic history of the rocks from this well differs from other areas described in the literature. Besides petrography, isotopic data also corroborated this hypothesis.

The comparison between punctual and bulk $\delta^{13}C$ and $\delta^{18}O$ values indicate that the fault-focused hydrothermal system acting in this well is probably the result of a mix of fluids prevenient of several sources such as interaction with sag and rift successions of Santos Basin, intrusive magmatic rocks, granitic-gneissic basement, and mantellic origin by the exhumation of the asthenosphere. So, the final fluid would be a blend of all these sources, and therefore very difficult to reliably quantify.

Exotic paragenesis compared to a typical carbonate system (barite, anhydrite, Sr-barite, fluorite, pyrite, bitumen), intense fracturing, and brecciated intervals hindering the original lithology supported by significant negative values in oxygen and carbon isotopic data allowed us to recognize that hydrothermal fluids percolated the reservoir of well SB-1. The first hydrothermal fluid was responsible for travertine precipitation (Aptian age). Later, a different fluid, likely associated with Late Cretaceous or Paleogene magmatic activity, had a strong post-depositional impact on this reservoir's porosity, permeability, and heterogeneity, affecting the production performance of this reservoir. Despite the cementing effect obliterating porosity and therefore negatively impacting reservoir production at first, other processes such as intense fracturing, brecciation, and creation of preferential paths generally improve the productivity of these pre-salt reservoirs.

REFERENCES

Altunel, E., and Hancock, P.L., 1993, Active fissuring and faulting in Quaternary travertines at Pamukkale, western Turkey: Zeitschrift fur Geomorphologie, Supplementband, v. 94, p. 285–302.

Artagão, V. de M., 2018, Universidade do Estado do Rio de Janeiro Centro de Tecnologia e Ciências Faculdade de Geologia Victor de Mello Artagão Análise estratigráfica de alta resolução aplicada aos depósitos da Formação Barra Velha , Bacia de Santos : identificação , correlação e:

Bargar, K., 1978, Geology and Thermal History of Mammoth Hot Springs, Yellowstone National Park, Wyoming: Geological Survey Bulletin, v. 1444.

Brogi, A., Capezzuoli, E., Alçiçek, M.C., and Gandin, A., 2014, Evolution of a fault-controlled fissure-ridge type travertine deposit in the western Anatolia extensional province: The Çukurbağ fissure-ridge (Pamukkale, Turkey): Journal of the Geological Society, v. 171, p. 425–441, doi:10.1144/jgs2013-034.

Cainelli, C., and Mohriak, W.U., 1999, Some remarks on the evolution of sedimentary basins along the Eastern Brazilian continental margin: Episodes, v. 22, p. 206–216, doi:10.18814/epiiugs/1999/v22i3/008.

Capezzuoli, E., Gandin, A., and Pedley, M., 2014, Decoding tufa and travertine (fresh water carbonates) in the sedimentary record : The state of the art: , p. 1–21, doi:10.1111/sed.12075.

Carminatti, M., Wolff, B., and Gamboa, L., 2008, New Exploratory Frontiers In Brazil: 19th World Petroleum Congress, p. 11, https://doi.org/.

Chafetz, H.S., and Folk, R.L., 1984, Travertines: deposicional morphology and bacterially constructed constituents: Journal of Sedimentary Petrology, v. 54, p. 289–316.

Chafetz, H.S., and Guidry, S.A., 1999, Bacterial shrubs, crystal shrubs, and ray-crystal shrubs: Bacterial vs. abiotic precipitation: Sedimentary Geology, v. 126, p. 57–74, doi:10.1016/S0037-0738(99)00032-9.

Claes, H., Soete, J., Van Noten, K., El Desouky, H., Erthal, M.M., Vanhaecke, F., Özkul, M., and Swennen, R., 2015, Sedimentology, three-dimensional geobody reconstruction and carbon dioxide origin of pleistocene travertine deposits in the Ballık area (South-west Turkey): Sedimentology, v. 62, p. 1408–1445, doi:10.1111/sed.12188.

Crossey, L.J., Fischer, T.P., Patchett, P.J., Karlstrom, K.E., Hilton, D.R., Newell, D.L., Huntoon, P., Reynolds, A.C., and de Leeuw, G.A.M., 2006, Dissected hydrologic system at the Grand Canyon: Interaction between deeply derived fluids and plateau aquifer waters in modern springs and travertine: Geology, v. 34, p. 25–28, doi:10.1130/G22057.1.

Deines, P., 2002, The carbon isotope geochemistry of mantle xenoliths: Earth-Science Reviews, v. 58, p. 247–278, doi:10.1016/S0012-8252(02)00064-8.

Dias, J.L., 2005, Tectonic Stratigraphy and Sedimentation during the Aptian along the Brazilian Eastern Margin: Boletim de Geociências da Petrobras, v. 13, p. 7–25.

Erthal, M.M., Capezzuoli, E., Mancini, A., Claes, H., Soete, J., and Swennen, R., 2017, Shrub morpho-types as indicator for the water flow energy - Tivoli travertine case (Central Italy): Sedimentary Geology, v. 347, p. 79–99, doi:10.1016/j.sedgeo.2016.11.008.

Falcão, L.C., 2015, Estudo faciológico de um intervalo aptiano do poço SB-1 (Bacia de Santos) e sua comparação com travertinos quaternários de San Juan, Argentina: Universidade Federal Fluminense.

Farias, F., Szatmari, P., Bahniuk, A., and França, A.B., 2019, Evaporitic carbonates in the pre-salt of Santos Basin – Genesis and tectonic implications: Marine and Petroleum Geology, v. 105, p. 251–272, doi:10.1016/j.marpetgeo.2019.04.020.

Fetter, M., Penteado, H., Madrucci, V., and Spadini, A., 2018, The Paleogeography of the Lacustrine Rift System of the Pre-Salt in Santos Basin, Offshore Brazil: AAPG 2018 Annual Convention & Exhibition, v. 11137, p. 39, doi:10.1306/11137Fetter2018.

Flugel, E., 2004, Microfacies of Carbonate Rocks: New York, Springer-Verlag.

Ford, T.D., and Pedley, H.M., 1996, A review of tufa and travertine deposits of the world: Earth-Science Reviews, v. 41, p. 117–175, doi:10.1016/s0012-8252(96)00030-x.

Gamboa, L., Ferraz, A., Baptista, R., and Santos Neto, E. V., 2019, Geotectonic controls on CO2formation and distribution processes in the Brazilian pre-salt basins: Geosciences (Switzerland), v. 9, p. 1–14, doi:10.3390/geosciences9060252.

Gomes, J.P., Bunevich, R.B., Tedeschi, L.R., Tucker, M.E., and Whitaker, F.F., 2020, Facies classification and patterns of lacustrine carbonate deposition of the Barra Velha Formation, Santos Basin, Brazilian Pre-salt: Marine and Petroleum Geology, v. 113, p. 104176, doi:10.1016/j.marpetgeo.2019.104176.

Gomes, P.O., Kilsdonk, B., Minken, J., Grow, T., and Barragan, R., 2009, The Outer High of the Santos Basin, Southern São Paulo Plateau, Brazil: Pre-Salt Exploration Outbreak, Paleogeographic Setting, and Evolution of the Syn-Rift Structures, #10193 (2009): AAPG 2008 International Convention & Exhibition, file:///Users/AOM/Dropbox/Papers2/Articles/Paulo Ot?vio Gomes/Paulo Ot?vio Gomes 2013.pdf%5Cnpapers2://publication/uuid/71AE335C-F853-4C08-86C4-59EFF1543145.

Grotzinger, J.R., and Knoll, A.H., 1999, Stromatolites in Precambrian carbonates: Evolutionary mileposts or environmental dipsticks? Annual Review of Earth and Planetary Sciences, v. 27, p. 313–358, doi:10.1146/annurev.earth.27.1.313.

Guo, L., and Riding, R., 1998, Hot-spring travertine facies and sequences, Late Pleistocene, Rapolano Terme, Italy: Sedimentology, v. 45, p. 163–180, doi:10.1046/j.1365-3091.1998.00141.x.

Hancock, P.L., Chalmers, R.M.L., Altunel, E., and Çakir, Z., 1999, Travitonics: Using travertines in active fault studies: Journal of Structural Geology, v. 21, p. 903–916, doi:10.1016/S0191-8141(99)00061-9.

Herlinger, R., Zambonato, E.E., and De Ros, L.F., 2017, Influence of diagenesis on the quality of lower cretaceous pre-salt lacustrine carbonate reservoirs from northern Campos Basin, Offshore Brazil: Journal of Sedimentary Research, v. 87, p. 1285–1313, doi:10.2110/jsr.2017.70.

Hutcheon, I., Abercrombie, H.J., and Krouse, H.R., 1990, Inorganic origin of carbon dioxide during low temperature thermal recovery of bitumen: Chemical and isotopic evidence: Geochimica et Cosmochimica Acta, v. 54, p. 165–171, doi:10.1016/0016-7037(90)90204-X.

Janssens, N., Capezzuoli, E., Claes, H., Muchez, P., Yu, T.L., Shen, C.C., Ellam, R.M., and Swennen, R., 2020, Fossil travertine system and its palaeofluid provenance, migration and evolution through time: Example from the geothermal area of Acquasanta Terme (Central Italy): Sedimentary Geology, v. 398, p. 105580, doi:10.1016/j.sedgeo.2019.105580.

Jones, B., and Renaut, R.W., 2010, Chapter 4 Calcareous Spring Deposits in Continental Settings, *in* Developments in Sedimentology, Elsevier, v. 61, p. 177–224, doi:10.1016/S0070-4571(09)06104-4.

Kampman, N., Burnside, N.M., Shipton, Z.K., Chapman, H.J., Nicholl, J.A., Ellam, R.M., and Bickle, M.J., 2012, Pulses of carbon dioxide emissions from intracrustal faults following climatic warming: Nature Geoscience, v. 5, p. 352–358, doi:10.1038/ngeo1451.

Lima, B.E.M., and De Ros, L.F., 2019, Deposition, diagenetic and hydrothermal processes in the Aptian Pre-Salt lacustrine carbonate reservoirs of the northern Campos Basin, offshore Brazil: Sedimentary Geology, v. 383, doi:10.1016/j.sedgeo.2019.01.006.

Lima, B.E.M., Tedeschi, L.R., Pestilho, A.L.S., Santos, R.V., Vazquez, J.C., Guzzo, J.V.P., and De Ros, L.F., 2020, Deep-burial hydrothermal alteration of the Pre-Salt carbonate reservoirs from northern Campos Basin, offshore Brazil: Evidence from petrography, fluid inclusions, Sr, C and O isotopes: Marine and Petroleum Geology, v. 113, p. 104143, doi:10.1016/j.marpetgeo.2019.104143.

Manatschal, G., and Bernoulli, D., 1999, Architecture and tectonic evolution of nonvolcanic margins: Present-day Galicia and ancient Adria: Tectonics, v. 18, p. 1099–1119, doi:10.1029/1999TC900041.

Melo Garcia, S.F. de, Letouzey, J., Rudkiewicz, J.L., Danderfer Filho, A., and Frizon de Lamotte, D., 2012, Structural modeling based on sequential restoration of gravitational salt deformation in the Santos Basin (Brazil): Marine and Petroleum Geology, v. 35, p. 337–353, doi:10.1016/j.marpetgeo.2012.02.009.

Mizusaki, A.M.P., Petrini, R., Bellieni, P., Comin-Chiaramonti, P., Dias, J., De Min, A., and Piccirillo, E.M., 1992, Basalt magmatism along the passive continental margin of SE Brazil (Campos basin): Contributions to Mineralogy and Petrology, v. 111, p. 143–160, doi:10.1007/BF00348948.

Moreira, J.L.P., Valdetaro, C., Gil, J.A., and Machado, M.A.P., 2007, Superseqüência Pós-Rifte: Boletim de Geociencias da Petrobras, v. 15, p. 531–549.

Mors, R.A., Astini, R.A., and Gomez, F.J., 2019, Coexisting active travertines and tufas in the southeastern border of the Puna plateau: Sedimentary Geology, v. 389, p. 200–217, doi:10.1016/j.sedgeo.2019.06.009.

Muir-Wood, R., and King, G.C.P., 1993, Hydrological signatures of earthquake strain: Journal of Geophysical Research, v. 98, doi:10.1029/93jb02219.

Muniz, M.C., and Bosence, D.W.J., 2015, Pre-salt microbialites from the Campos Basin (offshore Brazil): Image log facies, facies model and cyclicity in lacustrine carbonates: Geological Society Special Publication, v. 418, p. 221–242, doi:10.1144/SP418.10.

Özkul, M., Kele, S., Gökgöz, A., Shen, C.C., Jones, B., Baykara, M.O., Fórizs, I., Németh, T., Chang, Y.W., and Alçiçek, M.C., 2013, Comparison of the Quaternary travertine sites in the Denizli extensional basin based on their depositional and geochemical data: Sedimentary Geology, v. 294, p. 179–204, doi:10.1016/j.sedgeo.2013.05.018.

Özkul, M., Varol, B., and Cihat Alçiçek, M., 2002, Depositional Environments and Petrography oDenizli Travertines: Mineral Res. Expl. Bul, v. 125, p. 13–29.

Pedley, H.M., 1990, Classification and environmental models of cool freshwater tufas: Sedimentary Geology, v. 68, p. 143–154, doi:10.1016/0037-0738(90)90124-C.

Pentecost, A., 1993, British travertines : a review: Proceedings of the Geologists' Association, v. 104, p. 23–39, doi:10.1016/S0016-7878(08)80152-6.

Pentecost, A., 2005, Travertine: Springer Netherlands, 446 p., doi:10.1007/1-4020-3606-X.

Pentecost, A., and Viles, H., 1994, A Review and Reassessment of Travertine Classification: Géographie physique et Quaternaire, v. 48, p. 305–314, doi:10.7202/033011ar.

Pereira, M.J., and Feijó, F.J., 1994, Bacia de Santos. Estratigrafiadas Bacias Sedimentares do Brasil: Boletim de Geociênciasda Petrobrás, v. 8, p. 219–234.

Pereira, M.J., and Macedo, J.M., 1990, A Bacia de Santos: perspectivas de uma nova provincia petrolifera na plataforma continental sudeste Brasileira: Boletim de Geociencias - Petrobras, v. 4, p. 3–11.

Pietzsch, R., Oliveira, D.M., Tedeschi, L.R., Queiroz Neto, J. V., Figueiredo, M.F., Vazquez, J.C., and de Souza, R.S., 2018, Palaeohydrology of the Lower Cretaceous pre-salt lacustrine system, from rift to post-rift phase, Santos Basin, Brazil: Palaeogeography, Palaeoclimatology, Palaeoecology, v. 507, p. 60–80, doi:10.1016/j.palaeo.2018.06.043.

Della Porta, G., Capezzuoli, E., and De Bernardo, A., 2017, Facies character and depositional architecture of hydrothermal travertine slope aprons (Pleistocene, Acquasanta Terme, Central Italy): Marine and Petroleum Geology, v. 87, doi:10.1016/j.marpetgeo.2017.03.014.

Saller, A., Rushton, S., Buambua, L., Inman, K., McNeil, R., and Dickson, J.A.D.T., 2016, Presalt stratigraphy and depositional systems in the Kwanza Basin, offshore Angola: AAPG Bulletin, v. 100, p. 1135–1164, doi:10.1306/02111615216.

Santos Neto, E. V., Cerqueira, J.R., and Prinzhofer, A., 2012, Origin of CO2 in Brazilian Basins: AAPG Annual Convention and Exhibition, v. 40969.

Sartorato, C.L., 2018, Caracterização faciológica , estratigráfica e diagenética dos reservatórios carbonáticos da Formação Barra Velha , Bacia de Santos: Universidade do Estado do Rio de Janeiro, 276 p.

Souza, R.S. et al., 2018, Petrology of the hydrothermal and evaporitic continental Cretaceous (Aptian) pre-salt carbonates and associated rocks, South Atlantic Santos Basin, offshore Brazil: AAPG/ACE Annual Convention & Exhibition,.

Srdoc, D., Horvatincic, N., Obelic, B., and Sliepcevic, A., 1983, Radiocarbon dating of tufa in paleoclimatic studies: Radiocarbon, v. 25, p. 421–427.

Teboul, P.A., Durlet, C., Gaucher, E.C., Virgone, A., Girard, J.P., Curie, J., Lopez, B., and Camoin, G.F., 2016, Origins of elements building travertine and tufa: New perspectives provided by isotopic and geochemical tracers: Sedimentary Geology, v. 334, p. 97–114, doi:10.1016/j.sedgeo.2016.01.004.

Terra, G. et al., 2009, Classificação de rochas carbonáticas aplicável às bacias sedimentares brasileiras: Boletim de Geociencias da Petrobras, v. 18, p. 9–29.

Torsvik, T.H., Rousse, S., Labails, C., and Smethurst, M.A., 2009, A new scheme for the opening of the South Atlantic Ocean and the dissection of an Aptian salt basin: Geophysical Journal International, v. 177, p. 1315–1333, doi:10.1111/j.1365-246X.2009.04137.x.

Uysal, I.T., Feng, Y., Zhao, J. xin, Altunel, E., Weatherley, D., Karabacak, V., Cengiz, O., Golding, S.D., Lawrence, M.G., and Collerson, K.D., 2007, U-series dating and geochemical tracing of late Quaternary travertine in co-seismic fissures: Earth and Planetary Science Letters, v. 257, p. 450–462, doi:10.1016/j.epsl.2007.03.004.

Warwick, G.T., 1950, Calcite Bubbles - A new Cave Formation? National Speleological Society Bulletin, v. 12, p. 38–41.

Woodcock, N.H., and Mort, K., 2008, Classification of fault breccias and related fault rocks: Geological Magazine, v. 145, p. 435–440, doi:10.1017/S0016756808004883.

Wright, V.P., and Barnett, A.J., 2015, An abiotic model for the development of textures in some South Atlantic early Cretaceous lacustrine carbonates: Geological Society Special Publication, v. 418, p. 209–219, doi:10.1144/SP418.3.

Wright, P., and Barnett, A., 2017, Classifying Reservoir Carbonates When the Status Quo Simply Does Not Work : A Case Study from the Cretaceous of the South Atlantic: AAPG Annual Conference and Exhibition, v. 51419, p. 108–121.

Wright, P., and Tosca, N.J., 2016, A Geochemical Model for the Formation of the Pre-Salt Reservoirs , Santos Basin, Brazil : Implications for Understanding Reservoir Distribution: AAPG Annual Convention and Ehibition, v. 51304, p. 32.

Zalán, P.V., Severino, M.., Rigoti, C. a., and Magnavita, L.P., 2011, An entirely new 3-D view of the crustal and mantle structure of a South Atlantic Passive Margin, Santos, Campos and Espírito Santo Basins, Brazil: AAPG Annual Conference and Exhibition, p. 1–3.

APPENDIX 1

δ18O – δ13C (Punctual analyses)

CONSTITUENT	Depth (m)	CONSTITUINTE ANALISADO	$\delta^{13}C$	$\delta^{13}C$ St. Dev	$\delta^{18}O$	$\delta^{18}O$ St.Dev
Fascicular calcite	36,00	Calcita fascicular	-2,10	0.013	-0,639	0.043
Fascicular calcite	36,00	Calcita fascicular	-2,49	0.009	-0,553	0.016
Fascicular calcite	36,00	Calcita Fascicular	2,62	0,013	0,159	0,026
Fascicular calcite	36,00	Calcita Fascicular	2,41	0,011	0,285	0,026
Fascicular calcite	36,30	Calcita Fascicular	2,17	0,019	-0,276	0,042
Fascicular calcite	36,30	Calcita Fascicular	2,37	0,012	0,728	0,035
Fascicular calcite	36,30	Calcita fascicular	2,20	0.013	-1,114	0.034
Fascicular calcite	36,30	Calcita fascicular	2,04	0.019	-1,431	0.048
Fascicular calcite	40,85	Calcita fascicular	1,62	0.011	-0.247	0.023
Fascicular calcite	40,85	Calcita fibrorradial	-1,07	0,022	0,383	0,045
Fascicular calcite	40,85	Calcita fibrorradial	0,32	0,02	-1,214	0,041
Fascicular calcite	40,85	Calcita fibrorradial	1,71	0,018	-0,698	0,024
Fascicular calcite	47,60	Calcita fibrorradial	1,30	0.014	-2,322	0.044
Fascicular calcite	47,60	Calcita fibrorradial	1,04	0.013	-1,445	0.052
Micrit crust	47,60	Crosta Micrítica	1,26	0,009	-0,541	0,024
Micrit crust	48,10	Crosta Micrítica	0,49	0,024	-0,460	0,025
Micrit crust	48,10	Crosta Micrítica	1,39	0,011	-0,393	0,034
Micrit crust	48,10	Crosta Micrítica	1,47	0,023	0,218	0,067
Micrit crust	49,00	Crosta Micrítica	2,25	0,014	-0,782	0,042
Micrit crust	49,00	Crosta Micrítica	0,86	0,007	-1,549	0,044
Micrit crust	49,00	Crosta Micrítica	1,93	0,018	-0,641	0,018
Peloidal micrite	49,00	Crosta Micrítica	0,75	0,014	0,131	0,031
Peloidal micrite	111,45	Micrita Peloidal	-0,67	0,01	-4,460	0,015
Peloidal micrite	111,45	Micrita Peloidal	-0,01	0,019	-3,554	0,036
Peloidal micrite	111,75	Micrita Peloidal	0,29	0,011	-3,965	0,057
Peloidal micrite	111,75	Micrita Peloidal	0,68	0.015	-5,765	0.037
Peloidal micrite	111,75	Micrita Peloidal	0,55	0.012	-3,421	0.043
Peloidal micrite	116,00	Micrita Peloidal	-0,12	0,02	-3,498	0,017
Peloidal micrite	116,00	Micrita Peloidal	0,39	0,025	-3,145	0,025
Peloidal micrite	116,00	Micrita Peloidal	0,31	0,012	-3,448	0,037
Peloidal micrite	118,45	Micrita Peloidal	0,02	0,015	-3,806	0,019
Peloidal micrite	134,70	Micrita Peloidal	0,31	0,013	-0,015	0,012
Peloidal micrite	134,70	Micrita Peloidal	-0,76	0,009	0,478	0,022

APPENDIX 2

δ18O – δ13C (Bulk analyses)

Depth (m)	δ13C (‰ - VPDB)	St. Dev. δ13C (1σ - ‰)	δ18O (‰ - VPDB)	St. dev δ18O (1σ - ‰)	CORE SECTION
0,45	-11,47	0,08	0,05	0,08	UPPER
0,75	-12,78	0,04	0,26	0,08	UPPER
0,90	-11,01	0,02	0,79	0,07	UPPER
0,95	-10,54	0,01	0,52	0,07	UPPER
1,80	-12,18	0,10	0,73	0,09	UPPER
1,90	-11,86	0,05	0,85	0,10	UPPER
2,55	-14,63	0,07	-0,92	0,09	UPPER
2,70	-13	0,05	-0,98	0,11	UPPER
3,00	-13,73	0,06	-0,18	0,07	UPPER
3,50	-13,31	0,04	-0,03	0,07	UPPER
3,70	-13,33	0,10	-0,01	0,10	UPPER
3,95	-10,52	0,10	-0,15	0,08	UPPER
4,15	-13,31	0,03	0,72	0,06	UPPER
4,35	-12,88	0,06	0,64	0,07	UPPER
4,65	-12,38	0,02	0,48	0,08	UPPER
5,20	-11,31	0,05	0,45	0,10	UPPER
6,15	-12,72	0,10	-0,3	0,05	UPPER
6,25	-14,88	0,10	-1,12	0,14	UPPER
7,95	-15,42	0,10	-0,6	0,10	UPPER
8,50	-8,11	0,06	0,09	0,10	UPPER
8,60	-9,74	0,06	-0,28	0,09	UPPER
8,95	-13,24	0,08	-0,78	0,06	UPPER
10,25	-18,25	0,04	-0,85	0,06	UPPER
10,75	-21,94	0,02	-0,52	0,05	UPPER
11,05	-18,66	0,03	-0,93	0,10	UPPER
11,85	-18,83	0,07	-0,85	0,10	UPPER
12,05	-19,3	0,08	-0,96	0,07	UPPER
12,60	-25,64	0,10	-0,91	0,06	UPPER
12,75	-22,71	0,09	-1,4	0,13	UPPER
13,30	-13,5	0,09	-0,35	0,09	UPPER
13,65	-13,77	0,08	-0,19	0,09	UPPER
13,90	-23,18	0,05	-0,57	0,09	UPPER
14,05	-21,75	0,10	-0,87	0,07	UPPER
14,15	-18,05	0,06	-0,36	0,10	UPPER
14,50	-20,81	0,07	-0,34	0,09	UPPER
14,80	-13,45	0,04	0,23	0,08	UPPER
14,95	-15,7	0,05	-0,09	0,08	UPPER
15,20	-15,53	0,09	-0,17	0,09	UPPER
15,50	-11,44	0,04	-0,05	0,06	UPPER
15,80	-17,49	0,05	-0,61	0,09	UPPER
15,85	-15,55	0,07	-1,03	0,07	UPPER

15,90	-16,22	0,04	-0,5	0,09	UPPER
16,05	-17,13	0,09	-0,64	0,06	UPPER
16,35	-12,05	0,09	-0,05	0,07	UPPER
16,65	-13,07	0,05	0,13	0,04	UPPER
16,90	-16,07	0,08	-0,4	0,10	UPPER
17,25	-15,61	0,05	-0,38	0,08	UPPER
17,30	-10,67	0,07	0,18	0,04	UPPER
17,65	-12,13	0,04	0,09	0,09	UPPER
17,85	-12,37	0,07	-0,31	0,09	UPPER
17,90	-13,2	0,07	-0,18	0,04	UPPER
18,30	-14,94	0,10	0,22	0,06	UPPER
18,45	-9,99	0,05	-0,56	0,03	UPPER
18,50	-11,33	0,03	-1,72	0,06	UPPER
18,85	-11,51	0,03	-1,23	0,06	UPPER
19,15	-10,12	0,05	-1,74	0,10	UPPER
19,45	-11,83	0,09	-1,25	0,09	UPPER
19,75	-11,48	0,02	-1,25	0,06	UPPER
20,10	-13,39	0,03	-1,28	0,06	UPPER
20,15	-13,65	0,04	-1,28	0,04	UPPER
20,35	-14,74	0,09	-0,93	0,04	UPPER
20,65	-9,41	0,03	-1,45	0,08	UPPER
20,90	-10,42	0,03	-2,2	0,05	UPPER
21,30	-15,7	0,04	-1,02	0,03	UPPER
21,90	-18,43	0,05	-1,06	0,07	UPPER
21,95	-22,82	0,02	-0,78	0,04	UPPER
22,00	-20	0,07	-0,77	0,03	UPPER
22,15	-21,89	0,06	-0,9	0,03	UPPER
22,40	-21,28	0,09	-0,88	0,05	UPPER
22,75	-21,81	0,09	-0,67	0,03	UPPER
23,15	-18,09	0,06	-0,89	0,02	UPPER
23,40	-15,08	0,09	-0,38	0,05	UPPER
23,60	-14,98	0,05	-0,21	0,03	UPPER
23,90	-20,77	0,04	-0,64	0,03	UPPER
24,15	-20,45	0,03	-0,8	0,04	UPPER
24,25	-20,74	0,08	-0,92	0,04	UPPER
24,45	-21,07	0,02	-1,05	0,08	UPPER
24,55	-12,03	0,05	-1,13	0,06	UPPER
25,55	-1,55	0,09	0,21	0,05	UPPER
25,85	-5,9	0,06	-0,14	0,03	UPPER
25,95	-6,21	0,08	0,36	0,03	UPPER
26,05	-6,31	0,05	0,44	0,06	UPPER
26,40	-7,6	0,04	0,18	0,05	UPPER
26,50	-7,99	0,07	-0,07	0,04	UPPER
27,00	-7,73	0,06	0,39	0,02	UPPER
27,25	-11,67	0,03	-0,6	0,06	UPPER
27,35	-11,41	0,04	-0,95	0,07	UPPER
27,65	-2,17	0,10	1,23	0,02	UPPER
27,90	-0,03	0,03	1,06	0,07	UPPER
28,00	0,75	0,10	1,19	0,05	UPPER
28,10	-5,08	0,05	-0,18	0,02	UPPER

28,40	-15,23	0,07	-0,68	0,04	UPPER
28,55	-12,23	0,04	-0,53	0,04	UPPER
28,70	-14,51	0,04	-0,15	0,02	UPPER
30,75	-17,62	0,06	-1,4	0,09	UPPER
31,55	-5,41	0,09	-0,27	0,07	UPPER
31,8	-4,36	0,02	-0,45	0,05	UPPER
31,9	-3,94	0,07	0,01	0,05	UPPER
32,2	-4,66	0,06	-0,54	0,06	UPPER
33,25	-5,85	0,10	-1,82	0,05	UPPER
33,35	-3,12	0,05	-0,74	0,06	UPPER
34	-3,72	0,06	-1,83	0,08	UPPER
34,55	-10,32	0,08	-2,27	0,03	UPPER
34,8	-0,17	0,03	0,2	0,03	UPPER
35,1	-1,51	0,03	0,18	0,05	UPPER
35,4	0,87	0,10	0,29	0,10	INTERM
36,3	0,61	0,03	-0,61	0,06	INTERM
36,6	-1,27	0,05	-2,42	0,08	INTERM
36,8	-0,81	0,04	-1,57	0,09	INTERM
36,95	-0,7	0,06	-0,89	0,08	INTERM
37,2	-0,36	0,05	-0,34	0,06	INTERM
37,65	-1,69	0,02	-1,65	0,05	INTERM
37,95	-1,06	0,07	-1,46	0,07	INTERM
38,15	-0,65	0,07	-1,91	0,10	INTERM
38,25	-1,05	0,09	-0,9	0,08	INTERM
38,55	-1,41	0,07	-1,55	0,10	INTERM
38,95	-1,19	0,05	-1,34	0,11	INTERM
39,4	-1,09	0,06	-1,52	0,05	INTERM
39,5	-0,99	0,03	-1,63	0,05	INTERM
39,65	-0,16	0,07	-0,17	0,08	INTERM
40	-1,24	0,05	-1,79	0,09	INTERM
40,3	-0,88	0,04	0,36	0,06	INTERM
40,6	-2,35	0,02	-1,26	0,06	INTERM
40,8	-3,15	0,10	-1,22	0,09	INTERM
41,45	-2,09	0,07	-0,8	0,09	INTERM
41,75	-1,29	0,09	-1,79	0,09	INTERM
42,15	-1,83	0,08	-1,62	0,10	INTERM
42,6	-1,39	0,02	-0,35	0,05	INTERM
46,35	-0,5	0,04	-2,73	0,06	INTERM
46,90	-0,43	0,05	-3,01	0,07	INTERM
47,20	-1,19	0,05	-2,26	0,06	INTERM
47,60	-0,97	0,05	-2,53	0,06	INTERM
47,65	-1,16	0,07	-2,67	0,09	INTERM
47,75	-1,34	0,02	-2,32	0,09	INTERM
47,80	-1,27	0,03	-1,87	0,08	INTERM
48,20	-1,51	0,03	-2,55	0,04	INTERM
49,60	-1,77	0,03	-1,94	0,06	INTERM
49,65	-1,55	0,02	-2,69	0,05	INTERM
50,35	0,01	0,04	-1,52	0,05	INTERM
53,05	-1,31	0,05	-1,65	0,04	INTERM
53,45	-0,74	0,03	-1,07	0,09	INTERM

53,55	-1,26	0,02	-1,04	0,03	INTERM
54,3	0,04	0,02	-0,46	0,02	INTERM
55,2	-1,42	0,02	-1,55	0,07	INTERM
55,25	-1,76	0,04	-1,55	0,10	INTERM
108,05	-2,25	0,05	-1,48	0,10	INTERM
108,70	-2,17	0,04	-1,1	0,07	INTERM
109,00	-2,33	0,08	-1,16	0,07	INTERM
109,30	-1,64	0,08	0,48	0,05	INTERM
109,70	-0,41	0,05	-0,76	0,08	INTERM
109,75	-1,58	0,05	-1,5	0,07	INTERM
110,10	-1,59	0,05	-0,07	0,10	INTERM
110,80	-2,06	0,10	-1,42	0,08	INTERM
111,10	-1,4	0,10	-1,39	0,11	INTERM
111,45	-1,64	0,09	-1	0,05	INTERM
111,55	-1,35	0,03	0,02	0,05	INTERM
111,75	-0,54	0,02	0,48	0,04	INTERM
112,05	-0,96	0,05	-0,31	0,09	INTERM
112,40	-1,41	0,05	-0,77	0,06	INTERM
112,45	-0,86	0,07	-0,05	0,07	INTERM
116,00	-1,05	0,05	-0,07	0,07	INTERM
116,05	-0,77	0,10	-0,18	0,04	INTERM
116,60	-1,56	0,03	-1,27	0,06	INTERM
116,90	-1,23	0,04	-1,01	0,08	INTERM
116,95	-1,6	0,05	-0,27	0,08	INTERM
117,05	-1,82	0,06	-0,89	0,07	INTERM
117,15	-2,16	0,05	-0,4	0,07	INTERM
117,45	-1,57	0,07	-1,18	0,09	INTERM
118,10	-2,22	0,09	-1,13	0,10	INTERM
118,20	-2,26	0,04	-1,68	0,04	INTERM
118,45	-2,46	0,05	0,61	0,07	INTERM
118,75	-1,25	0,05	1,08	0,06	INTERM
119,10	-1,81	0,07	0,41	0,08	INTERM
119,45	-1,42	0,03	0,02	0,10	INTERM
119,55	-1,5	0,06	0,76	0,12	INTERM
119,75	-1,97	0,02	-1,26	0,05	INTERM
120,05	-1,25	0,06	-0,38	0,07	INTERM
120,45	-2,07	0,05	-0,55	0,06	INTERM
120,65	-1,85	0,03	-1,34	0,05	INTERM
120,75	-1,47	0,07	-1,02	0,07	INTERM
121,05	-1,54	0,08	-0,56	0,10	INTERM
121,30	-1,8	0,06	-0,64	0,08	INTERM
121,60	-2,05	0,04	-0,97	0,04	INTERM
121,85	-1,17	0,03	0,17	0,04	INTERM
122,15	-0,14	0,07	1,52	0,07	INTERM
122,25	-0,47	0,04	-0,1	0,05	INTERM
122,45	-0,46	0,02	-0,12	0,04	INTERM
122,60	0,83	0,13	1,5	0,10	INTERM
122,70	-1,17	0,08	1,16	0,06	INTERM
123,00	-0,83	0,03	0,24	0,07	INTERM
123,75	-2,14	0,04	-2,23	0,04	INTERM

123,85	-2,16	0,06	-2,51	0,07	INTERM
124,35	-1,25	0,11	-1,46	0,10	INTERM
124,75	-1,34	0,09	-1,15	0,08	INTERM
125,05	-1,61	0,06	-2,22	0,05	INTERM
125,35	-1,43	0,05	-1,92	0,07	INTERM
125,45	-1,76	0,06	-2,26	0,09	INTERM
125,65	-1,93	0,05	-1,42	0,05	INTERM
126,00	-1,7	0,03	-1,39	0,07	INTERM
126,30	-1,62	0,06	-1,51	0,10	INTERM
126,60	-1,62	0,05	-1,38	0,06	INTERM
126,65	-1,64	0,05	-1,77	0,10	INTERM
126,90	-1,48	0,04	-2,01	0,04	INTERM
127,15	-1,86	0,05	-2,66	0,15	INTERM
127,50	-1,69	0,09	-1,86	0,05	INTERM
127,55	-1,44	0,08	-1,5	0,10	INTERM
127,85	0,32	0,09	-0,02	0,07	INTERM
127,95	-1,3	0,09	-2,32	0,07	INTERM
128,10	0,35	0,06	-1,14	0,11	INTERM
128,40	-0,11	0,06	-0,81	0,07	INTERM
128,70	-1,05	0,07	-1,82	0,10	INTERM
129,30	-2,14	0,08	-1,24	0,06	INTERM
129,35	-1,98	0,06	-1,48	0,10	INTERM
129,65	-1,08	0,02	-0,83	0,08	INTERM
129,95	-0,98	0,05	-0,32	0,06	INTERM
130,20	-1,17	0,09	-0,98	0,05	INTERM
130,40	-1,89	0,08	-1,63	0,10	INTERM
130,50	-2,49	0,04	-2,19	0,09	INTERM
131,15	-1	0,02	-0,6	0,06	INTERM
131,70	-1,66	0,03	-0,82	0,03	INTERM
131,95	-2,72	0,05	-0,49	0,10	INTERM
132,60	-2,17	0,04	-2,6	0,07	INTERM
132,70	-2,2	0,04	-3,01	0,07	INTERM
133,35	-1,72	0,08	-2,83	0,10	INTERM
133,60	-1,17	0,02	-3,1	0,08	INTERM
133,70	-1,5	0,05	-3,67	0,08	INTERM
133,85	-1,19	0,03	-3,92	0,04	INTERM
134,45	-1,79	0,09	-2,24	0,08	INTERM
134,55	-1,65	0,05	-1,88	0,07	INTERM
134,70	-1,21	0,05	-1,97	0,06	INTERM
134,95	-2,76	0,07	-1,38	0,08	INTERM
135,00	-3,16	0,06	-2,32	0,06	INTERM
135,55	-0,71	0,09	-0,62	0,10	BASAL
135,90	-2,18	0,10	-1,91	0,09	BASAL
136,20	-1,85	0,03	-2,9	0,07	BASAL
136,45	-3,04	0,04	-2,17	0,05	BASAL
136,50	-2,65	0,02	-2,45	0,02	BASAL
136,85	-1,55	0,08	-2,64	0,05	BASAL
137,15	-1,5	0,04	-2,12	0,08	BASAL
137,35	-2,53	0,07	-1,84	0,09	BASAL
137,45	-4,79	0,04	-1,38	0,07	BASAL

APPENDIX 3 – QEMSCAN MINERALOGY (% AREA)

Depth (m)	Facies	Quartz	Apatite	Pores	Others	Pyrite	Al-Micas+Ilita+Al-Esmectitas	Calcite (1% a 4%MgO)	Calcite (0% a 1%MgO)	Calcite (4% a 7%MgO)	Dolomite (17% a 20%MgO)	Calcite (7% a 10%MgO)	Dolomite (20% a 23%MgO)	Barite	K-Feldspar	Bitumen	Sr-Barite	Goyazite	Celestite	Fluorite	Anhydrite	Estroncianite
34,55	**GST**	44,138	0,003	21,668	0,192	0,010	0,006	0,005	0,453	0,329	25,906	1,089	1,773	2,445	0,000	1,116	0,830	0,024	0,002	0,010	0,000	0,000
35,7	**GST**	0,362	0,025	26,591	0,106	0,025	0,002	24,215	18,437	15,814	11,371	2,294	0,106	0,004	0,001	0,492	0,000	0,002	0,142	0,012	0,000	0,000
36	**MCC**	30,473	0,003	24,675	0,310	0,029	0,007	9,991	15,495	9,184	7,673	0,990	0,193	0,000	0,000	0,936	0,001	0,017	0,017	0,004	0,000	0,000
36,3	**MCC**	0,319	0,017	23,022	0,137	0,021	0,017	14,677	27,532	22,027	7,585	2,260	0,080	0,107	0,009	2,155	0,004	0,014	0,004	0,008	0,004	0,000
38,55	**MCT-pe/CCL-sh**	0,012	0,033	7,770	0,043	0,002	0,026	19,930	64,210	6,308	0,845	0,642	0,015	0,047	0,041	0,050	0,000	0,003	0,000	0,008	0,000	0,017
49	**MCT-pe**	0,011	0,100	17,357	0,007	0,001	0,001	13,785	62,847	2,094	2,536	0,694	0,095	0,004	0,004	0,449	0,000	0,000	0,000	0,007	0,000	0,008
50,35	**CCL-sh**	0,028	0,067	5,142	0,035	0,002	0,014	26,288	47,001	17,552	2,406	1,279	0,041	0,028	0,024	0,065	0,001	0,010	0,000	0,007	0,000	0,008
111,75	**MCT-pe**	0,047	0,084	12,056	0,063	0,034	0,010	17,183	55,124	4,862	7,996	1,663	0,273	0,007	0,057	0,526	0,000	0,000	0,000	0,007	0,000	0,006
115,65	**CCL-ef**	0,158	0,108	2,187	0,038	0,594	0,012	15,666	73,148	1,760	4,558	0,606	0,206	0,096	0,054	0,762	0,001	0,002	0,000	0,005	0,000	0,038
119,45	**CCL-sh**	0,213	0,214	2,827	0,071	0,088	0,395	17,250	74,208	0,763	1,851	0,223	0,035	0,017	1,645	0,157	0,000	0,000	0,000	0,003	0,000	0,035
133,85	**CCL-ef**	2,503	0,011	2,111	0,094	0,099	0,254	18,134	73,585	0,937	0,383	0,161	0,007	0,000	1,197	0,486	0,000	0,000	0,000	0,006	0,000	0,029
135,55	**CCL-ef**	56,406	0,010	1,964	0,051	0,072	0,025	6,644	33,860	0,288	0,326	0,070	0,009	0,013	0,132	0,112	0,000	0,000	0,000	0,001	0,000	0,016
	Max	56,406	0,214	26,591	0,310	0,594	0,395	26,288	74,208	22,027	25,906	2,294	1,773	2,445	1,645	2,155	0,830	0,024	0,142	0,012	0,004	0,038
	Min	0,011	0,003	1,964	0,007	0,001	0,001	0,005	0,453	0,288	0,326	0,070	0,007	0,000	0,000	0,050	0,000	0,000	0,000	0,001	0,000	0,000
	Mean	11,223	0,056	12,281	0,096	0,082	0,064	15,314	45,492	6,827	6,120	0,998	0,236	0,231	0,264	0,609	0,070	0,006	0,014	0,006	0,000	0,013
	St.dev	19,480	0,060	9,399	0,081	0,158	0,120	6,934	24,569	7,309	6,885	0,727	0,471	0,669	0,527	0,570	0,229	0,008	0,039	0,003	0,001	0,013